Summer 8-8-2015

Development of a Modified Calcium-Based Composite Ceramic Bone Graft Material

Gavin Buckholtz

DEVELOPMENT OF A MODIFIED CALCIUM-BASED COMPOSITE CERAMIC BONE GRAFT MATERIAL

A Dissertation

Bayer School of Natural and Environmental Sciences

Duquesne University

In partial fulfillment of the requirements for

the degree of Doctor of Philosophy

By

Gavin Andrew Buckholtz

August 2015

DEVELOPMENT OF A MODIFIED CALCIUM-BASED COMPOSITE CERAMIC BONE GRAFT MATERIAL

By

Gavin Andrew Buckholtz

Approved June 8, 2015

_____	_____
Dr. Ellen S. Gawalt Associate Professor of Chemistry and Biochemistry (Committee Chair)	Dr. Jeffrey D. Evanseck Professor of Chemistry and Biochemistry (Committee Member)
_____	_____
Dr. Stephanie J. Wetzel Assistant Professor of Chemistry and Biochemistry (Committee Member)	Dr. Wilson S. Meng Associate Professor of Pharmaceutical Sciences (External Reviewer)
_____	_____
Dr. Philip P. Reeder Dean, Bayer School of Natural and Environmental Sciences Professor of Chemistry and Biochemistry	Dr. Ralph A. Wheeler Chair, Department of Chemistry and Biochemistry Professor of Chemistry and Biochemistry

ABSTRACT

DEVELOPMENT OF A MODIFIED CALCIUM-BASED COMPOSITE CERAMIC BONE GRAFT MATERIAL

By

Gavin Andrew Buckholtz

August 2015

Dissertation supervised by Professor Ellen S. Gawalt

Composites consisting of both calcium aluminum oxide and hydroxyapatite were tested for their applicability as bone replacement scaffolds. Implanted bone scaffolds may fail due to a variety of reasons, including mechanical and biological failure. Mechanical failure may occur as a result of dissimilar properties between the surrounding healthy bone and the scaffold. Biological failure can occur due to integration problems at the interface of the scaffold and the natural bone, or as a result of implant associated infections as a result of bacterial attachment and biofilm formation. Calcium aluminum oxide:hydroxyapatite composites were developed that address these three modes of implant failure through physical modification of the composition of the materials and chemical modification of the interface of the material.

The composites were evaluated for phase composition, elastic modulus, modulus of rupture, degradability, osteoblast attachment, percent viability and proliferation. Characterization was completed using powder x-ray diffraction (PXRD), a four point bending test, scanning electron microscopy (SEM), scanning electron microscopy-energy dispersive x-ray spectroscopy (SEM-EDS), diffuse reflectance infrared Fourier transform (DRIFT) spectroscopy, fluorescence spectroscopy, direct infusion quadrupole-time of flight mass spectrometry (Q-TOF MS), *Escherichia coli* N-phenylnaphthylamine (NPN) uptake and bacterial turbidity tests, and Live/Dead® and alamarBlue® tissue culture assays. Composites with greater than 10% HA by mass were mechanically weak and ruled out as scaffolds. However, 1-5% HA composites were mechanically similar to non-load bearing bone and all resulted in increased osteoblast response at extended time points. The antimicrobial peptide Inverso-CysHHC10 was successfully linked to the 5% HA composite using an interfacial alkene-thiol click reaction. The linked AMP retained its effectiveness against *Escherichia coli* based on NPN uptake assays and bacterial turbidity tests. Most importantly, the immobilization of the antimicrobial peptide did not affect the increased osteoblast response observed on the unmodified 5% HA. The Inverso-CysHHC10 modified composites present a new class of composite biomaterials that are able to simultaneously address issues with mechanical mismatching, osteoconductivity and implant site infection.

DEDICATION

To my wife Sarah, who supported me in my pursuit of this project. Her willingness to put my needs ahead of hers was instrumental to the success of this work.

And to my parents, who encouraged me to push myself. Their support has always meant a lot to me.

ACKNOWLEDGEMENT

I would first like to express my gratitude for the guidance, support, and encouragement from my research advisor, Dr. Ellen Gawalt, and members of my dissertation committee including Dr. Jeffrey Evanseck, Dr. Stephanie Wetzel, and Dr. Wilson Meng. Without their expertise and insight my work would not have been possible and their assistance is appreciated.

Dr. Kenneth McGowan and Bob Cullen of Westmoreland Advanced Materials were vital resources for me as well, primarily for providing the materials used but also providing valuable knowledge of calcium aluminum oxide.

Dr. Mark Miller from the Orthopaedic Biomechanics Research Laboratory at Allegheny-Singer Research Institute and his group members deserve a thank you for performing the mechanical analysis of the composites and for sharing their knowledge and skills with me.

Lastly I would like to thank the Duquesne University Department of Chemistry and Biochemistry, the NSF S-STEM fellowship and my fellow graduate students, previous and current, for providing me with funding, engaging discussion and relaxing events. All of your contributions have aided to my success over the previous five years.

TABLE OF CONTENTS

Abstract iv

Dedication vi

Acknowledgement vii

List of Tables xiv

List of Schemes xv

List of Figures xvi

List of Abbreviations xxi

Chapter 1: Background 1

1.1 Introduction 1

1.2 Bone Scaffold Requirements 1

1.2.1 Mechanical Requirements 2

1.2.2 Biological Requirements 3

1.3 Current Bone Replacement Materials 4

1.3.1 Autografts and Allografts 4

1.3.2 Metal Alloys and Metal Oxides 5

1.3.3 Ceramics 6

1.3.4 Bioactive Glasses 7

1.4 Failure of Graft Materials 8

1.4.1 Mechanical Failure 8

1.4.2 Biological Failure 10

1.5 Current Literature Approaches to Materials Modification 11
1.5.1 Metal Alloys and Metal Oxides 11
1.5.2 Composite Materials 12
1.5.3 Biomolecule Functionalization 13
1.6 Summary 15
1.7 Research Approach 15
1.8 References 17
Chapter 2: Physical Characterization of Composite CaAlO:HA 27
2.1 Introduction 27
2.2 Materials and Methods 29
2.2.1 Materials 29
2.2.2 Casting Calcium-Based Ceramics 29
2.2.2.1 Calcium Aluminum Oxide 29
2.2.2.2 Hydroxyapatite 30
2.2.2.3 Calcium Aluminum Oxide:Hydroxyapatite Composites 31
2.2.3 Powder X-ray Diffraction 32
2.2.4 Mechanical Evaluation 33
2.2.5 Scanning Electron Microscopy 34
2.2.6 Scanning Electron Microscopy-Energy Dispersive X-Ray Spectroscopy 34
2.2.7 Degradability Study 35
2.2.8 Statistics 36

2.3 Results 36
2.3.1 Powder X-Ray Diffraction 36
2.3.2 Mechanical Evaluation 37
2.3.2.1 Elastic Modulus 38
2.3.2.2 Modulus of Rupture 40
2.3.3 Scanning Electron Microscopy 41
2.3.4 Energy Dispersive X-Ray Spectroscopy 42
2.3.5 Degradability Study 44
2.4 Discussion 45
2.5 Conclusions 48
2.6 References 49
Chapter 3: Increased Osteoblast Response on 1-5% HA Composites 53
3.1 Introduction 53
3.2 Materials and Methods 55
3.2.1 Materials 55
3.2.2 Casting Calcium-Based Ceramics 56
3.2.2.1 Calcium Aluminum Oxide 56
3.2.2.2 Calcium Aluminum Oxide:Hydroxyapatite Composites 57
3.2.3 Osteoblast Cell Culture 57
3.2.4 Osteoblast Attachment to 1-5% HA 58
3.2.5 Osteoblast Viability on 1-5% HA 59

3.2.6 Osteoblast Proliferation on 1-5% HA 59

3.2.7 Statistics 60

3.3 Results 61

3.3.1 Osteoblast Attachment to 1-5% HA 61

3.3.2 Osteoblast Viability on 1-5% HA 63

3.3.3 Osteoblast Proliferation on 1-5% HA 65

3.4 Discussion 68

3.5 Conclusions 69

3.6 References 69

Chapter 4: Creating a Multifunctional Composite Ceramic by Antimicrobial Peptide Immobilization to the 5% HA 74

4.1 Introduction 74

4.2 Materials and Methods 78

4.2.1 Materials 78

4.2.2 Casting Composite 5% HA 79

4.2.3 Covalent Antimicrobial Peptide Immobilization 79

4.2.4 Diffuse Reflectance Infrared Fourier Transform Spectroscopy 80

4.2.5 Quantification of Antimicrobial Peptide Immobilization on 5% HA 81

4.2.6 Quantification of Antimicrobial Peptide Released from Modified 5% HA . 82

4.2.7 *Escherichia coli* Culture 83

4.2.8 *Escherichia coli* NPN Uptake Factor on Modified 5% HA 83

4.2.9 *Escherichia coli* Bacterial Turbidity Tests with Modified 5% HA 85

4.2.10 Inverso-CysHHC10 Antimicrobial Activity in Solution and on Modified 5% HA 86

4.2.11 Osteoblast Cell Culture 86

4.2.12 Osteoblast Attachment to Modified 5% HA 87

4.2.13 Osteoblast Viability on Modified 5% HA 87

4.2.14 Osteoblast Proliferation on Modified 5% HA 88

4.2.15 Statistics 88

4.3 Results 89

4.3.1 Covalent Antimicrobial Peptide Immobilization 89

4.3.2 Quantification of Antimicrobial Peptide Immobilization on 5% HA 92

4.3.3 Quantification of Antimicrobial Peptide Released from HHC10 Modified 5% HA 93

4.3.4 *Escherichia coli* NPN Uptake Factor on Modified 5% HA 94

4.3.5 *Escherichia coli* Bacterial Turbidity Tests with Modified 5% HA 95

4.3.6 Inverso-CysHHC10 Antimicrobial Activity in Solution and Linked to Modified 5% HA 96

4.3.7 Osteoblast Attachment to Modified 5% HA 98

4.3.8 Osteoblast Viability on Modified 5% HA 100

4.3.9 Osteoblast Proliferation on Modified 5% HA 101

4.4 Discussion 102

4.5 Conclusions 105

4.6 References 106

Chapter 5: Conclusions 112

5.1 Effect of Hydroxyapatite Incorporation into Calcium Aluminum Oxide 112

5.1.1 Phase Composition of Cast Composites 112

5.1.2 Mechanical Properties of Cast Composites 113

5.1.3 Osteoblast Response on 1-5% HA 114

5.2 Inverso-CysHHC10 Antimicrobial Activity: Surface Immobilized vs. in Solution 114

5.3 Osteoblast Response on Inverso-CysHHC10 Modified 5% HA 115

5.4 Impact and Future Work 116

5.5 References 118

LIST OF TABLES

Table 1.1: Mechanical properties of natural bone and materials of interest in implant procedures. 2

Table 2.1: Elastic modulus of the sintered and RT-formed CaAlO:HA composites. 39

Table 2.2: Modulus of rupture of the sintered and RT-formed CaAlO:HA composites. 41

Table 5.1: Mechanical properties of natural bone and the 5% HA developed in this work. 113

LIST OF SCHEMES

Scheme 2.1: Proposed reactions for the synthesis of hydroxyapatite from calcium phosphate tribasic. 28

Scheme 4.1: Inverso-CysHHC10 containing the hydrophobic tryptophan and isoleucine amino acids and hydrophilic arginine and lysine amino acids. The sacrificial cysteine is appended to the N-terminus. 77

Scheme 4.2: Reaction sequence utilized for the covalent immobilization of HHC10 to composite 5% HA. First the material is modified with 16-heptadecenoic acid, then an alkene-thiol click reaction is used to link HHC10 at the interface. 80

LIST OF FIGURES

Figure 1.1: Modes of artificial graft failure including a) healthy bone resorption due to mechanical mismatching, b) fibrous encapsulation due to non-specific protein adsorption and c) biofilm formation due to attachment of bacteria and polysaccharide matrix production. 9

Figure 2.1: Casting 100% CaAlO in a 2:1:1 ratio of three different aggregate sizes. Through hydration the aggregates can be cast into a variety of shapes. 30

Figure 2.2: Casting 100% HA using ground $Ca_3(PO_4)_2$ with 25 mM H_3PO_4. After casting the materials are sintered for strength. 31

Figure 2.3: CaAlO:HA composite beam loaded in the four point bending apparatus, prior to load application. 33

Figure 2.4: A) PXRD pattern for the 5% HA composite and phases contained within the composite. Including the calcium aluminum oxide based phases B) $CaAl_4O_7$, C) $CaAl_2O_4$ and D) $Ca_3Al_2(OH)_{12}$ and the calcium phosphate based phases E) $Ca_5(PO_4)_3(OH)$ and F) $CaHPO_4{\cdot}2H_2O$. 37

Figure 2.5: Average elastic modulus of the composites of sintered and RT-formed 0-5, 10, 15, 20 and 25% HA composites, shown as mean ± standard error, $p<0.05$. RT-formed composites are statistically higher for all percentages evaluated. 38

Figure 2.6: Average modulus of rupture of the composites of sintered and RT-formed 0-5, 10, 15, 20 and 25% HA composites, shown as mean ± standard error, $p<0.05$. RT-formed composites are statistically higher for 1-5% HA and statistically equal at greater percentages of HA. 40

Figure 2.7: Morphological SEM images of surface structures observed on CaAlO, 5% HA and HA. A) Needle-like formation of CaAlO. B) Plate-like formation of CaAlO. C) Cube-like formation of CaAlO. D) Increased surface uniformity observed on 5% HA, similar to interfacial characteristics of HA. E) Interfacial structure of 100% HA. 42

Figure 2.8: EDS spectra for 0, 1, 3 and 5% HA exhibit the presence of calcium, aluminum, and oxygen from the CaAlO phases. The 1, 3 and 5% HA composites contain phosphorus due to the HA and brushite phases. Elemental mapping shows the distribution of the HA phase at the composite interface based on the location of the phosphorus atoms and the aluminum atoms show that the majority of the interface is CaAlO. 43

Figure 2.9: Average change in mass from week to week for 0-5% HA composites over a 3 month time span. 45

Figure 3.1: Fluorescent based Live/Dead® Viability/Cytotoxicity assay where calcein AM enters a live cell and is digested by an esterase to result in the green fluorescent cells. The ethidium homodimer enters a dead cell and binds to the DNA in the nucleus resulting in the red fluorescent cells. 59

Figure 3.2: AlamarBlue® assay for osteoblast proliferation. If there are living, dividing cells in the wells, the alamarBlue® reagent is reduced and a color change can be observed and quantified by UV-VIS. If there are dead cells in the wells, the alamarBlue® reagent is not reduced. 60

Figure 3.3: Representative Live/Dead® fluorescent images of osteoblasts attached to control 100% CaAlO and 1-5% HA composites on Days 1, 4 and 7. 61

Figure 3.4: Day 1 normalized average number of live osteoblasts attached to control and 1-5% HA composites. * = statistically higher than control and all other composites. Data represented as mean ± standard error, $p<0.05$. 62

Figure 3.5: Day 4 normalized average number of live osteoblasts attached to control and 1-5% HA composites. # = statistically higher than control and * = statistically higher than control and all other composites. Data represented as mean ± standard error, $p<0.05$. ...62

Figure 3.6: Day 7 normalized average number of live osteoblasts attached to control and 1-5% HA composites. # = statistically higher than control and * = statistically higher than control and all other composites. Data represented as mean ± standard error, $p<0.05$. ...63

Figure 3.7: Day 1 percent viability of attached cells on control and 1-5% HA composites. # = statistically higher than control. Data represented as mean ± standard error, $p<0.05$. 64

Figure 3.8: Day 4 percent viability of attached cells on control and 1-5% HA composites. # = statistically higher than control. Data represented as mean ± standard error, $p<0.05$. 64

Figure 3.9: Day 7 percent viability of attached cells on control and 1-5% HA composites. # = statistically higher than control. Data represented as mean ± standard error, $p<0.05$. 65

Figure 3.10: Representative OBM solutions for Day 7 of the alamarBlue® assay for control and 1-5% HA. 66

Figure 3.11: Day 1 normalized absorbance at 570 nm of control and 1-5% HA composites. # = statistically higher than control. Data represented as mean ± standard error, $p<0.05$. 66

Figure 3.12: Day 4 normalized absorbance at 570 nm of control and 1-5% HA composites. # = statistically higher than control and * = statistically higher than control and all other composites. Data represented as mean ± standard error, $p<0.05$. 67

Figure 3.13: Day 7 normalized absorbance at 570 nm of control and 1-5% HA composites. # = statistically higher than control and * = statistically higher than control and all other composites. Data represented as mean ± standard error, $p<0.05$. 67

Figure 4.1: Steps in biofilm formation on the implant surface include irreversible bacterial attachment of planktonic bacteria, bacterial replication and polysaccharide matrix production and shedding of biofilm clusters and release of planktonic cells. 75

Figure 4.2: A proposed mechanism of AMP action is membrane pore formation where hydrophobic amino acids allow for intercalation of the peptide into the phospholipid membrane of bacteria, and hydrophilic amino acids form the interior of the pore. 76

Figure 4.3: NPN uptake assay for determination of *E. coli* membrane permeability. If the HHC10 effectively lyses the membrane the NPN can enter the hydrophobic environment and increased fluorescence of NPN can be observed. If the membrane remains intact the NPN cannot enter and fluorescence is not observed. 83

Figure 4.4: Bacterial turbidity test for the evaluation of *E. coli* growth in culture. If HHC10 reduces bacterial growth, the concentration of *E. coli* in solution will be smaller and the $OD_{600\ nm}$ will be lower than untreated bacteria. 85

Figure 4.5: DRIFT spectra indicating successful surface modification of 5% HA with 16-heptadecenoic acid. A) Methylene stretching region, $\nu_{CH2\ asymm}$= 2921 cm^{-1} and $\nu_{CH2\ symm}$= 2852 cm^{-1} indicating the presence of the acid film after solvent rinse. B) Acid head group binding region with peaks indicative of a bidentate binding mode for the attached acid (red spectra) at 1558, 1538 and 1521 cm^{-1} and the free interfacial $\nu_{C=C}$ at 1651 cm^{-1}. 90

Figure 4.6: DRIFT spectra indicating successful immobilization of HHC10. A) Thiol stretching before (blue) and after (red) peptide linking, showing the loss of the S-H stretch. B) Sulfide bond stretches before (blue) and after (red) peptide immobilization corresponding to $\nu_{C\text{-}S\ cysteine,\ solid}$ at 702 cm^{-1} and $\nu_{C\text{-}S\ cysteine}$ and $\nu_{C\text{-}S\ acid\ to\ peptide}$ at 735, 716, 673 and 652 cm^{-1}. C) Amide I ($\nu_{C=O}$) and amide II ($\nu_{N\text{-}H}$) bands for solid (blue) and linked peptide (red) indicating the presence on the peptide on the 5% HA composite. 91

Figure 4.7: Calibration curve used for the quantification of the amount of immobilized HHC10 on the 5% HA composites. 92

Figure 4.8: Calibration curve used to quantify the amount of HHC10 released into solution. 93

Figure 4.9: The percentage of Inverso-CysHHC10 that remains linked to 5% HA using the alkene-thiol linker system through a 24 hour soak in ddH_2O, shown as mean ± standard error, $p<0.05$. 94

Figure 4.10: Normalized NPN uptake factor for untreated *E. coli* and *E. coli* treated with HHC10 modified 5% HA discs. Data shown as mean ± standard error, $p<0.05$. *E. coli* treated with modified discs exhibit increased membrane permeability. 95

Figure 4.11: Normalized $OD_{600\ nm}$ for untreated *E. coli* and *E. coli* treated with HHC10 modified 5% HA discs. Data shown as mean ± standard error, $p<0.05$. *E. coli* treated with modified discs exhibit decreased $OD_{600\ nm}$ and decreased bacterial growth in culture. ...96

Figure 4.12: NPN uptake assay for *E.* coli treated with 10 μM and linked HHC10, shown as mean ± standard error, $p<0.05$. Both treated *E. coli* solutions have a statistically higher NPN uptake factor than untreated *E. coli* and are statistically equivalent. 97

Figure 4.13: Bacterial turbidity tests for *E. coli* treated with 10 μM and linked HHC10, shown as mean ± standard error, $p<0.05$. Both treated *E. coli* solutions have a statistically lower $OD_{600\ nm}$ than untreated *E. coli* and are statistically equivalent. 98

Figure 4.14: Representative Live/Dead® fluorescent images of osteoblasts attached to control unmodified and HHC10 modified 5%HA composites on Days 1, 4 and 7. 98

Figure 4.15: Days 1, 4 and 7 normalized average number of live osteoblasts attached to control unmodified and HHC10 modified 5% HA composites. Data represented as mean ± standard error, $p<0.05$. The average number of attached live cells is statistically equal on all days examined. 99

Figure 4.16: Days 1, 4 and 7 percent viability of attached cells on control unmodified and HHC10 modified 5% HA composites. * = statistically higher than control for that day. Data represented as mean ± standard error, $p<0.05$. The percent viability is equal on Day 1 and 4 and statistically higher on Day 7. 101

Figure 4.17: Days 1, 4 and 7 normalized absorbance of OBM for control unmodified and HHC10 modified 5% HA composites. Data represented as mean ± standard error, $p<0.05$. The amount of cell proliferation is statistically equal on all days examined. 102

LIST OF ABBREVIATIONS

0% HA	Non-composite ceramic, 100% CaAlO
16-ene	16-heptadecenoic acid
5% HA	Composite consisting of 5% HA and 95% CaAlO, by mass
AMP	Antimicrobial peptide
ANOVA	Analysis of variance
ATCC	American Type Culture Collection
CaAlO	Calcium aluminum oxide
CaAlO:HA	Composite calcium aluminum oxide:hydroxyapatite (not a specific composition)
$Ca_3(PO_4)_2$	Calcium phosphate tribasic
ddH_2O	Distilled deionized water
DMF	Dimethylformamide
DRIFT	Diffuse reflectance infrared Fourier transform
E. coli	*Escherichia coli*
EDS	Energy dispersive x-ray spectroscopy
GPa	Gigapascals
H_3PO_4	Phosphoric acid
HA	Hydroxyapatite
HEPES	4-(2-hydroxyethyl)-piperazine ethanesulfonic acid
HHC10	Inverso-CysHHC10
Irgacure 2959	2-hydroxy-4’-(2-hydroxyethoxy)-2-methylpropiophenone

LB media	Luria Bertani medium
MPa	Megapascals
NHOsts	Normal human osteoblasts
NPN	N-phenylnaphthylamine
OBM	Osteoblast basal medium
$OD_{600\ nm}$	Optical density at 600 nm
P. aeruginosa	*Pseudomonas aeruginosa*
PBS	Phosphate buffered saline
PMMA	Polymethylmethacrylate
PXRD	Powder x-ray diffraction
Q-TOF MS	Quadrupole-time of flight mass spectrometry
RT-formed	Composites dried at room temperature after hydration
S. aureus	*Staphylococcus aureus*
S. epidermidis	*Staphylococcus epidermidis*
SEM	Scanning electron microscopy
Sintered	Composites sintered at 1000°C for 4 hours after hydration
THF	Tetrahydrofuran

Chapter 1: Background

1.1 Introduction

There are more than 3 million musculoskeletal procedures performed annually in the United States, with approximately half of those involving bone graft procedures.[1] Bone grafts are frequently used to treat skeletal injuries including fractures, tissue degenerative diseases and bone resection, generally as a result of cancer.[2-6] The autograft and the allograft are currently the two most common methods of bone replacement, comprising about 90% of the performed procedures.[7] Only the remaining 10% of bone grafts utilize a synthetic graft source.[7] Whatever the graft source may be, the material must be able to address the physiological stresses placed on it when it is used in an *in vivo* setting. The primary stresses placed on a graft material are mechanical and biological, and due to the nature of the autograft, it remains the most desirable source of boney tissue.[8,9] However, the extent of skeletal injury can often limit the opportunity for an autograft to be used, based on the size and severity of the bone loss. But, with recent progress in biomaterials research, tissue engineering and mechanical engineering, there is hope that a synthetic bone graft material can be developed and tuned for its applicability.[10-12] The ideal synthetic bone graft material would be mechanically similar to natural bone and biologically similar to the autograft.

1.2 Bone Scaffold Requirements

The mechanical strength and biological activity of a bone graft material are both critical aspects in determining the applicability of a synthetic scaffold material used to fill

a critically-sized bone defect, anything larger than 4 mm in size.[13-16] Synthetic graft materials must be mechanically similar to the natural bone that will surround them upon implantation, resistant to corrosion and degradation under physiological condition, non-cytotoxic to healthy cells, able to stimulate increased cellular attachment, viability and proliferation and resistant to bacterial attachment and colonization.[17-20]

1.2.1 Mechanical Requirements

The scaffold should have similar strength to the cortical or cancellous bone that it will be used to replace.[9,21,22] This is important for a couple reasons. First, it is important because most scaffolds are designed to act as mechanical supports for the injury site, with the long term goal of healthy tissue eventually replacing the graft. Second, the location of the graft will dictate the mechanical properties necessary. Natural load bearing cortical bone, such as the femur, is much stronger than non-load bearing cancellous bone, such as the skull or jaw, and the mechanical properties of the scaffold should be similar to those of the natural surrounding bone.

Table 1.1: Mechanical properties of natural bone and materials used in implant procedures.

	Elastic Modulus (GPa)	Modulus of Rupture (MPa)
Load Bearing Cortical Bone[23]	15-22	60-75
Non-Load Bearing Cancellous Bone[23]	3-11	4-9
Ti-6Al-4V Alloy Biomaterial[24]	100-115	800-1000
Hydroxyapatite (Sintered)[25]	80-110	600-800

Biomaterials that are too weak provide poor mechanical support and result in fracture or dislocation of the scaffold. But biomaterials that are stronger than the surrounding tissue result in the stress shielding of the surrounding natural bone by the biomaterials and can lead to bone resorption, weakening and fracture.[26-28]

Since bone scaffolds are designed to act as mechanical support while new, healthy bone regenerates the material should not rapidly degrade.[29] If the scaffold degrades too rapidly, it does not give the healthy tissue an opportunity to integrate and vascularize, both critical steps in new bone formation. Also, too rapid of degradation can lead to implant loosening and failure. However, if the scaffold does not break down at a rate approximately equal to the rate of new bone regeneration it can result in the buildup of boney tissue at the scaffold-tissue interface and can also lead to implant rejection.

1.2.2 Biological Requirements

The biological requirements of a biomaterial are the most important and can often be tuned to overcome minor mechanical differences. An ideal bone scaffold material should be osteoconductive, osteoinductive, osteogenic and osteointegrative.[21,22,30] Osteoconductivity is the ability of the scaffold to support attachment and growth of osteoblasts, cells necessary for new bone formation.[21,22,30] Osteoinductivity is the ability of the scaffold to induce the differentiation of mesenchymal stem cells into osteoblasts.[21,22,30] The ability of a material to induce this differentiation is important in the formation of new bone cells and bone tissue. A scaffold that is osteogenic allows living cells to proliferate on and within the material, leading to the eventual replacement of graft material with natural tissue.[21,22,30] Finally, osteointegration is the capability of the scaffold material to

bind with the natural bone. Improper osteointegration can lead to implant dislocation and graft failure.[21,22,30]

The physical properties of a scaffold material often play a role in the osteoconductivity and osteoinductivity.[19] Primarily the porosity, including size and connectivity, of a material effect the osteoconductivity and osteoinductivity. Natural bone can be up to 90% porous which leads to the ability to vascularize the tissue and leads to healthy tissue formation.[31-33] If a material is non-porous the cells tend to only grow on the surface and the graft may fail.[34]

However, the chemical composition of the scaffold has also been shown to effect the osteoconductivity and osteoinductivity. Where CaAlO based materials have demonstrated the necessity of chemical functionalization for the addition of these characteristics.[35-37] Calcium phosphate materials, including β-tricalcium phosphate and hydroxyapatite, have shown increased material osteoconductivity and osteoinductivity through the simple addition of these phases to a variety of materials.[37,38] By incorporating these phases, it has been shown that the physical shortcomings of a material can be overcome.

1.3 Current Bone Replacement Materials

1.3.1 Autografts and Allografts

The autograft and allograft are the only types of bone graft materials that are based on natural human tissue. The autograft is considered the gold standard of bone graft technology because it is the only material that supports osteoconductivity, osteoinductivity and osteointegration.[9] The autograft is a piece of bone tissue harvested from the patient's

own body.[39,40] This graft is the most desirable because the tissue is from the patient and therefore the risk of immune response and disease transmission are minimized.[41] However, the procedure to acquire the autograft presents significant concerns. Obtaining the autograft tissue requires a second surgical site and risks donor site infection, morbidity and possible chronic pain.[41,42] The final drawback to the autograft is the limitation of tissue availability.[43] The autograft has been successful in small applications, however a patient only has a finite amount of donatable tissue. If the skeletal injury is too severe, then despite the advantages of the autograft, an allograft is often used.

The allograft is a piece of boney tissue that is harvested from a donor, typically shortly following death.[40] Upon removal the bones are cleaned of all soft tissue and sterilized using ethanol or gamma radiation.[44,45] The sterilized bone can then be stored until it is needed for a surgical procedure. Allografts have the benefit of a larger size availability and they minimize the donor site complications associated with autografts.[46] However, allografts have several significant risks associated with them. Due to post resection processing the tissue lacks osteoinductive properties and becomes mechanically weaker.[21,47] Also despite the sterilization process disease transmission from donor to recipient has been observed.[45,48,49] Finally, the biggest risk is long-term host rejection which requires drug therapy.[50,51]

1.3.2 Metal Alloys and Metal Oxides

As mentioned, only about 10% of bone replacement procedures utilize a synthetic bone scaffold material. The majority of these are metal replacements utilized when the bone defect is critically-sized and the location of the injury is to load bearing bone.

Frequently stainless steel, titanium and cobalt-chromium alloys are utilized in these types of applications.[52,53] Stainless steel alloys are useful as biomaterials because they are more ductile than other alloys and the surface can be physically adjusted for surface roughness, surface oxygen content and surface energy demonstrated that osteoblast cell adhesion, spreading and growth rate was increased for one-day adhesion tests on CO_2 laser-treated samples.[54] Also they showed that the mechanically roughened surface results in a slight enhancement in cell proliferation.[54] Titanium based alloys are regularly used as total replacement materials because they have a high strength to weight ratio and tend to be the most bio-inert alloy.[55] Titanium alloys, including Ti-6Al-4V, have shown increased osteoblast adhesion, differentiation and calcification when the alloy surface was rough.[56] Nano-patterned titanium substrates demonstrated improved osteoblast adhesion and morphology on linearly aligned features similar to the size and orientation of collagen and hydroxyapatite in long bones.[57] Cobalt-chromium alloys are widely used due to high mechanical strength and hardness that limits wear over time.[28] Co-Cr alloys modified with BMP-2 showed a two-fold increase in osteoblast differentiation after two weeks and a four-fold increase in calcium deposition after three weeks.[58] Both physical and chemical modification have demonstrated their ability to increase the biocompatibility of synthetic metal replacement devices.

1.3.3 Ceramics

Due to their chemical stability and mechanical strength, calcium aluminum oxide cements have been evaluated for use a synthetic graft materials.[59-61] CaAlO possesses a variety of desirable characteristics for bone grafting procedures. The material is easily

prepared using hydration, making it easy to fabricate necessary shapes and designs.[35,36] In addition to the ease of fabrication, CaAlO has low degradability and cytotoxicity, under normal physiological conditions. CaAlO has also been shown to not lose its mechanical strength through autoclave sterilization and is readily functionalized with cell adhesion peptides and antibiotics using interfacial reactions.[35,36]

Due to the chemical similarity to natural bone, calcium phosphate ceramics have also been investigated.[16,62,63] When cast as HA, the material has been shown to be osteoconductive and osteointegrative.[38,63] The material can also be slowly resorbed through cell mediated resorption, allowing for replacement with natural tissue.[64,65] Many available biomaterials utilize HA as part of their material, including the Vitoss Bone Graft Substitute. HA demonstrates increased osteoconductivity and osteoinductivity, but work has also shown that this material can be further functionalized with adsorbed antibiotics (including vancomycin, gentamicin and ciprofloxacin) and linked antibiotics (tetracycline) to make them even more attractive options as multifunctional synthetic bone graft materials.[66-68]

1.3.4 Bioactive Glasses

Bioactive glasses are hard, non-porous materials typically composed of a combination of sodium oxide, calcium oxide, silicon dioxide and diphosphorus pentoxide that are being investigated for bone repair.[21,69] These materials are safe to implant and can be engineered for specific purposes. First the sodium ions in the glass are replaced by protons, then hydrolysis of the silicon dioxide leads to the precipitation of a calcium phosphate on the material that mineralizes into HA.

Ajita et al examined the effect of particle size on mesenchymal stem cell proliferation of bioactive glasses.[70] They have shown that the smaller the bioactive glass nanoparticles the greater the amount of cell proliferation. Bi et al studied the effect of bioactive glass microstructure (trabecular, fibrous and oriented) on bone regeneration in a rat calvarial defect model.[71] Twelve weeks after implantation the trabecular bioactive glass formed new bone over 33% of the initial defect, as opposed to 23% and 15% for fibrous and oriented. The new bone formed with trabecular bioactive glass also had a higher average blood vessel area.

1.4 Failure of Graft Materials

1.4.1 Mechanical Failure

Failure of bone grafts is most commonly the result of mechanical issues. Corrosion and degradation of the synthetic material *in vivo* often leads to decreased osteointegration at the tissue:bone graft interface.[72,73] Often the result of this is loosening of the graft in the implant site and subsequent failure. Although metallic biomaterials tend to be made from metals that are thought to be corrosion resistant, crevice and stress corrosion can still occur in load bearing implants.[74]

Mechanical mismatching of the biomaterial to the surrounding natural tissue is frequently a cause of failure.[75,76] If the mechanical properties of the graft are different than the tissue it is replacing then stress shielding, healthy bone resorption, implant loosening and implant fracture can occur (Figure 1.1a).[26-28] Specifically a mismatch of the elastic modulus between natural bone (3-11 GPa for non-load bearing cancellous bone, 15-30 GPa for load bearing cortical bone) and metallic biomaterials (~100 GPa for Ti and ~200 GPa

for CoCr). When a biomaterial is more stiff than the surrounding natural bone, it takes away the mechanical requirements of the natural bone.[77] When the natural bone is exposed less mechanical stress, the bone begins to resorb, weakening the tissue:graft interface and resulting in graft failure.[28]

Ceramics and bioactive glasses are frequently used in non-load bearing applications because when they are used in load bearing applications they are unable to withstand the stresses placed on them, often ending in graft fracture.[22,78] Bioactive glasses are quick to degrade and convert to hydroxyapatite, which is an issue if the healthy tissue is not growing back at a rate appropriate to its degradation. Ceramics, on the other hand, tend to degrade slowly, which leads to slow integration. If the material is subjected to a stress prior to integration, fracture and dislodging can occur.

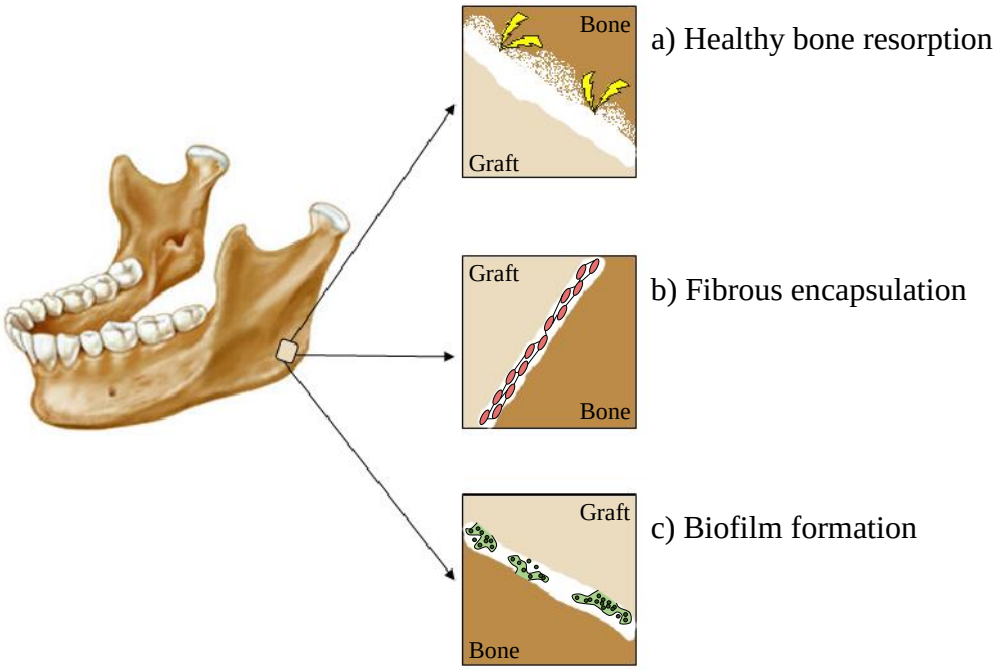

Figure 1.1: Modes of artificial graft failure including a) healthy bone resorption due to mechanical mismatching, b) fibrous encapsulation due to non-specific protein adsorption and c) biofilm formation due to attachment of bacteria and polysaccharide matrix production.

1.4.2 Biological Failure

Biomaterials can also fail as a result of biological issues. The ideal graft would be osteoconductive, osteoinductive, osteogenic and osteointegrative, however current biomaterials are not able to address all four of these characteristic simultaneously, and can result in a variety of bone tissue-graft merger issues.[21,22,30] Two methods of biological failure include fibrous tissue encapsulation and infection.[18,22,79-81]

In the case of fibrous encapsulation, the failure is the result of an immune response that leads to problems with implant integration and eventual implant rejection. Biomaterial implantation results in the non-specific adhesion of proteins and cells.[77,82] The presence of blood at the surgical site leads to the production of fibrin and recruitment of white blood cells.[18] Macrophages then settle on the implant and recruit fibroblasts that create a barrier between the tissue and the biomaterial (Figure 1.1b). Also, the adhesion of fibrinogen to the material, which can cross-link with other proteins, can result in fibrous encapsulation.[77,83-85] If either of these two encapsulation events were to take place, the biological response of the host would lead to significant implant loosening and eventual failure.

Biological failure can also result from infection.[82,86-88] Implant infection generally occurs at the time of implant surgery or early on in the wound healing process.[89,90] Bacteria can adhere to the surface of the implant shortly before or immediately after surgery; since the non-specific adhesion of proteins can form a conditioning film on the material.[91] Once the bacteria are attached they can begin to grow into bacterial colonies known as biofilms, where the bacteria are enclosed in a polysaccharide matrix that protects them from conventional antibiotic treatment (Figure 1.1c).[82,89] Further the bacteria undergo a

phenotype change to sessile organisms which have reduced need for nutrients. While enclosed in the biofilm the bacteria can become more virulent, which becomes an issue when the biofilm releases planktonic cells or biofilm clusters that can spread to other areas of the body.[92,93] Frequently the best approach to eradicate a biofilm infection is to remove the initial implant, treat the infection, then insert a new implant.[81,89,90]

1.5 Current Literature Approaches to Materials Modification

1.5.1 Metal Alloys and Metal Oxides

Metals possess the mechanical strength necessary for load bearing boney applications, but these materials tend to not be biodegradable, do not allow for cell ingrowth, lead to increased fibrous tissue formation and can lead to stress-shielding and healthy tissue weakening. As mentioned previously, different research strategies are being evaluated to help increase the biocompatibility of the materials. Physical modification, including etching and porous material fabrication, of stainless steels, titanium and cobalt-chromium are being investigated to increase *in vitro* bone cell attachment and *in vivo* bone cell in growth. By introducing pores on the metal surfaces, *in vivo* performance is enhanced through increased vascularization, leading to increased nutrient supply, and increased new bone in growth and regeneration.

Chemical modification of the surfaces of metal replacement materials has been more widely performed as a means to improve biocompatibility of metal oxides. Stainless steel alloys have been chemically modified with antibiotics that operate synergistically to reduce bacterial colonization for up to 48 hours.[94] The surface of the nitinol alloy has been modified to reduce its corrosion subsequently reducing the amount of metal ions that are

released into the body that can cause cytotoxic and genotoxic effects.[95] Through the implementation of these types of interfacial modifications the surface properties of a variety of metals and alloys can be improved to increase their efficacy and applicability.

To overcome the issues associated with mechanical mismatching and failure associated with stress shielding there has been work examining biodegradable metal and alloys, including magnesium and iron.[96] Using these mechanically strong, but degradable metals, provides the temporary mechanical support with the ability to degrade in a physiological environment while allowing for new bone regeneration.

1.5.2 Composite Materials

Composite materials aim to combine the best attributes of one material with those of another material, to design a synthetic graft material with better function than any of the parts individually. Composites consisting of hydroxyapatite and other bioactive ceramic coatings on metals have shown promise by providing the bioactive properties of the coating with the enhanced mechanical properties of the metal beneath the coating.

Chen and coworkers created a composite consisting of a titanium core with a calcium coating. Their material was shown to induce apatite formation on the surface of the material when submerged in simulated body fluid.[97] Gu et al produced a composite material that consisted of Ti-6Al-4V plasma-sprayed with HA. They also demonstrated the formation of a carbonate-apatite layer after a 2 week soaking in simulated body fluid.[98]

Composites of HA and collagen fibers have also been investigated. Natural bone is approximately 60% HA and 40% collagen by dry mass, so a composite of these materials may closely mimic natural bone. Du et al and Wu et al both demonstrated that a collagen

and HA composite produced mineralized bone in 21 days.[99] Rovira and coworkers showed that an HA-collagen-elastin composite produced mineralized bone in 15 days.[99]

1.5.3 Biomolecule Functionalization

Another approach to improving current biomaterials is interfacial modification with an assortment of active biomolecules. Molecules of interest include antibiotics to limit bacterial attachment and infection, cell adhesion peptides to promote specific cell adhesion improving osteoconductivity, and other proteins that have been shown to induce bone formation and vascularization. Although these modifications utilize different types of biomolecules, they all aim to improve the surface characteristics of the biomaterials and reduce the chance for implant failure.

The localized delivery of peptides and proteins on the biomaterial would be an advantageous approach to increasing biocompatibility and the osteoconductive properties of the material. Previous work has shown that modifying biomaterials with osteoblast adhesion peptides and bone morphogenetic proteins results in better bone cell performance and new bone formation.[58,100] Several binding domains from the extracellular matrix peptides and proteins have been revealed and incorporated into short peptides. The most widely used is the arginine-glycine-aspartic acid (RGD) sequence.[16,100] Cook et al first showed enhanced cell spreading on RGD modified poly(lactic acid-co-lysine) polymers.[101] Since that time, RGD modified materials have been used to increase fibroblast adhesion and spreading, endothelial cell attachment and osteoblast attachment on orthopaedic materials.[36,102,103] Another example is the FDA approved InFUSE® Bone Graft that is used in primarily in spinal surgery. This device is a composite synthetic graft that is a titanium

cage with collagen located on the interior. The collagen is used to deliver recombinant human bone morphogenetic protein-2 (BMP-2). This protein has been shown to induce new bone growth by attracting osteoblast cells to the delivery site of the BMP-2.[104]

The delivery of active antimicrobials is also a critical part of implant success. Research has been conducted on antimicrobial surfaces that are (1) non-fouling (surfaces that avoid protein adsorption and cell adhesion) (2) colonized with non-pathogenic bacteria (occupy the surface to prevent attachment of pathogenic bacteria) (3) modified with biocidal substances (non-antibiotic molecules that have shown activity, including silver, quaternary ammonium compounds and nitric oxide) and (4) modified with antibiotics (vancomycin, tobramycin, ampicillin, gentamicin, etc.).[105] Zhao et al and Subramani et al have successfully immobilized vancomycin to titanium and it was proven to be bactericidal to *Staphylococcus aureus* (*S. aureus*) and *Staphylococcus epidermidis* (*S. epidermidis*).[106,107] Palchesko et al linked vancomycin to CaAlO and demonstrated its efficacy against *S. aureus*.[35,108] However the utility of antibiotic coatings is dependent upon the activity of the linked antibiotic and the growing concern over the risk of development of antibiotic resistance in bacteria.

For these reasons, the focus has shifted for some to using antimicrobial peptides (AMP). These antimicrobials have broad spectrum efficacy, minimize the development of bacterial resistance and maintain effectiveness, even through sterilization.[109-111] Glinel et al, Haynie et al, Humblot et al and Bagheri et al have all linked the AMP magainin I to a variety of materials through a variety of approaches.[105] Despite different approaches the AMP was shown to be active against bacteria including, *E. coli*, *S. aureus*, *Pseudomonas aeruginosa* (*P. aeruginosa*) and *Listeria ivanovii*.[105] Wilcox et al and Chen et al have linked

melimine to contact lenses and glass cover slips and shown its activity against *S. aureus* and *P. aeruginosa*.[105] Finally, Gabriel and coworkers immobilized cathelin LL37 to silanized titanium surfaces and demonstrated activity against *E. coli*.[105]

1.6 Summary

Although the autograft remains the optimal bone graft material due to its osteogenic properties, the growing concerns over the source of autologous bone and the risk of infection is driving the need to develop a better synthetic material. Currently, most synthetic materials, including metals, alloys, ceramics, bioactive glasses and composite materials, are not able to address all of the mechanical and biological stresses that will be places on them in an *in vivo* setting. Although significant progress has been made through the creation of composite materials and the tuning of interfacial properties through organic functionalization with biomolecules, these synthetic materials still underachieve when compared to the autograft. Therefore, continuing research on the development of synthetic materials is necessary before the use of the autograft can be phased out and eliminated.

1.7 Research Approach

Artificial bone graft materials must meet several requirements. They should be osteoconductive, osteoinductive, osteogenic and osteointegrative, all while being mechanically similar to the surrounding natural tissue and being resistant to bacterial attachment and colonization. Conferring all of these attributes into a single material has been a formidable task thus far.

This project aimed to modify the composition of the previously, physically optimized CaAlO ceramic to enhance osteoblast response and to further develop the antimicrobial functionalization of the composite material. A composite CaAlO material was formed that included the osteoconductive and osteoinductive HA. As has been shown in previous literature, the goal was to increase the osteoconductivity and osteoinductivity of the CaAlO through this incorporation. Composites containing different percentages of HA were cast and evaluated to find the percentages that were mechanically similar to natural non-load bearing bone, and resulted in the greatest increase in osteoblast attachment and proliferation.

Further, the previously designed CaAlO material required a five-step reaction sequence to immobilize active antibiotic, vancomycin. In this project, the highly efficient, single step alkene-thiol click reaction was used to link the antimicrobial peptide Inverso-CysHHC10. This linkage presents an improvement over the previous approach in multiple regards. First, the linkage approach is shorter, more efficient and introduces the synthetic material to less chemicals, as alkene-thiol click reactions can be performed without initiators. Secondly, the linking of an antimicrobial peptide is advantageous over antibiotics because antimicrobial peptides have broad spectrum efficacy, their mode of action does not rely on bacteria growth and division and the risk of development of bacterial resistance to antimicrobial peptides is limited.

This work evaluated the mechanical similarity of the developed composites to non-load bearing cancellous bone, examined the increased osteoconductivity of the composite materials and determined the loading, stability and efficacy of the linked Inverso-CysHHC10 antimicrobial peptide.

1.8 References

1. Jahangir, A. A.; Nenley, R. M.; Mehta, S.; Sharan, A. Bone-graft substitutes in orthopaedic surgery. *AAOS Now* **2008**.

2. Gustilo, R.; Anderson, J. Prevention of infection in the treatment of one thousand and twenty-five open fractures of long bones: Retrospective and prospective analyses. *J. Bone Joint Surg* **1976**, *58*, 453-458.

3. Govender, S.; Csimma, C.; Genant, H. K.; Valentin-Opran, A.; Amit, Y.; Arbel, R.; Aro, H.; Atar, D.; Bishay, M.; Börner, M. G. Recombinant human bone morphogenetic protein-2 for treatment of open tibial fractures. *J. Bone Joint Surg* **2002**, *84*, 2123-2134.

4. Bridwell, K. H.; Sedgewick, T. A.; O'Brien, M. F.; Lenke, L. G.; Baldus, C. The role of fusion and instrumentation in the treatment of degenerative spondylolisthesis with spinal stenosis. *J. Spinal Disord Tech* **1993**, *6*, 461-472.

5. Wood, G. W.; Boyd, R. J.; Carothers, T. A.; Mansfield, F. L.; Rechtine, G. R.; Rozen, M. J.; Sutterlin III, C. E. The effect of pedicle screw/plate fixation on lumbar/lumbosacral autogenous bone graft fusions in patients with degenerative disc disease. *Spine* **1995**, *20*, 819-830.

6. Blackley, H.; Wunder, J.; Davis, A.; White, L.; Kandel, R.; Bell, R. Treatment of giant-cell tumors of long bones with curettage and bone-grafting. *J. Bone Joint Surg* **1999**, *81*, 811-820.

7. Laurencin, C.; Khan, Y.; El-Amin, S. F. Bone graft substitutes. *Expert Rev. Med. Devic.* **2006**, *3*, 49-57.

8. Misch, C. M. Autogenous bone: Is it still the gold standard?. *Implant dent.* **2010**, *19*, 361.

9. Giannoudis, P. V.; Dinopoulos, H.; Tsiridis, E. Bone substitutes: An update. *Injury* **2005**, *36*, S20-S27.

10. Kao, S. T.; Scott, D. D. A review of bone substitutes. *Oral Maxillofac. Surg. Clin. North Am.* **2007**, *19*, 513-521.

11. Urban, R. M.; Turner, T. M.; Hall, D. J.; Inoue, N.; Gitelis, S. Increased bone formation using calcium sulfate-calcium phosphate composite graft. *Clin. Orthop. Relat. R.* **2007**, *459*, 110-117.

12. Chan, C. K.; Kumar, T. S.; Liao, S.; Murugan, R.; Ngiam, M.; Ramakrishnan, S. Biomimetic nanocomposites for bone graft applications. *Nanomedicine* **2006**, *1*, 177-188.

13. Levi, B.; James, A. W.; Nelson, E. R.; Vistnes, D.; Wu, B.; Lee, M.; Gupta, A.; Longaker, M. T. Human adipose derived stromal cells heal critical size mouse calvarial defects. *PLoS ONE* **2010**, *5*, e11177.

14. Dupont, K. M.; Sharma, K.; Stevens, H. Y.; Boerckel, J. D.; García, A. J.; Guldberg, R. E. Human stem cell delivery for treatment of large segmental bone defects. *Proc. Natl. Acad. Sci. U.S.A.* **2010**, *107*, 3305-3310.

15. Chou, J.; Hao, J.; Kuroda, S.; Ben-Nissan, B.; Milthopre, B.; Otsuka, M. Bone regeneration of calvarial defect using marine calcareous-derived beta-tricalcium phosphate macrospheres. *J. Tissue Eng.* **2014**, *5*, 1-7.

16. Miljkovic, N. D.; Cooper, G. M.; Hott, S. L.; DiSalle, B. F.; Gawalt, E. S.; Smith, D. M.; McGowan, K.; Marra, K. G. Calcium aluminate, RGD-modified calcium aluminate, and β-tricalcium phosphate implants in a calvarial defect. *J. Craniofac. Surg.* **2009**, *20*, 1538-1543.

17. Bigi, A.; Incerti, A.; Roveri, N.; Foresti-Serantoni, E.; Mongiorgi, R.; di Sanseverino, L. R.; Krajewski, A.; Ravaglioli, A. Characterization of synthetic apatites for bioceramic implants. *Biomaterials* **1980**, *1*, 140-144.

18. Duan, K.; Wang, R. Surface modifications of bone implants through wet chemistry. *J. Mater. Chem.* **2006**, *16*, 2309-2321.

19. Herath, H.; Di Silvio, L.; Evans, J. Porous hydroxyapatite ceramics for tissue engineering. *J. Appl. Biomater. Biom.* **2004**, *3*, 192-198.

20. Arciola, C. R.; Campoccia, D.; Speziale, P.; Montanaro, L.; Costerton, J. W. Biofilm formation in Staphylococcus implant infections. A review of molecular mechanisms and implications for biofilm-resistant materials. *Biomaterials* **2012**, *33*, 5967-5982.

21. Moore, W. R.; Graves, S. E.; Bain, G. I. Synthetic bone graft substitutes. *Aust. N. Z. J. Surg.* **2001**, *71*, 354-361.

22. Ryan, G.; Pandit, A.; Apatsidis, D. P. Fabrication methods of porous metals for use in orthopaedic applications. *Biomaterials* **2006**, *27*, 2651-2670.

23. Charriere, E.; Terrazzoni, S.; Pittet, C.; Mordasini, P.; Dutoit, M.; Lemaıtre, J.; Zysset, P. Mechanical characterization of brushite and hydroxyapatite cements. *Biomaterials* **2001**, *22*, 2937-2945.

24. Cvijović-Alagić, I.; Cvijović, Z.; Mitrović, S.; Panić, V.; Rakin, M. Wear and corrosion behaviour of Ti–13Nb–13Zr and Ti–6Al–4V alloys in simulated physiological solution. *Corros. Sci.* **2011**, *53*, 796-808.

25. Katti, K. S. Biomaterials in total joint replacement. *Colloids Surf., B* **2004**, *39*, 133-142.

26. Brown, C.; Knickerbocker, W. Radiologic studies in the investigation of the causes of total hip replacement failure. *J. Can. Assoc. Radiol.* **1973**, *24*, 245-253.

27. Buford, A.; Goswami, T. Review of wear mechanisms in hip implants: Paper I–General. *Mater. Des.* **2004**, *25*, 385-393.

28. Siopack, J.; Jergesen, H. Total hip arthroplasty. *West. J. Med.* **1995**, *162*, 243-249.

29. Misch, C. E. *Dental Implant Prosthetics*, 2nd ed; Elsevier: Missouri, 2005.

30. Brems, J. J. Role of bone graft substitutes for glenoid bone defects. *J. Shoulder Elb. Surg.* **2007**, *16*, S282-S285.

31. Kaplan, F.; Hayes, W.; Keaveny, T.; Boskey, A.; Einhorn, T.; Iannotti, J. Form and function of bone. *Orthop. Basic Sci.* **1994**, 127-185.

32. Karageorgiou, V.; Kaplan, D. Porosity of 3D biomaterial scaffolds and osteogenesis. *Biomaterials* **2005**, *26*, 5474-5491.

33. Knabe, C.; Koch, C.; Rack, A.; Stiller, M. Effect of β-tricalcium phosphate particles with varying porosity on osteogenesis after sinus floor augmentation in humans. *Biomaterials* **2008**, *29*, 2249-2258.

34. Chang, B. S.; Hong, K. S.; Youn, H. J.; Ryu, H. S.; Chung, S. S.; Park, K. W. Osteoconduction at porous hydroxyapatite with various pore configurations. *Biomaterials* **2000**, *21*, 1291-1298.

35. Palchesko, R. N.; Buckholtz, G. A.; Romeo, J. D.; Gawalt, E. S. Co-immobilization of active antibiotics and cell adhesion peptides on calcium based biomaterials. *Mater. Sci. Eng., C* **2014**, *40*, 398-406.

36. Palchesko, R. N.; Romeo, J. D.; McGowan, K. A.; Gawalt, E. S. Increased osteoblast adhesion on physically optimized KRSR modified calcium aluminate. *J. Biomed. Mater. Res., Part A* **2012**, *100*, 1229-1238.

37. Clafshenkel, W. P.; Rutkowski, J. L.; Palchesko, R. N.; Romeo, J. D.; McGowan, K. A.; Gawalt, E. S.; Witt-Enderby, P. A. A novel calcium aluminate-melatonin scaffold enhances bone regeneration within a calvarial defect. *J. Pineal Res.* **2012**, *53*, 206-218.

38. Pino-Mínguez, J.; Jorge-Mora, A.; Couceiro-Otero, R.; García-Santiago, C. Study of the viability and adhesion of osteoblast cells to bone cements mixed with hydroxyapatite at different concentrations to use in vertebral augmentation techniques. *Rev. Esp. Cir. Ortop. Traumatol.* **2015**, *59*, 122-128.

39. Rogers, G. F.; Greene, A. K. Autogenous bone graft: Basic science and clinical implications. *J. Craniofac. Surg.* **2012**, *23*, 323-327.

40. Zimmermann, G.; Moghaddam, A. Allograft bone matrix versus synthetic bone graft substitutes. *Injury* **2011**, *42*, S16-S21.

41. Kuremsky, M. A.; Schaller, T. M.; Hall, C. C.; Roehr, B. A.; Masonis, J. L. Comparison of autograft vs allograft in opening-wedge high tibial osteotomy. *J. Arthroplasty* **2010**, *25*, 951-957.

42. Gibson, S.; McLeod, I.; Wardlaw, D.; Urbaniak, S. Allograft versus autograft in instrumented posterolateral lumbar spinal fusion: A randomized control trial. *Spine* **2002**, *27*, 1599-1603.

43. Woo, K. M.; Seo, J.; Zhang, R.; Ma, P. X. Suppression of apoptosis by enhanced protein adsorption on polymer/hydroxyapatite composite scaffolds. *Biomaterials* **2007**, *28*, 2622-2630.

44. Grover, V.; Kapoor, A.; Malhotra, R.; Sachdeva, S. Bone allografts: A review of safety and efficacy. *Indian J. Dent. Res.* **2011**, *22*, 496.

45. Mikhael, M. M.; Huddleston, P. M.; Zobitz, M. E.; Chen, Q.; Zhao, K. D.; An, K. N. Mechanical strength of bone allografts subjected to chemical sterilization and other terminal processing methods. *J. Biomech.* **2008**, *41*, 2816-2820.

46. Buck, B.; Malinin, T. I. Human bone and tissue allografts: Preparation and safety. *Clin. Orthop. Relat. Res.* **1994**, *303*, 8-17.

47. Malloy, K. M.; Hilibrand, A. S. Autograft versus allograft in degenerative cervical disease. *Clin. Orthop. Relat. Res.* **2002**, *394*, 27-38.

48. Kainer, M. A.; Linden, J. V.; Whaley, D. N.; Holmes, H. T.; Jarvis, W. R.; Jernigan, D. B.; Archibald, L. K. Clostridium infections associated with musculoskeletal-tissue allografts. *N. Engl. J. Med.* **2004**, *350*, 2564-2571.

49. Shutkin, N. M. Homologous-serum hepatitis following the use of refrigerated bone-bank bone. *J. Bone Joint Surg. Am.* **1954**, 160-162.

50. Mankin, H. J.; Gebhardt, M. C.; Jennings, L. C.; Springfield, D. S.; Tomford, W. W. Long-term results of allograft replacement in the management of bone tumors. *Clin. Orthop. Relat. Res.* **1996**, *324*, 86-97.

51. Fändrich, F.; Lin, X.; Chai, G. X.; Schulze, M.; Ganten, D.; Bader, M.; Holle, J.; Huang, D. S.; Parwaresch, R.; Zavazava, N. Preimplantation-stage stem cells induce long-term allogeneic graft acceptance without supplementary host conditioning. *Nat. Med.* **2002**, *8*, 171-178.

52. Hao, L.; Dadbakhsh, S.; Seaman, O.; Felstead, M. Selective laser melting of a stainless steel and hydroxyapatite composite for load-bearing implant development. *J. Mater. Process. Tech.* **2009**, *209*, 5793-5801.

53. Pilliar, R.; Cameron, H.; Welsh, R.; Binnington, A. Radiographic and morphologic studies of load-bearing porous-surfaced structured implants. *Clin. Orthop. Relat. Res.* **1981**, *156*, 249-257.

54. Hao, L.; Lawrence, J.; Phua, Y.; Chian, K.; Lim, G.; Zheng, H. Enhanced human osteoblast cell adhesion and proliferation on 316 LS stainless steel by means of CO_2 laser surface treatment. *J. Biomed. Mater. Res., Part B* **2005**, *73*, 148-156.

55. Geetha, M.; Singh, A.; Asokamani, R.; Gogia, A. Ti based biomaterials, the ultimate choice for orthopaedic implants–A review. *Prog. Mater. Sci.* **2009**, *54*, 397-425.

56. Lincks, J.; Boyan, B.; Blanchard, C.; Lohmann, C.; Liu, Y.; Cochran, D.; Dean, D.; Schwartz, Z. Response of MG63 osteoblast-like cells to titanium and titanium alloy is dependent on surface roughness and composition. *Biomaterials* **1998**, *19*, 2219-2232.

57. Puckett, S.; Pareta, R.; Webster, T. J. Nano rough micron patterned titanium for directing osteoblast morphology and adhesion. *Int. J. Nanomed.* **2008**, *3*, 229-241.

58. Poh, C. K.; Shi, Z.; Tan, X. W.; Liang, Z. C.; Foo, X. M.; Tan, H. C.; Neoh, K. G.; Wang, W. Cobalt chromium alloy with immobilized BMP peptide for enhanced bone growth. *J. Orthop. Res.* **2011**, *29*, 1424-1430.

59. Lööf, J. Calcium-aluminate as biomaterial: Synthesis, design and evaluation. Ph.D. Thesis, Uppsala University, Uppsala, Sweden, 2008.

60. Engqvist, H.; Schultz-Walz, J. E.; Loof, J.; Botton, G. A.; Mayer, D.; Phaneuf, M. W.; Ahnfelt, N. O.; Hermansson, L. Chemical and biological integration of a mouldable bioactive ceramic material capable of forming apatite in vivo in teeth. *Biomaterials* **2004**, *25*, 2781-2787.

61. Engqvist, H.; Persson, T.; Lööf, J.; Faris, A.; Hermansson, L. Chemical stability of a novel bioceramic for stabilisation of vertebral compression fractures. *Trends Biomater. Artif. Organs* **2008**, *21*, 98-106.

62. Jarcho, M. Calcium phosphate ceramics as hard tissue prosthetics. *Clin. Orthop. Relat. Res.* **1981**, *157*, 259-278.

63. LeGeros, R. Z. Properties of osteoconductive biomaterials: Calcium phosphates. *Clin. Orthop. Relat. Res.* **2002**, *395*, 81-98.

64. Theiss, F.; Apelt, D.; Brand, B.; Kutter, A.; Zlinszky, K.; Bohner, M.; Matter, S.; Frei, C.; Auer, J. A.; Von Rechenberg, B. Biocompatibility and resorption of a brushite calcium phosphate cement. *Biomaterials* **2005**, *26*, 4383-4394.

65. Yamada, S.; Heymann, D.; Bouler, J. M.; Daculsi, G. Osteoclastic resorption of calcium phosphate ceramics with different hydroxyapatite/β-tricalcium phosphate ratios. *Biomaterials* **1997**, *18*, 1037-1041.

66. Chai, F.; Hornez, J. C.; Blanchemain, N.; Neut, C.; Descamps, M.; Hildebrand, H. Antibacterial activation of hydroxyapatite (HA) with controlled porosity by different antibiotics. *Biomol. Eng.* **2007**, *24*, 510-514.

67. Murugan, R.; Ramakrishna, S. Coupling of therapeutic molecules onto surface modified coralline hydroxyapatite. *Biomaterials* **2004**, *25*, 3073-3080.

68. Murugan, R.; Rao, K. P. Controlled release of antibiotic from surface modified coralline hydroxyapatite. *Trends Biomater. Artif. Organs* **2002**, *16*, 43-45.

69. Rahaman, M. N.; Day, D. E.; Bal, B. S.; Fu, Q.; Jung, S. B.; Bonewald, L. F.; Tomsia, A. P. Bioactive glass in tissue engineering. *Acta Biomater.* **2011**, *7*, 2355-2373.

70. Ajita, J.; Saravanan, S.; Selvamurugan, N. Effect of size of bioactive glass nanoparticles on mesenchymal stem cell proliferation for dental and orthopedic applications. *Mater. Sci. Eng., C* **2015**, *53*, 142-149.

71. Bi, L.; Rahaman, M. N.; Day, D. E.; Brown, Z.; Samujh, C.; Liu, X.; Mohammadkhah, A.; Dusevich, V.; Eick, J. D.; Bonewald, L. F. Effect of bioactive borate glass microstructure on bone regeneration, angiogenesis, and hydroxyapatite conversion in a rat calvarial defect model. *Acta Biomater.* **2013**, *9*, 8015-8026.

72. Jacobs, J. J.; Gilbert, J. L.; Urban, R. M. Current concepts review-Corrosion of metal orthopaedic implants. *J. Bone Joint Surg.* **1998**, *80*, 268-282.

73. Ulrich, S. D.; Seyler, T. M.; Bennett, D.; Delanois, R. E.; Saleh, K. J.; Thongtrangan, I.; Kuskowski, M.; Cheng, E. Y.; Sharkey, P. F.; Parvizi, J. Total hip arthroplasties: What are the reasons for revision?. *Int. Orthop.* **2008**, *32*, 597-604.

74. Kamachimudali, U.; Sridhar, T.; Raj, B., Corrosion of bio implants. *Sadhana* **2003**, *28*, 601-637.

75. Li, X.; Hao, Q.; Shi, Y.; Lei, Y.; Marquis, G. Influence of mechanical mismatching on the failure of welded joints by void nucleation and coalescence. *Int. J. Pressure Vessels Piping* **2003**, *80*, 647-654.

76. Hench, L. L. Biomaterials: A forecast for the future. *Biomaterials* **1998**, *19*, 1419-1423.

77. Ratner, B.; Hoffman, A.; Schoen, F.; Lemons, J. *Biomaterials Science: An Introduction to Materials in Medicine*, 3rd ed; Elsevier: London, 2004.

78. Ambard, A. J.; Mueninghoff, L. Calcium phosphate cement: Review of mechanical and biological properties. *J. Prosthodont.* **2006**, *15*, 321-328.

79. McKay, W. F.; Peckham, S. M.; Badura, J. M. A comprehensive clinical review of recombinant human bone morphogenetic protein-2 (INFUSE® Bone Graft). *Int. Orthop.* **2007**, *31*, 729-734.

80. Ramage, G.; Martínez, J. P.; López-Ribot, J. L. Candida biofilms on implanted biomaterials: A clinically significant problem. *FEMS Yeast Res.* **2006**, *6*, 979-986.

81. Campoccia, D.; Montanaro, L.; Arciola, C. R. A review of the clinical implications of anti-infective biomaterials and infection-resistant surfaces. *Biomaterials* **2013**, *34*, 8018-8029.

82. Childs, S. G. Biofilm: The pathogenesis of slime glycocalyx. *Orthop. Nurs.* **2008**, *27*, 361-369.

83. Adamczyk, Z.; Barbasz, J.; Cieśla, M. Mechanisms of fibrinogen adsorption at solid substrates. *Langmuir* **2011**, *27*, 6868-6878.

84. Fuss, C.; Palmaz, J. C.; Sprague, E. A. Fibrinogen: Structure, function, and surface interactions. *J. Vasc. Interv. Radiol.* **2001**, *12*, 677-682.

85. Siegismund, D.; Keller, T. F.; Jandt, K. D.; Rettenmayr, M. Fibrinogen adsorption on biomaterials–A numerical study. *Macromol. Biosci.* **2010**, *10*, 1216-1223.

86. Del Pozo, J. L.; Patel, R. Infection associated with prosthetic joints. *N. Engl. J. Med.* **2009**, *361*, 787-794.

87. Trampuz, A.; Widmer, A. F. Infections associated with orthopedic implants. *Curr. Opin. Infect. Dis.* **2006**, *19*, 349-356.

88. Zimmerli, W.; Trampuz, A.; Ochsner, P. E. Prosthetic-joint infections. *N. Engl. J. Med.* **2004**, *351*, 1645-1654.

89. Katsikogianni, M.; Missirlis, Y. Concise review of mechanisms of bacterial adhesion to biomaterials and of techniques used in estimating bacteria-material interactions. *Eur. Cell. Mater.* **2004**, *8*, 37-57.

90. Sampedro, M. F.; Patel, R. Infections associated with long-term prosthetic devices. *Infect. Dis. Clin. N. Am.* **2007**, *21*, 785-819.

91. Banerjee, I.; Pangule, R. C.; Kane, R. S. Antifouling coatings: Recent developments in the design of surfaces that prevent fouling by proteins, bacteria, and marine organisms. *Adv. Mater.* **2011**, *23*, 690-718.

92. Hall-Stoodley, L.; Stoodley, P. Biofilm formation and dispersal and the transmission of human pathogens. *Trends Microbiol.* **2005**, *13*, 7-10.

93. Stoodley, P.; Hall-Stoodley, L.; Lappin-Scott, H. M. Detachment, surface migration, and other dynamic behavior in bacterial biofilms revealed by digital time-lapse imaging. *Methods Enzymol.* **2001**, *337*, 306-319.

94. Kruszewski, K. M.; Nistico, L.; Longwell, M. J.; Hynes, M. J.; Maurer, J. A.; Hall-Stoodley, L.; Gawalt, E. S. Reducing Staphylococcus aureus biofilm formation on stainless steel 316L using functionalized self-assembled monolayers. *Mater. Sci. Eng., C* **2013**, *33*, 2059-2069.

95. Bansiddhi, A.; Sargeant, T.; Stupp, S.; Dunand, D. Porous NiTi for bone implants: A review. *Acta Biomater.* **2008**, *4*, 773-782.

96. Staiger, M. P.; Pietak, A. M.; Huadmai, J.; Dias, G. Magnesium and its alloys as orthopedic biomaterials: A review. *Biomaterials* **2006**, *27*, 1728-1734.

97. Chen, X. B.; Li, Y.-C.; Du Plessis, J.; Hodgson, P. D.; Wen, C. e. Influence of calcium ion deposition on apatite-inducing ability of porous titanium for biomedical applications. *Acta Biomater.* **2009**, *5*, 1808-1820.

98. Gu, Y.; Khor, K.; Cheang, P. In vitro studies of plasma-sprayed hydroxyapatite/Ti-6Al-4V composite coatings in simulated body fluid (SBF). *Biomaterials* **2003**, *24*, 1603-1611.

99. Wahl, D.; Czernuszka, J. Collagen-hydroxyapatite composites for hard tissue repair. *Eur. Cell. Mater.* **2006**, *11*, 43-56.

100. Dee, K. C.; Andersen, T. T.; Bizios, R. Design and function of novel osteoblast-adhesive peptides for chemical modification of biomaterials. *J. Biomed. Mater. Res.* **1998**, *40*, 371-377.

101. Cook, A. D.; Hrkach, J. S.; Gao, N. N.; Johnson, I. M.; Pajvani, U. B.; Cannizzaro, S. M.; Langer, R. Characterization and development of RGD-peptide-modified poly (lactic acid-co-lysine) as an interactive, resorbable biomaterial. *J. Biomed. Mater. Res.* **1997**, *35*, 513-523.

102. Hersel, U.; Dahmen, C.; Kessler, H. RGD modified polymers: Biomaterials for stimulated cell adhesion and beyond. *Biomaterials* **2003**, *24*, 4385-4415.

103. Walluscheck, K.; Steinhoff, G.; Kelm, S.; Haverich, A. Improved endothelial cell attachment on ePTFE vascular grafts pretreated with synthetic RGD-containing peptides. *Eur. J. Vasc. Endovasc.* **1996**, *12*, 321-330.

104. Riew, K.; Wright, N.; Cheng, S. L.; Avioli, L.; Lou, J. Induction of bone formation using a recombinant adenoviral vector carrying the human BMP-2 gene in a rabbit spinal fusion model. *Calcif. Tissue Int.* **1998**, *63*, 357-360.

105. Costa, F.; Carvalho, I. F.; Montelaro, R. C.; Gomes, P.; Martins, M. C. L. Covalent immobilization of antimicrobial peptides (AMPs) onto biomaterial surfaces. *Acta Biomater.* **2011**, *7*, 1431-1440.

106. Subramani, K., Titanium surface modification techniques for implant fabrication–From microscale to the nanoscale. *J. Biomimetics, Biomater., Tissue Eng.* **2010**, *5*, 39-56.

107. Zhao, L.; Chu, P. K.; Zhang, Y.; Wu, Z. Antibacterial coatings on titanium implants. *J. Biomed. Mater. Res., Part B* **2009**, *91*, 470-480.

108. Palchesko, R. N.; McGowan, K. A.; Gawalt, E. S. Surface immobilization of active vancomycin on calcium aluminum oxide. *Mater. Sci. Eng., C* **2011**, *31*, 637-642.

109. Brogden, K. A. Antimicrobial peptides: Pore formers or metabolic inhibitors in bacteria?. *Nat. Rev. Microbiol.* **2005**, *3*, 238-250.

110. Peschel, A.; Sahl, H. G. The co-evolution of host cationic antimicrobial peptides and microbial resistance. *Nat. Rev. Microbiol.* **2006**, *4*, 529-536.

111. Wimley, W. C.; Hristova, K. Antimicrobial peptides: Successes, challenges and unanswered questions. *J. Membr. Biol.* **2011**, *239*, 27-34.

Chapter 2: Physical Characterization of Composite CaAlO:HA

2.1 Introduction

Calcium aluminum oxide materials were previously utilized as bone graft materials and showed some promise in initial work, but they had since been discounted because of concerns over biocompatibility.[1-6] However, *in vivo* work has shown that the calcium aluminum oxide materials do not illicit an inflammatory response demonstrating the biotolerability of the CaAlO material.[7-11] More recent work has further demonstrated that through covalent chemical modification of CaAlO the biocompatibility of these materials can be increased and biological applicability can be tuned.[7,12-14] However, other work has demonstrated that a different class of calcium ceramics, calcium phosphates, are biocompatible and are intriguing options for synthetic bone graft materials.[8,15-17] Composites of CaAlO and calcium phosphates, namely hydroxyapatite, were examined in this project because the materials are mechanically strong and through the introduction of the biocompatible HA, the biocompatibility of the CaAlO based material may be increased.

CaAlO casts are formed through a three-step mechanism.[18,19] First the surface of the CaAlO aggregates are hydroxylated and they begin to dissolve until the saturation limit has been reached (dissolution).[18,19] After dissolution the nuclei continue to grow in critical size and quantity, known as the nucleation phase.[18,19] Finally, the precipitation phase occurs where the hydrates precipitate out of the solution.[18,19] This process continues until all of the dissolved CaAlO has been precipitated. During the hydration process the phases bind together and interlock with one another, increasing the mechanical strength and forming the cast CaAlO.

In a previous study, a variety of different ratios of CaAlO aggregates within casts was examined to physically optimize the material.[14] The outcome was a ratio that produced CaAlO materials that were optimized for porosity, strength and degradability.[14] Despite the optimization of the physical properties of the CaAlO material, the study revealed that the material was not optimized for its biological performance, and required total interfacial modification for biological activity.[14]

HA is formed through the hydration of calcium phosphate with phosphoric acid (Scheme 2.1). In the first step of the formation of HA, the $Ca_3(PO_4)_2$ reacts with protons in solution to from the HA precursor brushite, $CaHPO_4$.[20] The brushite molecules then react with water molecules and generate the solid HA phase.[20] The formed solid HA molecules are not interlocked like those in the CaAlO material, therefore the HA is mechanically weak. To add mechanical strength to the HA, it can be sintered which fuses the powder together by heating and compacting without reaching the melting point of the material.[21-24]

$$Ca_3(PO_4)_2 + 2\ H^+ \longrightarrow 2\ CaHPO_4 + Ca^{2+}$$

$$5\ CaHPO_4 + H_2O \longrightarrow Ca_5(PO_4)_3(OH) + 2\ H_3PO_4$$

Scheme 2.1: Proposed reactions for the synthesis of hydroxyapatite from calcium phosphate tribasic.

Many prior studies have examined HA materials for their applicability as synthetic bone graft materials.[8,25-27] These studies consistently demonstrate that biomaterials intended for boney applications often have increased biological activity when HA is present in the material.[8,27]

In casting a composite of CaAlO and HA, the mechanical integrity of the material must be evaluated because CaAlO derives strength from through the hydration process and HA derives strength from sintering after hydration.[18-20] If the post hydration treatment effects the mechanical integrity of the composite, then it must be determined which procedure is more appropriate for casting materials relevant to natural bone. By using the previously established methods for casting CaAlO and HA, to create a method to cast composite CaAlO:HA, the physical attributes of the new CaAlO:HA material can be physically characterized.

2.2 Materials and Methods

2.2.1 Materials

Calcium aluminum oxide (CaAlO) was supplied by Westmoreland Advanced Materials. Calcium phosphate tribasic ($Ca_3(PO_4)_2$) and phosphate buffered saline (PBS, $MgCl_2$ and $CaCl_2$ free) were purchased from Sigma-Aldrich. Phosphoric acid (H_3PO_4) was purchased from Fisher Scientific (Certified ACS). All materials and chemicals were used as received unless otherwise noted.

2.2.2 Casting Calcium-Based Ceramics

2.2.2.1 Calcium Aluminum Oxide

Calcium aluminum oxide discs were prepared using a room temperature casting (20°C) of different sized aggregates of CaAlO containing the two phases, $CaAl_2O_4$ and $CaAl_4O_7$. The aggregate sizes utilized were -30+60, -60 and -200, in a 1:1:2 ratio, that are

previously separated using a sifting process that sorts out the particles based on their mesh size (Figure 2.1).[13,14] The appropriate mass of each CaAlO aggregate size were thoroughly dry mixed at room temperature to ensure even particle distribution. Distilled deionized water (ddH_2O) was then added to the aggregate powders at an amount equal to 0.3 mL of ddH_2O per gram of CaAlO. The paste was allowed to thicken at room temperature for 10 minutes. Afterwards, the CaAlO was poured into either: 1) a 6x2 mm (diameter x height) cylindrical disc mold or a 2) 17.75x2.5x1.67 cm (length x width x height) rectangular prism mold, where it was allowed to set for four hours. The CaAlO casts were rehydrated in their molds with ddH_2O, and allowed to set overnight. The next day the casts were hydrated in their molds using ddH_2O, then allowed to set for the night. The following day casts were removed from their molds and immersed into ddH_2O for 24 hours to ensure hydration of the material.

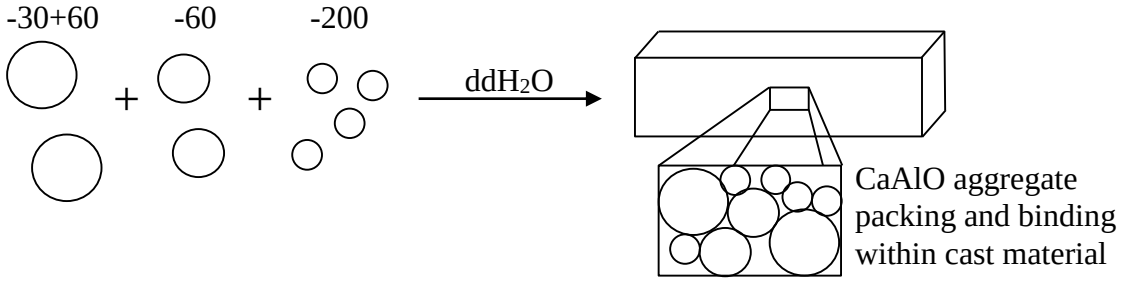

Figure 2.1: Casting 100% CaAlO in a 2:1:1 ratio of three different aggregate sizes. Through hydration the aggregates can be cast into a variety of shapes.

2.2.2.2 Hydroxyapatite

Hydroxyapatite discs were also prepared using a room temperature cast approach.[28,29] Fine particles of calcium phosphate tribasic were first obtained by grinding the $Ca_3(PO_4)_2$ powder in a mortar and pestle for 10 minutes. Once the powder was ground, it was hydrated using a dilute phosphoric acid (H_3PO_4, 25 mM) solution at an amount equal

to 1.1 mL of H_3PO_4 per gram of $Ca_3(PO_4)_2$ (Figure 2.2). Again the paste was allowed to thicken at room temperature for 10 minutes. After thickening the $Ca_3(PO_4)_2$ was poured in the same molds as above, where it was allowed to set for four hours. After four hours the material was rehydrated in the molds using H_3PO_4, then allowed to set overnight. The following day the casts were rehydrated with H_3PO_4 in the molds and set for another night. The next day the casts were removed from their molds, rehydrated with H_3PO_4 for 24 hours and then were sintered for four hours at 1000°C using a programmable Lindberg/Blue Moldatherm Box Furnace (Model: BF51866A). The furnace was programmed to heat up from room temperature to 1000°C over a span of two hours, then remain at 1000°C for four hours, followed by a two hour cool down from 1000°C to room temperature.

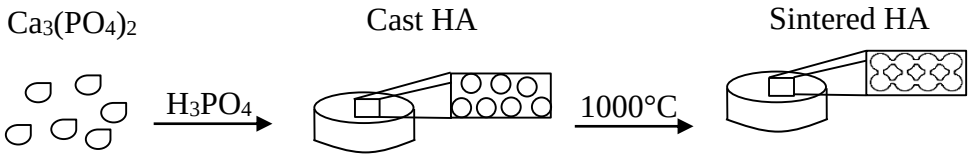

Figure 2.2: Casting 100% HA using ground $Ca_3(PO_4)_2$ with 25 mM H_3PO_4. After casting the materials are sintered for strength.

2.2.2.3 Calcium Aluminum Oxide:Hydroxyapatite Composites

Calcium aluminum oxide:hydroxyapatite (HA) composite discs (1-5, 10, 15, 20 and 25%, by mass) were cast using a room temperature method that combined both the CaAlO and the HA methods. First the three different aggregate sizes of CaAlO (-30+60, -60 and -200) were dry mixed in a 1:1:2 ratio. Upon thorough mixing, ground $Ca_3(PO_4)_2$ was added to the mixed CaAlO powder at a mass appropriate for the desired composite composition (1-5, 10, 15, 20 or 25% HA, by mass). The powders were again thoroughly dry mixed to distribute the particles and then were hydrated with 0.3 mL of ddH_2O per gram CaAlO and

1.1 mL H_3PO_4 per gram $Ca_3(PO_4)_2$ in the composite. For example, 15 grams of a composite that is 95% CaAlO and 5% HA (known as 5% HA), required 7.125 grams of -200 mesh CaAlO, 3.563 grams each of the -60 and -30+60 mesh CaAlO, and 0.75 grams of $Ca_3(PO_4)_2$. Upon mixing, 4.28 mL of ddH_2O and 0.83 mL of H_3PO_4 was used to hydrate the powder. The paste was allowed to thicken for 10 minutes. Afterwards the paste was poured into the same molds mentioned above, where it was allowed to set for four hours, then was rehydrated using H_3PO_4 and allowed to set overnight. Composites were hydrated again the next day with H_3PO_4 and permitted to set overnight. The following day composites were removed from their casts and were rehydrated in ddH_2O for 24 hours.

Once hydrated, half of the composite discs/beams were allowed to dry at room temperature (simulating exclusive CaAlO casting) and half were subjected to a four hour sintering at 1000°C (simulating exclusive HA casting). The two post hydration processes were examined because CaAlO derives much of its mechanical strength through using ddH_2O to create chemical bonds between the aggregate powders during hydration, whereas mechanical integrity of HA is the result of sintering, the high temperature compaction and fusion of powders into solids.

2.2.3 Powder X-ray Diffraction

Phases present in the cast composites were determined using powder x-ray diffraction (PXRD).[14,30,31] Six discs of each material (100% CaAlO, 100% HA and 1-5, 10, 15, 20 and 25% HA) were ground with a mortar and pestle for 20 minutes. Samples were then loaded onto an X'Pert PANalytical Pro and scanned from 5-70° 2Θ with a time per step of 720.090 seconds and a scan speed of 0.002947° per second. Collected diffraction

patterns were analyzed using X'Pert High Score Plus to match peaks in the collected sample patterns to reference database patterns. Peak overlap between the sample and reference patterns indicated a matched phase.

2.2.4 Mechanical Evaluation

Eight total beams of each composite (0-5, 10, 15, 20 and 25% HA) were cast. Four composite beams were sintered at 1000°C for four hours and the other four were dried at room temperature. All composite beams were evaluated independently by mounting in an MTS 858 Bionix test machine in a fully articulated four point bending fixture (Figure 2.3). The middle supports were placed at 25% and 75% of the distance from the left, and a light, hollow, square brass structural beam of 6x6 mm with 0.4 mm walls was attached to the midpoint of the lower side of the beam, perpendicular to the axis of symmetry. Each side of the beam was in contact with a linear variable differential transformer. A tare load of 70 N was applied to the beam and the deflection at the midpoint was recorded. Beams were then loaded at a speed of 0.5mm/s until failure, and the load and deflection were recorded. The average elastic modulus and the average modulus of rupture of each composite was then calculated and compared to the value for non-load bearing cancellous bone.

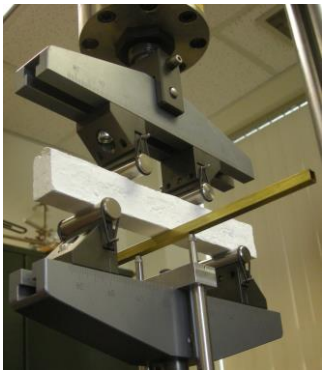

Figure 2.3: CaAlO:HA composite beam loaded in the four point bending apparatus, prior to load application.

The elastic modulus and modulus of rupture were calculated according to equations 1 and 2, respectively. Where "l" is the distance between the two outer most loading points, "F_{max}" is the maximum applied load, "b" is the specimen width, "h" is the specimen thickness, "ΔF" is the load range between a maximum 350 N load and the 70 N tare load and "f" is the difference in the midpoint beam deflections at 350 N load and the 70 N tare load.

$$\textbf{Equation 1}.\ \text{Elastic Modulus} = \frac{11 \cdot \Delta F \cdot l^3}{64 \cdot f \cdot b \cdot h^3}$$

$$\textbf{Equtaion 2}.\ \text{Modulus of Rupture} = \frac{3 \cdot F_{max} \cdot l}{4 \cdot b \cdot h^2}$$

2.2.5 Scanning Electron Microscopy

Morphological characteristics of the cast composite materials (0-5% HA) were examined using scanning electron microscopy (SEM). Characteristics including composite topography and interfacial porosity were examined. Micrographs were collected between 250-1400x magnification using a 2.00-7.00 kV accelerating voltage, dependent upon the surface feature and material being examined. Substrates were analyzed on a Hitachi S-3400N-II SEM under full vacuum.

2.2.6 Scanning Electron Microscopy-Energy Dispersive X-Ray Spectroscopy

Interfacial composition and interfacial phase distribution of the cast composite materials (0-5% HA) were examined using scanning electron microscopy-energy

dispersive x-ray spectroscopy (SEM-EDS) and elemental mapping. EDS spectra were collected on areas of the substrates that were large and flat, allowing for data collection over an area instead of a single point. Spectra were collected for two minutes from 0-20 eV. Maps of all elements detected using EDS were also obtained. Elemental maps were collected on the same region of the substrate as the EDS spectra was collected. Maps for all elements were simultaneously collected for the duration of four minutes. All substrates were analyzed and spectra/maps collected on a Hitachi S-3400N-II SEM under vacuum using a Bruker XFlash with ESPIRIT software, under a magnification of 1400x and accelerating voltage of 15.0 kV.

2.2.7 Degradability Study

The long term stability of the composite material in an aqueous environment was evaluated through immersion in phosphate buffered saline (PBS) for three months at 37°C and 5% CO2. Ten discs each of 0-5% HA were cast and weighed for their initial mass, recorded as week 0 (n=10). Discs were then added to individual wells of a 48 well plate, immersed in 1 mL of PBS and placed into an incubator at 37°C and 5% CO2. Well plates were removed from the incubator weekly, and the discs were transferred from the well plate into test tubes and then were heated at 120°C for 4.5 hours to ensure the removal of the liquid. Each disc was individually massed at the weekly time point. The discs were then placed into individual wells of a new 48 well plates, immersed in 1 mL of fresh PBS and they were returned to the incubator for another week. This process was carried out weekly for the duration of three months and the average change in mass between weeks was determined for each composite.

2.2.8 Statistics

A one-way analysis of variance (ANOVA) with a Bonferroni post-hoc test was used to determine the averages and examine statistical differences between the elastic moduli and moduli of rupture of the cast composites (0-5, 10, 15, 20 and 25% HA) and between the sintered and RT-formed composites. Additionally, the average weekly change in mass of all of the composites was compared. Both were evaluated at the $p<0.05$ level of significance and all data is reported as mean ± standard error.

2.3 Results

2.3.1 Powder X-Ray Diffraction

To determine the phases present in the composite materials, PXRD was utilized. The phases of the CaAlO starting aggregates are $CaAl_4O_7$ and $CaAl_2O_4$. Phases present in the room temperature cast 100% CaAlO include $CaAl_4O_7$, $CaAl_2O_4$, and a new hydrated calcium aluminum phase, $Ca_3Al_2(OH)_{12}$.[14] In the composite materials (1-5, 10, 15, 20 and 25% HA) $Ca_3(PO_4)_2$, was added in as the source of HA. PXRD analysis of the RT-formed composites revealed the same three phases of CaAlO, as well as $Ca_5(PO_4)_3(OH)$, which is HA, and trace amounts of the HA precursor, $CaHPO_4{\cdot}2H_2O$ (Figure 2.4).

The presence of the same phases in both the RT-formed composites and the exclusively cast CaAlO and $Ca_3(PO_4)_2$ demonstrates that the phases are not mixing and no cross reactions are taking place when the composites are cast. Thus the osteogenic benefits of the HA phase may be preserved through the RT casting.

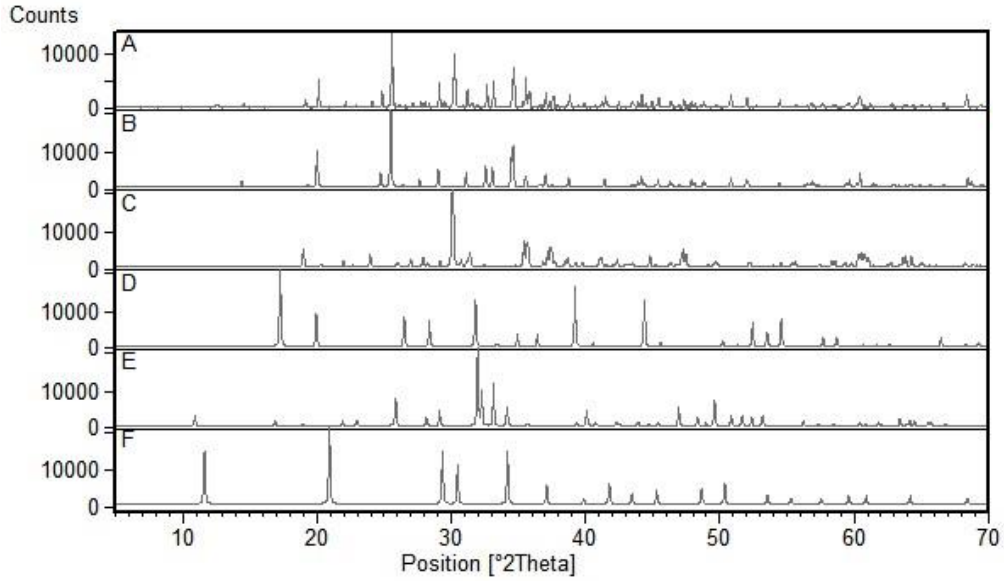

Figure 2.4: A) PXRD pattern for the 5% HA composite and phases contained within the composite. Including the calcium aluminum oxide based phases B) $CaAl_4O_7$, C) $CaAl_2O_4$ and D) $Ca_3Al_2(OH)_{12}$ and the calcium phosphate based phases E) $Ca_5(PO_4)_3(OH)$ and F) $CaHPO_4{\cdot}2H_2O$.

2.3.2 Mechanical Evaluation

Different post hydration procedures were examined because CaAlO derives its mechanical strength from hydration, whereas the mechanical integrity of HA is the result of sintering. Composites ranging from 0-5, 10, 15, 20 and 25% HA were cast into two groups (sintered: heated at 1000°C for 4 hours and RT-formed: dried at room temperature) and evaluated for their elastic modulus and modulus of rupture.[32,33] When examining bone for these properties, the value depends largely on the bone type, location and purpose.[32,34] Cortical bone is the dense, rigid bone tissue that is found largely in load bearing locations, whereas cancellous bone is the porous, more flexible bone tissue found primarily in non-load bearing locations.[32] Both the elastic modulus and modulus of rupture of cortical bone have been shown to be higher than those of cancellous bone.[32] However, mechanically

matching a composite CaAlO to either of these types of bone would be useful for guiding the materials applicability.

2.3.2.1 Elastic Modulus

The elastic modulus of a material is a measure of the resistance to non-permanent deformation when an external force is applied. Beams composed of 100% CaAlO cast at room temperature were found to have an average elastic modulus of 14.5 ± 0.9 GPa. As HA was incorporated into the mixture it was found that the elastic modulus of the CaAlO:HA composites tended to decrease as the mass percent of HA increased. Specifically, the 1%, 3% and 4% HA composites were statistically equivalent to control 100% CaAlO, the 2% HA composite was statistically higher (16.2 ± 0.5 GPa) than control and the 5, 10, 15, 20 and 25% HA composites had a statistically lower elastic moduli than control (Figure 2.5).

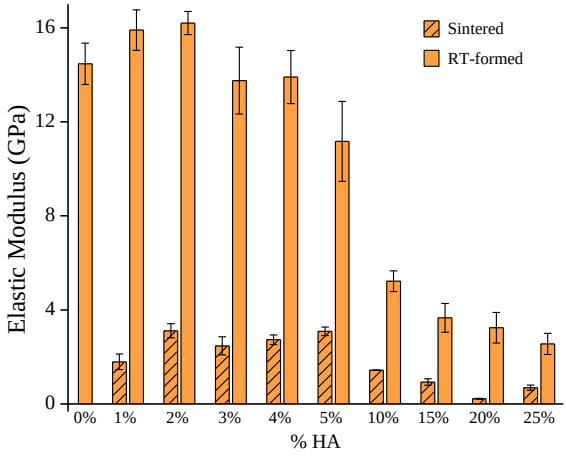

Figure 2.5: Average elastic modulus of the composites of sintered and RT-formed 0-5, 10, 15, 20 and 25% HA composites, shown as mean ± standard error, $p<0.05$. RT-formed composites are statistically higher for all percentages evaluated.

Table 2.1: Elastic modulus of the sintered and RT-formed CaAlO:HA composites.

Material	Sintered/RT-formed	Elastic Modulus (GPa)
0% HA	RT-formed	14.5 ± 0.9
1% HA	Sintered	1.8 ± 0.3
	RT-formed	15.9 ± 0.9
2% HA	Sintered	3.1 ± 0.3
	RT-formed	16.2 ± 0.5
3% HA	Sintered	2.5 ± 0.4
	RT-formed	13.8 ± 1.4
4% HA	Sintered	2.7 ± 0.2
	RT-formed	13.9 ± 1.1
5% HA	Sintered	2.6 ± 0.3
	RT-formed	9.9 ± 1.1
10% HA	Sintered	1.4 ± 0.1
	RT-formed	5.2 ± 0.4
15% HA	Sintered	0.9 ± 0.1
	RT-formed	3.7 ± 0.6
20% HA	Sintered	0.2 ± 0.02
	RT-formed	3.2 ± 0.7
25% HA	Sintered	0.7 ± 0.1
	RT-formed	2.6 ± 0.5

In spite of the statistical differences amongst the composites, the elastic moduli for the 5, 10, 15, 20 and 25% HA RT-formed composites were all within the reported range for non-load bearing, structural cancellous bone, between 3-11 GPa (Table 2.1).[32,35] All of the composites, 1-5, 10, 15, 20 and 25% HA, had elastic moduli lower than that reported for cortical bone.

The RT-formed beams were also compared to their sintered counterparts. The results demonstrate that sintering the composites at 1000°C for 4 hours significantly decreases the elastic modulus of the material for all of the composites examined. The 5% HA composite had the smallest average difference (70% decrease) between sintered and RT-formed materials and the maximum difference found was for the 1% HA composite (90% decrease).

2.3.2.2 Modulus of Rupture

The modulus of rupture of a material is a measure of the ultimate force necessary to cause failure. Composites that were 100% CaAlO cast at room temperature were found to have an average modulus of rupture of 8.8 ± 0.9 MPa. As HA was incorporated into the mixture it was found that at low percentages the modulus of rupture was not significantly affected and at high percentages the modulus of rupture decreased. Specifically, the RT-formed 1% and 3-5% HA composites were statistically equal to control 100% CaAlO, the 2% HA composites were statistically higher (10.8 ± 0.6 MPa) than control CaAlO and the 10, 15, 20 and 25% HA composites were lower than control (Figure 2.6).

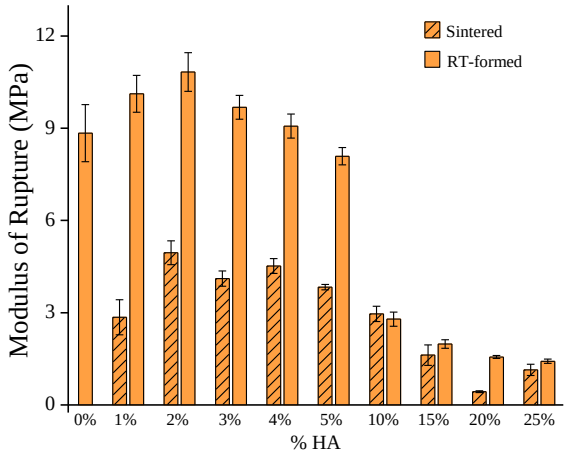

Figure 2.6: Average modulus of rupture of the composites of sintered and RT-formed 0-5, 10, 15, 20 and 25% HA composites, shown as mean ± standard error, $p<0.05$. RT-formed composites are statistically higher for 1-5% HA and statistically equal at greater percentages of HA.

Despite statistical differences among the composites, the moduli of rupture for the RT-formed 1, and 3-5% HA composites were all within the reported range for non-load bearing, structural cancellous bone, between 4-9 MPa (Table 2.2).[32,35] The modulus of rupture of all of the composites were significantly lower than cortical bone.

Table 2.2: Modulus of rupture of the sintered and RT-formed CaAlO:HA composites.

Material	Sintered/RT-formed	Moduli of Rupture (MPa)
0% HA	RT-formed	8.8 ± 0.9
1% HA	Sintered	2.9 ± 0.6
	RT-formed	10.1 ± 0.6
2% HA	Sintered	5.0 ± 0.4
	RT-formed	10.8 ± 0.6
3% HA	Sintered	4.1 ± 0.3
	RT-formed	9.7 ± 0.4
4% HA	Sintered	4.5 ± 0.2
	RT-formed	9.1 ± 0.4
5% HA	Sintered	3.9 ± 0.1
	RT-formed	6.4 ± 0.7
10% HA	Sintered	3.0 ± 0.3
	RT-formed	2.8 ± 0.2
15% HA	Sintered	1.6 ± 0.3
	RT-formed	2.0 ± 0.1
20% HA	Sintered	0.4 ± 0.03
	RT-formed	1.6 ± 0.1
25% HA	Sintered	1.1 ± 0.2
	RT-formed	1.4 ± 0.1

RT-formed beams were again compared to their sintered counterparts, revealing that sintering the 1-5% HA composites caused a significant decrease in the modulus of rupture, but at higher percentages of HA sintering did not significantly affect the modulus of rupture. The smallest percent difference in average strength between sintered and RT-formed materials was found for the higher percentage composite 10%, 15% and 25% HA composite (10-20% decrease) and the largest difference was for the 1% HA composite (70% decrease).

2.3.3 Scanning Electron Microscopy

After using the mechanical evaluation to focus the study on mechanically-relevant composites, the 0-5% HA composites were qualitatively evaluated using SEM to determine

material morphology. It was found that the 100% CaAlO material adopted a topography that was rough and non-uniform, containing surface structures that were needle-like, plate-like and cubic (Figure 2.7 A-C). As small mass percentages of HA were added into the CaAlO, the topography of the composites became more uniform and the distinct surface structures observed in 100% CaAlO were no longer present. The interface of the composites appear smoother, like that of cast 100% HA (Figure 2.7 D-E).

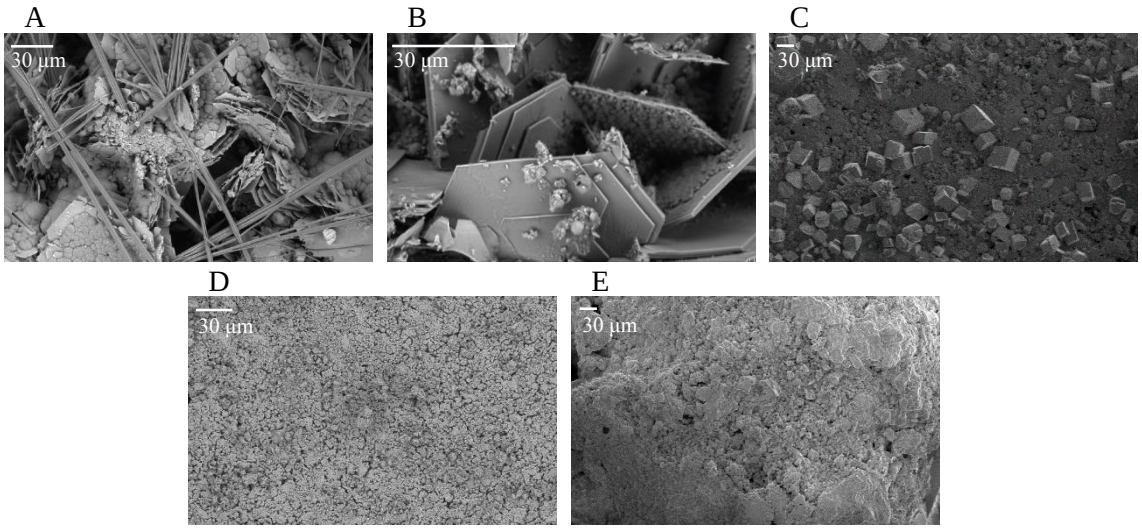

Figure 2.7: Morphological SEM images of surface structures observed on CaAlO, 5% HA and HA. A) Needle-like formation of CaAlO. B) Plate-like formation of CaAlO. C) Cube-like formation of CaAlO. D) Increased surface uniformity observed on 5% HA, similar to interfacial characteristics of HA. E) Interfacial structure of 100% HA.

2.3.4 Energy Dispersive X-Ray Spectroscopy

The interfacial composition of the 0-5% HA composites was evaluated using SEM-EDS and elemental mapping to determine the elemental and phase composition. Interfacial analysis confirmed the presence of the elements calcium, aluminum and oxygen in all 0-5% HA composites examined, as a result of the $CaAl_4O_7$, $CaAl_2O_4$ and $Ca_3Al_2(OH)_{12}$ in cast CaAlO (determined using PXRD). As $Ca_3(PO_4)_2$ was incorporated into the material, it

cast as the phase HA, $Ca_5(PO_4)_3(OH)$ (determined using PXRD), and was present at the composite interface, determined by the presence of the EDS peak corresponding to phosphorus at 2.0 eV and elemental mapping of phosphorus. Additionally, the intensity of the EDS peak corresponding to phosphorus increased as the composite increased from 1% to 5% HA, indicating that as the mass percentage of HA in the composite increased, the amount of HA present at the interface also increased. A greater interfacial amount of HA is significant because it can lead to increased exposure and interaction between osteoblasts and the osteogenic phase of the composite.

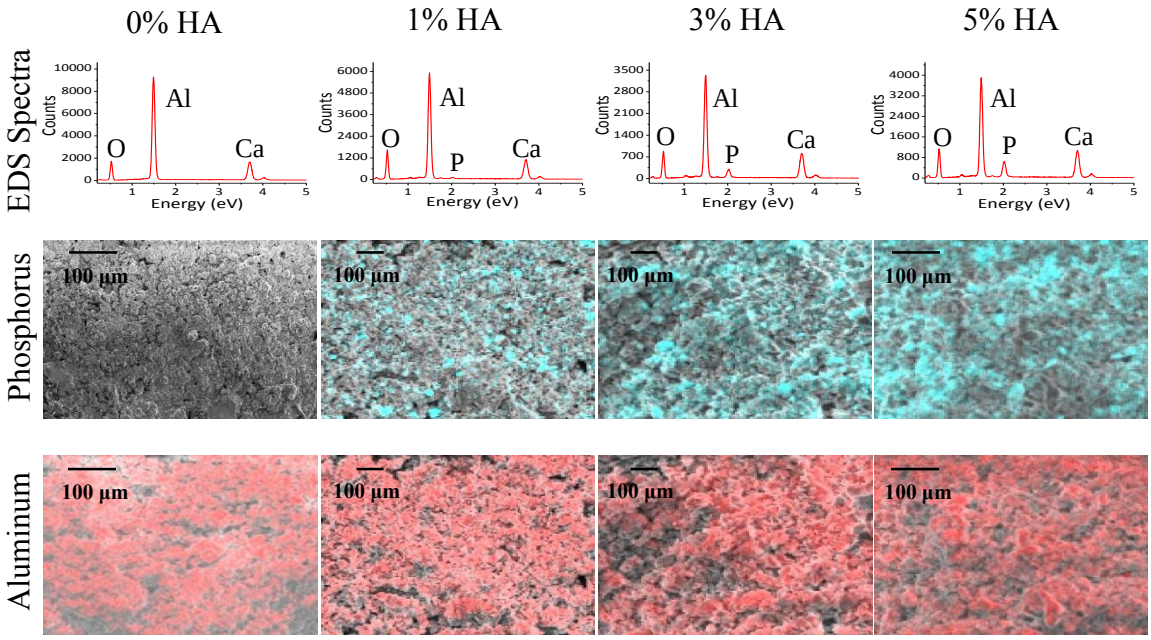

Figure 2.8: EDS spectra for 0, 1, 3 and 5% HA exhibit the presence of calcium, aluminum, and oxygen from the CaAlO phases. The 1, 3 and 5% HA composites contain phosphorus due to the HA and brushite phases. Elemental mapping shows the distribution of the HA phase at the composite interface based on the location of the phosphorus atoms and the aluminum atoms show that the majority of the interface is CaAlO.

2.3.5 Degradability Study

The long term stability of the 1-5% HA composites and control CaAlO was evaluated by immersion in PBS for 3 months. Substrates were placed into individual wells of a 48 well plate, immersed in 1 mL of fresh PBS and put into an incubator at 37°C and 5% CO_2. Substrates were removed from the incubator weekly and PBS was driven off then substrates were weighed.

Overall, the 1-5% HA composites exhibited a similar trend in their average week-to-week change in mass when compared to one another. However, between Week 0 and 1 the composites (1-5% HA) experienced a statistically significant drop in mass compared to the control CaAlO. For example, the average decrease in mass of control during Week 1 was 0.23 ± 0.34 milligrams and for 5% HA it was 1.94 ± 0.35 milligrams. This decrease in mass can be attributed to the dissolution of solid CaAlO and/or $Ca_3(PO_4)_2$ that remains in the composites after the casting process, because these phases are soluble in water. However, the observed decrease in mass during the first week was not statistically different among the 1-5% HA composites (Figure 2.9).

Between Weeks 1 and 2 the mass of control CaAlO and 1%, 2%, and 5% HA all increased by statistically the same mass, and 3% HA and 4% HA increased by a significantly greater amount than the others. Specifically, in Week 2 the control increased by 2.22 ± 0.30 milligrams and the 5% HA by 2.20 ± 0.28 milligrams, whereas the 3% HA increased by 3.01 ± 0.18 milligrams. Despite the differences in the mass changes in the early weeks of the assay, the mass change of all samples (0-5% HA) converged to zero grams when the degradability assay was extended through 3 months, indicating that the material was not degrading and remained stable in the PBS (Figure 2.9).

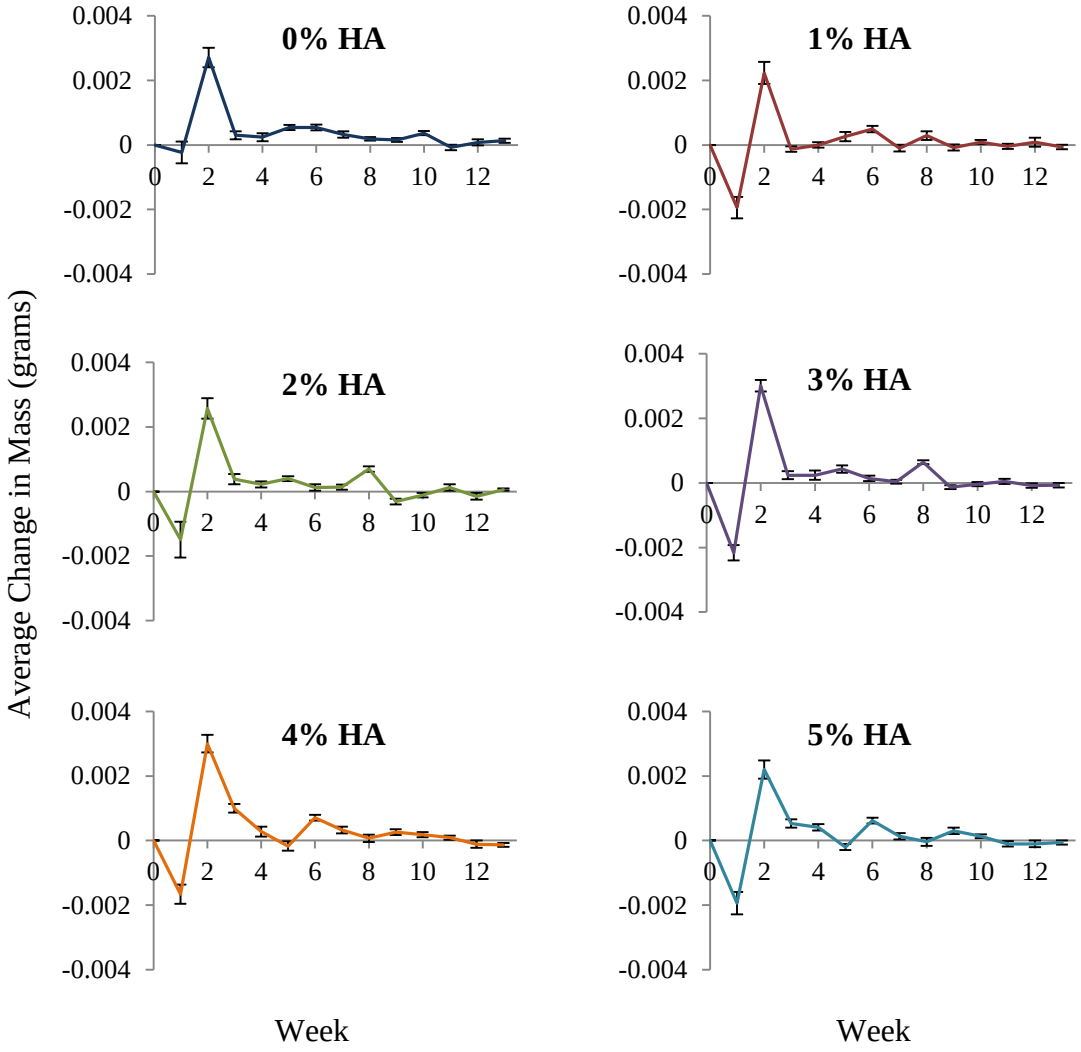

Figure 2.9: Average change in mass from week to week for 0-5% HA composites over a 3 month time span.

2.4 Discussion

The 100% CaAlO had previously been physically characterized for interfacial pore size and volume, phase presence, degradability and fibroblast attachment.[14] It was determined that the 2:1:1 ratio of -200, -30+60 and -60 CaAlO aggregate sizes resulted in the material that was physically the most applicable, with pores of 100 µm diameter, no free Al^{3+} ions, long term stability in PBS and increased fibroblast (scar tissue cells)

adhesion at short time points.[14] In spite of the fact that the material was physically optimized and increased fibroblast adhesion, it required chemical optimization to allow for bone cell attachment.[12,14] This chemical modification was important because it introduced a five-step reaction sequence that culminated in the linkage of KRSR, an osteoblast adhesion peptide, and vancomycin, an antibiotic active against gram-positive strains of bacteria.[12,13] Through the introduction of the osteogenic HA into the materials, the goal was to maintain the material's mechanical strength while increasing osteoblast response, and decreasing the extent of chemical modification necessary to develop a multifunctional bone graft material.

$Ca_3(PO_4)_2$ was added to the CaAlO powder as the source of HA for the composite material. When the composite materials are cast, PXRD demonstrated that the $Ca_3(PO_4)_2$ does cast into HA. However, to analyze the composites using PXRD the discs had to be ground into a fine powder following the casting, therefore PXRD demonstrated the presence of the HA phase in the disc, but the location of the HA in the discs is also very important. Also, when exclusive HA materials are used, the material must be sintered in order to provide mechanical strength and decrease solubility, therefore these characteristics needed to be reexamined for the composites.

The strength of the CaAlO phase is due to the hydrated phases that form during the casting process and interlock the different aggregates within the material. Despite the hydration steps in the HA casting phase, its strength comes from sintering and fusing the powders. Since the two materials being cast into one composite differ in their mechanism for obtaining strength, both processes were examined. Sintering the composites had a significant effect on the elastic modulus and modulus of rupture for the composites with

less than 5% HA. All of these composites had significantly reduced values as a result of sintering. This is due to the removal of the hydrating waters of the CaAlO phases. By driving these waters out of the composite at 1000°C, the CaAlO phases weaken and therefore weaken the composite as a whole. Conversely, when the 1-5% HA composites were simply hydrated and dried at room temperature, the elastic modulus and modulus of rupture was not affected. This is because the materials are between 95-99% CaAlO and CaAlO strength is the results of interlocked phases from hydration. Further when the elastic modulus of the composites was compared to non-load bearing cancellous bone, it was found that the 5, 10, 15, 20 and 25% HA composites were within the reported range of 3-11 GPa.[32,35] The 1-4% HA composites were very close to this value, no more than 4 GPa higher (observed with 2% HA). The modulus of rupture of non-load bearing cancellous bone is reported between 4-9 MPa.[32,35] The 1 and 3-5% HA composites had moduli of rupture within this range and the 2% HA was 1 MPa higher. As the composites became >10% HA they were significantly lower than this range. Structural cancellous bone is 100% stronger than composites with >10% HA. Mechanical evaluation demonstrated that RT-formed composites with between 1-5% HA were the most mechanically relevant materials to natural, structural cancellous bone.

The results of the mechanical evaluation indicated that the RT-formed 1-5% HA composites were mechanically similar to non-load bearing bone. The distribution of the HA phase within the cast composites is important to their success. The distribution is important for a few reasons, first, cellular interactions will take place at the scaffold-tissue interface, so when cast some HA must be present at the interface, and secondly because

sintering reduces the degradability of HA *in vitro*. But, since the composites were not being sintered, the presence of HA at the interface may lead to increased material degradability.

The presence and distribution of HA at the interface of all 1-5% HA composites was demonstrated using SEM-EDS. The EDS spectra collected on all composites revealed the presence of the elements calcium, aluminum, oxygen and phosphorus. Based on the data collected with PXRD, it can be established that the presence of phosphorus is the result of HA or the HA precursor and not starting $Ca_3(PO_4)_2$ or any mixed calcium aluminum oxide-calcium phosphate phases. It was also found that as the amount of HA in the composite increases from 1% to 5% the interfacial amount of phosphorus increased. This indicates that by increasing the amount of $Ca_3(PO_4)_2$ in the cast powder, the amount of HA at the interface will increase accordingly. This is important because it shows that the HA phase is distributed and abundant at the material-tissue interface. Furthermore, the degradability assay was carried out on the composite materials at physiological temperature and verified that the *in vitro* stability of the materials was not significantly affected.

2.5 Conclusions

Composite materials consisting of calcium aluminum oxide and hydroxyapatite were successfully cast at room temperature to contain 1-5, 10, 15, 20 and 25% HA by mass. By casting the composites of CaAlO with small mass percentages of HA, the mechanical strength of the CaAlO material was not significantly affected. The 1-5% HA composites were up to 190% stronger than other composites and were better mechanical matches for non-load bearing cancellous bone. Importantly, the incorporated HA (1-5%) was present and distributed at the composite interface where cellular interactions could occur, and the

composites were stable *in vitro* in PBS at 37°C and 5% CO_2 for 3 months. Based on these results the 1-5% HA composites were investigated for their ability to increase osteoblast response *in vitro*.

2.6 References

1. Franz, A.; Konradsson, K.; König, F.; Van Dijken, J. W.; Schedle, A. Cytotoxicity of a calcium aluminate cement in comparison with other dental cements and resin-based materials. *Acta Odontol. Scand.* **2006**, *64*, 1-8.

2. Graves, G.; Noyes, F.; Villanueva, A. The influence of compositional variations on bone ingrowth of implanted porous calcium aluminate ceramics. *J. Biomed. Mater. Res.* **1975**, *9*, 17-22.

3. Kalita, S.; Bose, S.; Bandyopadhyay, A.; Hosick, H. Porous calcium aluminate ceramics for bone-graft applications. *J. Mater. Res.* **2002**, *17*, 3042-3049.

4. Klawitter, J.; Hulbert, S. Application of porous ceramics for the attachment of load bearing internal orthopedic applications. *J. Biomed. Mater. Res.* **1971**, *5*, 161-229.

5. Uchida, A.; Nade, S.; McCartney, E.; Ching, W. Bone ingrowth into three different porous ceramics implanted into the tibia of rats and rabbits. *J. Orthop. Res.* **1985**, *3*, 65-77.

6. Uchida, A.; Nade, S.; McCartney, E.; Ching, W. Growth of bone marrow cells on porous ceramics in vitro. *J. Biomed. Mater. Res.* **1987**, *21*, 1-10.

7. Clafshenkel, W. P.; Rutkowski, J. L.; Palchesko, R. N.; Romeo, J. D.; McGowan, K. A.; Gawalt, E. S.; Witt-Enderby, P. A. A novel calcium aluminate-melatonin scaffold enhances bone regeneration within a calvarial defect. *J. Pineal Res.* **2012**, *53*, 206-218.

8. Miljkovic, N. D.; Cooper, G. M.; Hott, S. L.; DiSalle, B. F.; Gawalt, E. S.; Smith, D. M.; McGowan, K.; Marra, K. G. Calcium aluminate, RGD-modified calcium aluminate, and β-tricalcium phosphate implants in a calvarial defect. *J. Craniofac. Surg.* **2009**, *20*, 1538-1543.

9. Oliveira, I.; Pandolfelli, V.; Jacobovitz, M. Chemical, physical and mechanical properties of a novel calcium aluminate endodontic cement. *Int. Endod. J.* **2010**, *43*, 1069-1076.

10. Palmquist, A.; Jarmar, T.; Hermansson, L.; Emanuelsson, L.; Taylor, A.; Taylor, M.; Engqvist, H.; Thomsen, P. Calcium aluminate coated and uncoated free form fabricated CoCr implants: A comparative study in rabbit. *J. Biomed. Mater. Res., Part B* **2009**, *91*, 122-127.

11. Pameijer, C. H.; Zmener, O.; Alvarez Serrano, S.; Garcia-Godoy, F. Sealing properties of a calcium aluminate luting agent. *Am. J. Dent.* **2010**, *23*, 121-124.

12. Palchesko, R. N.; Buckholtz, G. A.; Romeo, J. D.; Gawalt, E. S. Co-immobilization of active antibiotics and cell adhesion peptides on calcium based biomaterials. *Mater. Sci. Eng., C* **2014**, *40*, 398-406.

13. Palchesko, R. N.; McGowan, K. A.; Gawalt, E. S. Surface immobilization of active vancomycin on calcium aluminum oxide. *Mater. Sci. Eng., C* **2011**, *31*, 637-642.

14. Palchesko, R. N.; Romeo, J. D.; McGowan, K. A.; Gawalt, E. S. Increased osteoblast adhesion on physically optimized KRSR modified calcium aluminate. *J. Biomed. Mater. Res., Part A* **2012**, *100*, 1229-1238.

15. LeGeros, R. Z. Properties of osteoconductive biomaterials: Calcium phosphates. *Clin. Orthop. Relat. Res.* **2002**, *395*, 81-98.

16. Yuan, H.; Yang, Z.; Li, Y.; Zhang, X.; De Bruijn, J.; De Groot, K. Osteoinduction by calcium phosphate biomaterials. *J. Mater. Sci. Mater. Med.* **1998**, *9*, 723-726.

17. Shadanbaz, S.; Dias, G. J. Calcium phosphate coatings on magnesium alloys for biomedical applications: A review. *Acta Biomater.* **2012**, *8*, 20-30.

18. Luz, A.; Pandolfelli, V. $CaCO_3$ addition effect on the hydration and mechanical strength evolution of calcium aluminate cement for endodontic applications. *Ceram. Int.* **2012**, *38*, 1417-1425.

19. Parr, C. Calcium aluminate cement- What happens when things go wrong?. *IRE Annual Conference* **2008**.

20. Oliveira, M.; Mansur, H. S. Synthetic tooth enamel: SEM characterization of a fluoride hydroxyapatite coating for dentistry applications. *Mat. Res.* **2007**, *10*, 115-118.

21. Rossi, A. L.; Barreto, I. C.; Maciel, W. Q.; Rosa, F. P.; Rocha-Leão, M. H.; Werckmann, J.; Rossi, A. M.; Borojevic, R.; Farina, M. Ultrastructure of regenerated bone mineral surrounding hydroxyapatite–alginate composite and sintered hydroxyapatite. *Bone* **2012**, *50*, 301-310.

22. Dasgupta, S.; Tarafder, S.; Bandyopadhyay, A.; Bose, S. Effect of grain size on mechanical, surface and biological properties of microwave sintered hydroxyapatite. *Mater. Sci. Eng., C* **2013**, *33*, 2846-2854.

23. Zhu, X.; Zhang, H.; Li, D.; Fan, H.; Zhang, X. Study on the enhanced protein adsorption of microwave sintered hydroxyapatite nanoceramic particles: Role of microstructure. *J. Biomed. Mater. Res., Part B* **2012**, *100*, 516-523.

24. Tripathi, G.; Basu, B. A porous hydroxyapatite scaffold for bone tissue engineering: Physico-mechanical and biological evaluations. *Ceram. Int.* **2012**, *38*, 341-349.

25. Gosain, A. K.; Song, L.; Riordan, P.; Amarante, M. T.; Nagy, P. G.; Wilson, C. R.; Toth, J. M.; Ricci, J. L. A 1-year study of osteoinduction in hydroxyapatite-derived biomaterials in an adult sheep model: Part I. *Plast. Reconstr. Surg.* **2002**, *109*, 619-630.

26. Ozawa, S.; Kasugai, S. Evaluation of implant materials (hydroxyapatite, glass-ceramics, titanium) in rat bone marrow stromal cell culture. *Biomaterials* **1996**, *17*, 23-29.

27. Pino-Mínguez, J.; Jorge-Mora, A.; Couceiro-Otero, R.; García-Santiago, C. Study of the viability and adhesion of osteoblast cells to bone cements mixed with hydroxyapatite at different concentrations to use in vertebral augmentation techniques. *Rev. Esp. Cir. Ortop. Traumatol.* **2015**, *59*, 122-128.

28. Bouler, J. M.; Trécant, M.; Delécrin, J.; Royer, J.; Passuti, N.; Daculsi, G. Macroporous biphasic calcium phosphate ceramics: Influence of five synthesis parameters on compressive strength. *J. Biomed. Mater. Res.* **1996**, *32*, 603-609.

29. Gauthier, O.; Bouler, J. M.; Aguado, E.; Pilet, P.; Daculsi, G. Macroporous biphasic calcium phosphate ceramics: Influence of macropore diameter and macroporosity percentage on bone ingrowth. *Biomaterials* **1998**, *19*, 133-139.

30. Kontoyannis, C. G.; Vagenas, N. V. Calcium carbonate phase analysis using XRD and FT-Raman spectroscopy. *Analyst* **2000**, *125*, 251-255.

31. Tampieri, A.; Celotti, G.; Szontagh, F.; Landi, E. Sintering and characterization of HA and TCP bioceramics with control of their strength and phase purity. *J. Mater. Sci. Mater. Med.* **1997**, *8*, 29-37.

32. Charriere, E.; Terrazzoni, S.; Pittet, C.; Mordasini, P.; Dutoit, M.; Lemaıtre, J.; Zysset, P. Mechanical characterization of brushite and hydroxyapatite cements. *Biomaterials* **2001**, *22*, 2937-2945.

33. Currey, J. The mechanical properties of bone. *Clin. Orthop. Relat. Res.* **1970**, *73*, 210-231.

34. Currey, J. D. Mechanical properties of bone tissues with greatly differing functions. *J. Biomech.* **1979**, *12*, 313-319.

35. Røhl, L.; Larsen, E.; Linde, F.; Odgaard, A.; Jørgensen, J. Tensile and compressive properties of cancellous bone. *J. Biomech.* **1991**, *24*, 1143-1149.

Chapter 3: Increased Osteoblast Response on 1-5% HA Composites

3.1 Introduction

When synthetic bone graft materials are used they can lead to the formation of fibrous tissue around the implant which may inhibit new bone growth and integration at the graft-tissue interface.[1-4] This encapsulation is caused by non-specific cell and protein adhesion due to the normal wound healing response.[3] If fibrous encapsulation does occur it can lead to bone resorption at the graft-tissue interface which can lead to implant loosening and graft failure. One approach to increasing cell adhesion has been to link cell adhesion peptides to the surfaces of the graft materials.[5-10] Initially studies demonstrated that the peptide RGD increased the attachment of a variety of cells (osteoblast, fibroblasts, mesenchymal stem cells) to an assortment of materials (calcium ceramics, titanium, polymers).[5,11-14] The biggest issue with RGD is that it is a non-cell specific adhesion peptide and as a result it may lead to increased fibrous tissue at the graft-tissue interface.[12,15-18] To address this, research has shifted to cell specific adhesion peptides.[6,19] The osteoblast specific adhesion peptide KRSR has been shown to bind an increased number of osteoblasts compared to unmodified surfaces (titanium, calcium ceramics).[6,20-22] KRSR has also been shown to preferentially bind osteoblasts over fibroblasts when immobilized to 100% CaAlO.[6] These cell adhesion peptide based approaches do result in increased osteoblast response on modified materials, but materials based approaches have shown that calcium phosphate containing materials can increase osteoblast response.[23-25]

Miljkovic and coworkers compared three calcium based ceramics in an *in vivo* rat calvarial critical-sized defect model.[23] They compared CaAlO, RGD-modified CaAlO and a calcium phosphate, β-tricalcium phosphate, and demonstrated that CaAlO and RGD-CaAlO did not have osteoconductive or osteoinductive properties on their own and both cause a mild immune reaction at the site of implantation.[23] Conversely, the β-tricalcium phosphate did not illicit an immune response and showed signs of implant integration into the host tissue at 4 weeks.[23] This work showed that unmodified calcium phosphate ceramics were a more viable option for increased *in vivo* bone regeneration over CaAlO and modified CaAlO.

Ball and coworkers used pulsed laser ablation as a method for deposition of HA onto titanium surfaces.[24] Human osteoblasts were seeded onto the material surfaces and examined for a variety of cellular responses. The HA coated surfaces supported greater cell attachment, were more supportive of proliferation and growth and caused increased differentiation based on alkaline phosphatase presence.[24] The osteoblasts on HA coated titanium also had a more organized actin cytoskeleton and had more contacts with the surface, determined by vinculin staining.[24] They showed that by coating the mechanically strong titanium with a thin HA layer, the *in vitro* osteoblast performance was greatly improved.

Finally, Pino-Minguez and coworkers created composites of polymethyl-methacrylate alone and mixed with HA in different concentrations.[25] They examined composite PMMA:HA with 5%, 10%, 15% and 20% HA.[25] PMMA has been studied due to its strength, however osteoblasts have shown limited activity when they are in contact with it, and it is common to observe fibroblastic cells at the PMMA-bone interface.[25]

PMMA:HA composites were investigated in an attempt to enhance the biocompatibility of the PMMA. They demonstrated the maximum amount of osteoblast growth and differentiation between 15% and 20% and that the transition between encapsulation and bone growth was at 15%.[25] They revealed that by creating a composite of the mechanically strong PMMA and the osteoinductive HA, the *in vitro* bone cell response was significantly improved when the composites contained 15% and 20% HA.

In this study, the composite CaAlO:HA materials that were mechanically similar to non-load bearing bone (1-5% HA composites) were evaluated for their ability to increase *in vitro* osteoblast response. Based on the literature, it has been shown that the presence of calcium phosphates, either as β-tricalcium phosphate or HA, in biomaterials causes an increase in the biocompatibility of the coated or composite materials. Here, the effect of the addition of HA to the CaAlO material was examined through osteoblast attachment, viability and proliferation of cells seeded on the sterilized composites.

3.2 Materials and Methods

3.2.1 Materials

Calcium aluminum oxide (CaAlO) was supplied by Westmoreland Advanced Materials. Calcium phosphate tribasic ($Ca_3(PO_4)_2$) and phosphate buffered saline (PBS, $MgCl_2$ and $CaCl_2$ free) were purchased from Sigma-Aldrich. Phosphoric acid was purchased from Fisher Scientific (Certified ACS). Normal human osteoblasts (NHOsts), osteoblast subculturing reagents (HEPES buffered saline, Trypsin/EDTA, Trypsin neutralizing solution) and osteoblast basal medium (OBM) were purchased from LONZA. The Live/Dead® Viability/Cytotoxicity assay kit and alamarBlue® reagent were

purchased from Life Technologies. All materials and chemicals were used as received unless otherwise noted.

3.2.2 Casting Calcium-Based Ceramics

3.2.2.1 Calcium Aluminum Oxide

Calcium aluminum oxide discs were prepared using the same method described in Chapter 2. The three different aggregate sizes of CaAlO utilized were -30+60, -60 and -200, in a 1:1:2 ratio, that are previously separated using a sifting process that sorts out the particles based on their mesh size. The appropriate mass of each CaAlO aggregate size were thoroughly dry mixed at room temperature to ensure even particle distribution. Distilled deionized water (ddH_2O) was then added to the aggregate powders at an amount equal to 0.3 mL of ddH_2O per gram of CaAlO. The paste was allowed to thicken at room temperature for 10 minutes. Afterwards, the CaAlO was poured into either a 6x2 mm (diameter x height) cylindrical disc mold where it was allowed to set for four hours. The CaAlO casts were rehydrated in their molds with ddH_2O, and allowed to set overnight. The next day the casts were hydrated in their molds using ddH_2O, then allowed to set for the night. The following day casts were removed from their molds and immersed into ddH_2O for 24 hours to ensure hydration of the material. CaAlO discs were sterilized before cellular studies by autoclaving at 121°C and 18 psi of steam for 60 minutes with fast exhaust.

3.2.2.2 Calcium Aluminum Oxide:Hydroxyapatite Composites

Calcium aluminum oxide:hydroxyapatite (HA) composite discs (1-5% HA) were cast using the same method described in Chapter 2. First the three different aggregate sizes of CaAlO (-30+60, -60 and -200) were dry mixed in a 1:1:2 ratio. Upon thorough mixing, ground $Ca_3(PO_4)_2$ was added to the mixed CaAlO powder at a mass appropriate for the final composition to be 5% HA. The powders were thoroughly dry mixed together and hydrated with 0.3 mL of ddH_2O per gram CaAlO and 1.1 mL H_3PO_4 per gram $Ca_3(PO_4)_2$ in the composite. The paste thickened for 10 minutes, then was poured into the 6x2 mm cylindrical molds. The paste set for four hours, then was rehydrated using H_3PO_4 and allowed to set overnight. Composites were hydrated again the next day with H_3PO_4 and permitted to set overnight. The following day composites were removed from the mold and rehydrated in H_3PO_4 for 24 hours. The 5% HA discs were sterilized before cellular and bacterial studies by autoclaving at 121°C and 18 psi of steam for 60 minutes with fast exhaust.

3.2.3 Osteoblast Cell Culture

Normal human osteoblasts (NHOsts) isolated from a 2 year old male (LONZA) were thawed from a -200°C liquid N_2 dewar and plated into T-25 cm^2 tissue culture flasks with at least 125,000 cells per flask in 5 mL of osteoblast basal medium (OBM). Tissue culture flasks were then placed into an incubator at 37°C and 5% CO_2 for 24 hours, so live osteoblasts could adhere to the interior. In the flasks, osteoblast attachment and division was monitored daily until attached cells achieved approximately 80% confluence. OBM

was changed daily after initial seeding during the days leading up to 80% confluence in the flask.

Once cells reached 80% confluence they were subcultured out of the flasks and a cell trial was begun. Osteoblasts were subcultured according to the protocol provided by LONZA and counted using the hemocytometer with Trypan Blue. Nine autoclaved composite discs per time point (0-5% HA) were placed into individual wells of 48 well plates labeled as Days 1, 4 and 7. Osteoblasts were then diluted to 10,000 cells per mL in OBM, and 1 mL of this osteoblast solution was added to each well containing a disc. OBM was changed daily in the individual wells leading up to each time point.

3.2.4 Osteoblast Attachment to 1-5% HA

NHOsts isolated from a 2 year old male were purchased from LONZA, cultured until 80% confluent and diluted to a concentration of 10,000 cells per mL of OBM. Three sample sets of three discs per time point (Days 1, 4 and 7, nine total discs) were autoclaved and seeded with 10,000 osteoblasts. After 1, 4 and 7 days the number of attached live and dead cells was determined using the Live/Dead® Viability/Cytotoxicity assay kit from Life Technologies (Figure 3.1).[6,26-28]

Using this assay kit, live cells will fluoresce green and dead cells will fluoresce red. Five spots on each sample with an area of 0.6 mm^2 were imaged under 10x magnification using the Axioskop2 with AxioVision software and fluorescence filters. The number of live cells was then counted on all 45 images for each composite percentage for each day (1-5% HA), then normalized to the control 100% CaAlO.

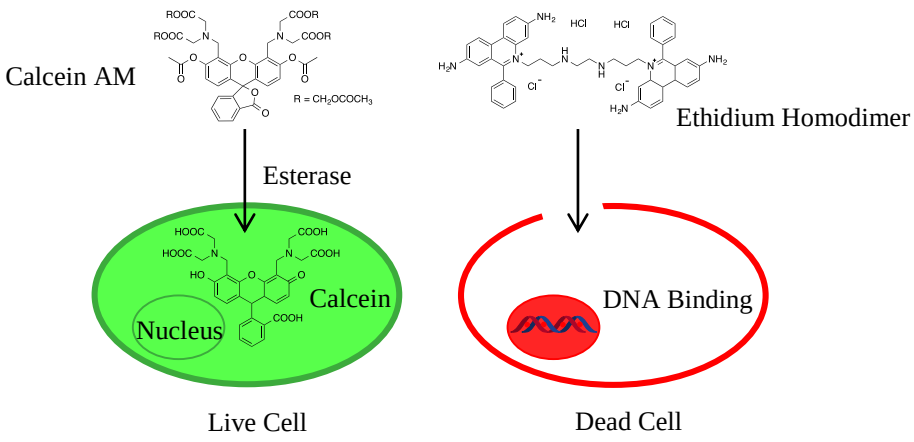

Figure 3.1: Fluorescent based Live/Dead® Viability/Cytotoxicity assay where calcein AM enters a live cell and is digested by an esterase to result in the green fluorescent cells. The ethidium homodimer enters a dead cell and binds to the DNA in the nucleus resulting in the red fluorescent cells.

3.2.5 Osteoblast Viability on 1-5% HA

NHOsts isolated from a 2 year old male were cultured and treated the same as described in Section 3.2.4. Cells were again assayed using the Live/Dead® Viability/Cytotoxicity assay kit and Axioskop2. In this assay, however, both the living (green) and dead (red) cells were counted on the 45 images of each composite for each day, getting a total number of cells. The percent viability was determined by dividing the number of live cells in each image by the total number of cells in each image.

3.2.6 Osteoblast Proliferation on 1-5% HA

NHOsts isolated from a 2 year old male were cultured to 80% confluence and diluted to 10,000 cell per mL of OBM. Then 1 mL of the osteoblast solution was added to nine wells containing autoclaved discs (0-5% HA). Cell proliferation was evaluated using the alamarBlue® assay from Life Technologies (Figure 3.2).[29-32] In this assay the

alamarBlue reagent, resazurin, is reduced to resorufin through metabolic processes that take place during cell division and the extent of reduction is correlated to the amount of cellular growth. The alamarBlue® reagent was added to the OBM in the wells in a 1:40 dilution 24 hours prior to UV-VIS analysis on Days 1, 4 and 7. The absorbance of the alamarBlue reagent at 570 nm, corresponding to resorufin, was collected for all nine samples at each day using an Agilent Technologies Cary 100 UV-VIS spectrometer. The absorbance values of all of the composites on all days were normalized to the control 100% CaAlO.

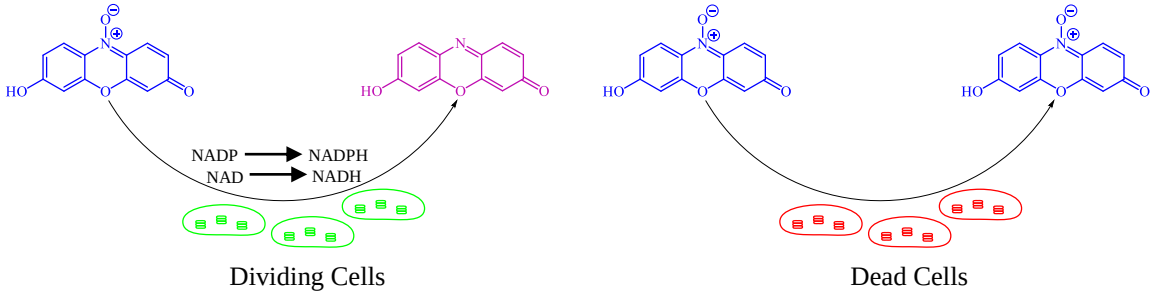

Figure 3.2: AlamarBlue® assay for osteoblast proliferation. If there are living, dividing cells in the wells, the alamarBlue® reagent is reduced and a color change can be observed and quantified by UV-VIS. If there are dead cells in the wells, the alamarBlue® reagent is not reduced.

3.2.7 Statistics

A one-way analysis of variance (ANOVA) with a Bonferroni post-hoc test was used to determine the averages and statistical differences between the NHOst attachment, viability and proliferation at the $p<0.05$ level of significance and all data is reported as mean ± standard error.

3.3 Results

3.3.1 Osteoblast Attachment to 1-5% HA

To determine if the incorporation of the osteogenic HA into the CaAlO:HA material increased osteoblast attachment over control 100% CaAlO, NHOsts (LONZA) were cultured and seeded onto autoclaved discs (0-5% HA). Nine sterilized discs per time point were placed into a 48 well plate and loaded with 10,000 NHOsts. After 1, 4 and 7 days the cells were imaged using the Live/Dead® Viability/Cytotoxicity assay kit (Figure 3.3). Five images per disc were collected and the number of live cells was normalized to CaAlO.

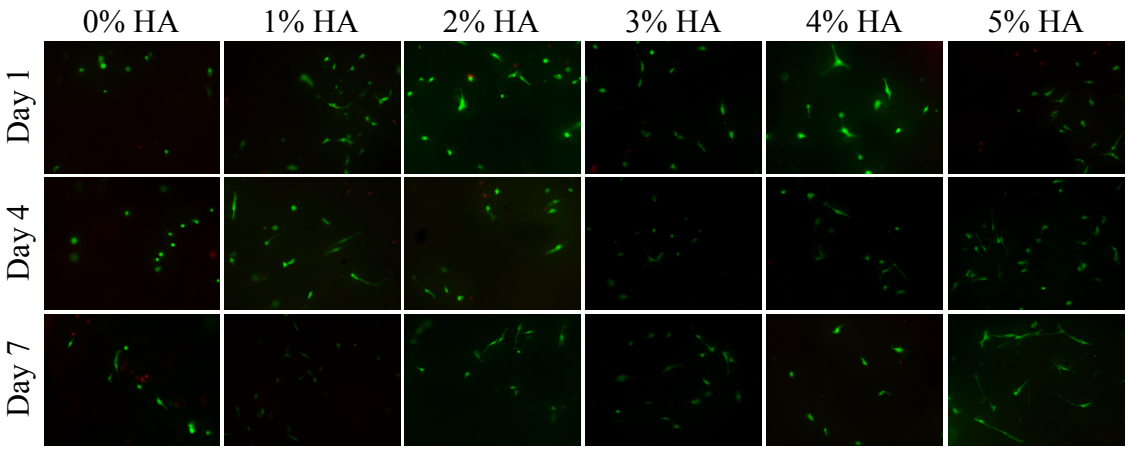

Figure 3.3: Representative Live/Dead® fluorescent images of osteoblasts attached to control 100% CaAlO and 1-5% HA composites on Days 1, 4 and 7.

On Day 1 the normalized average number of live osteoblast cells per view was: control CaAlO: 100.0 ± 11.9; 1% HA: 96.4 ± 5.8; 2% HA: 101.5 ± 5.8; 3% HA: 96.0 ± 5.9; 4% HA: 104.1 ± 4.8; 5% HA: 125.4 ± 6.0 (Figure 3.4). Only the 5% HA had a statistically greater number of attached live cells than control CaAlO.

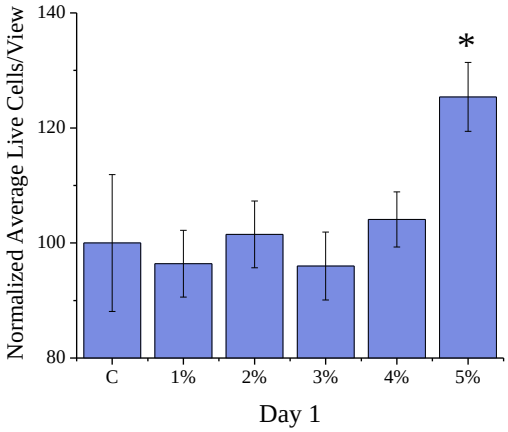

Figure 3.4: Day 1 normalized average number of live osteoblasts attached to control and 1-5% HA composites. * = statistically higher than control and all other composites. Data represented as mean ± standard error, $p<0.05$.

On Day 4 the normalized average number of live osteoblast cells per view was: control CaAlO: 100.0 ± 12.0; 1% HA: 141.9 ± 11.2; 2% HA: 146.2 ± 11.5; 3% HA: 143.2 ± 7.8; 4% HA: 145.8 ± 6.6; 5% HA: 185.7 ± 10.2 (Figure 3.5). Composites consisting of 1-4% HA had a statistically greater number of live cells than control, but were equivalent to one another. However, the 5% HA composite exhibited statistically increased live osteoblast attachment when compared to both the control and the 1-4% HA composites.

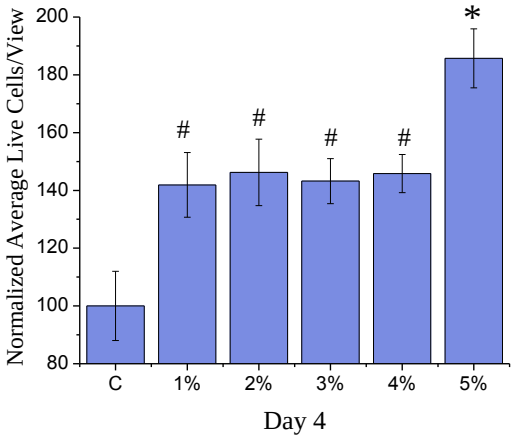

Figure 3.5: Day 4 normalized average number of live osteoblasts attached to control and 1-5% HA composites. # = statistically higher than control and * = statistically higher than control and all other composites. Data represented as mean ± standard error, $p<0.05$.

On Day 7 the normalized average number of live osteoblast cells per view was: control CaAlO: 100.0 ± 11.8; 1% HA: 121.2 ± 9.3; 2% HA: 124.7 ± 6.8; 3% HA: 126.4 ± 8.9; 4% HA: 117.4 ± 5.4; 5% HA: 142.4 ± 5.6 (Figure 3.6). Composites with 1-4% HA had a statistically greater number of live cells when compared to control CaAlO, but similar to Day 4 they were all statistically equal to one another. The 5% HA had a statistically the greater number of live cells than the control CaAlO and 1-4% HA composites.

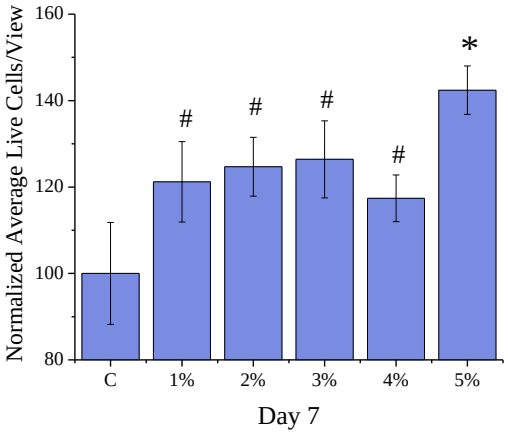

Figure 3.6: Day 7 normalized average number of live osteoblasts attached to control and 1-5% HA composites. # = statistically higher than control and * = statistically higher than control and all other composites. Data represented as mean ± standard error, $p<0.05$.

3.3.2 Osteoblast Viability on 1-5% HA

To examine the effect of HA on osteoblast viability, NHOsts (LONZA) were cultured and seeded onto autoclaved discs (0-5% HA). Nine sterilized discs per time point were placed into a 48 well plate and loaded with 10,000 NHOsts. After 1, 4 and 7 days the cells were imaged using the Live/Dead® Viability/Cytotoxicity assay kit. Five images per disc were collected. The number of live cells was divided by the total number of cells to determine the percent viability of the attached NHOsts.

On Day 1 the percent cell viability was: control CaAlO: 60.7 ± 4.7; 1% HA: 73.2 ± 2.3; 2% HA: 67.6 ± 2.5; 3% HA: 67.8 ± 2.5; 4% HA: 81.4 ± 1.6; 5% HA: 83.0 ± 1.7

(Figure 3.7). The 1%, 4% and 5% HA composites had statistically higher percent cell viability than control CaAlO. The 2% and 3% HA composites did not have an increased percent cell viability on Day 1 over control.

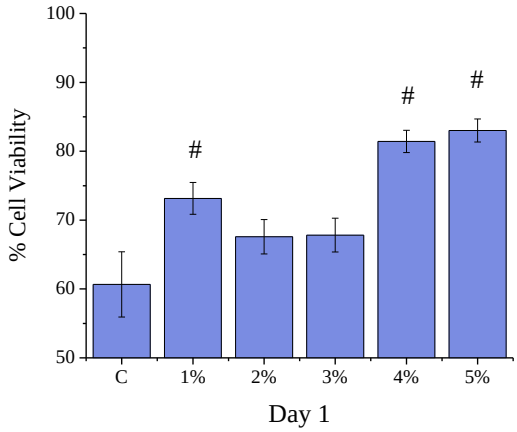

Figure 3.7: Day 1 percent viability of attached cells on control and 1-5% HA composites. # = statistically higher than control. Data represented as mean ± standard error, $p<0.05$.

The percent cell viability on Day 4 was: control CaAlO: 57.5 ± 4.2; 1% HA: 74.2 ± 2.3; 2% HA: 77.0 ± 2.5; 3% HA: 81.6 ± 1.6; 4% HA: 79.5 ± 1.6; 5% HA: 81.7 ± 2.1 (Figure 3.8). All of the 1-5% HA composites had statistically increased percent cell viability when compared to control CaAlO.

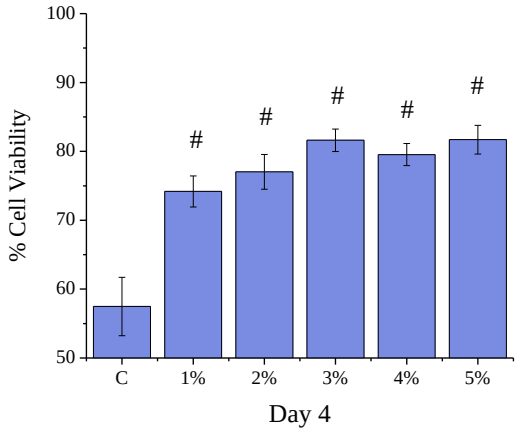

Figure 3.8: Day 4 percent viability of attached cells on control and 1-5% HA composites. # = statistically higher than control. Data represented as mean ± standard error, $p<0.05$.

On Day 7 the percent cell viability was: control CaAlO: 69.6 ± 4.2; 1% HA: 81.2 ± 2.8; 2% HA: 88.1 ± 1.5; 3% HA: 84.6 ± 1.9; 4% HA: 87.6 ± 1.3; 5% HA: 84.9 ± 1.6 (Figure 3.9). Again, the percent viability was significantly higher on all of the composites compared to control CaAlO.

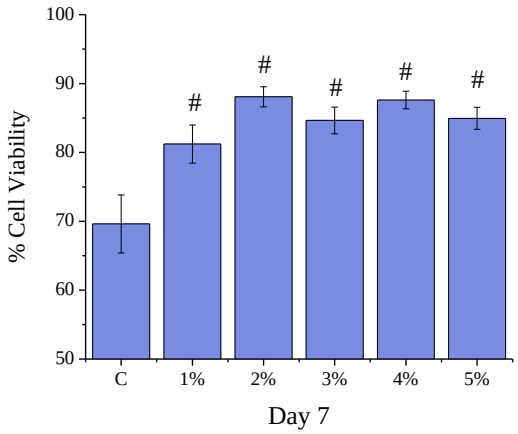

Figure 3.9: Day 7 percent viability of attached cells on control and 1-5% HA composites. # = statistically higher than control. Data represented as mean ± standard error, $p<0.05$.

3.3.3 Osteoblast Proliferation on 1-5% HA

To determine if the presence of HA had an effect on osteoblast proliferation, NHOsts were cultured and seeded onto sterilized discs (0-5% HA). Nine discs at each time point were placed into 48 well plates and loaded with 10,000 NHOsts. Before evaluating osteoblast proliferation, the alamarBlue® reagent was diluted in the OBM. After 1, 4 and 7 days the OBM was examined using UV-VIS spectroscopy (Figure 3.10). The absorbance of the OBM from each well was collected and normalized to control CaAlO.

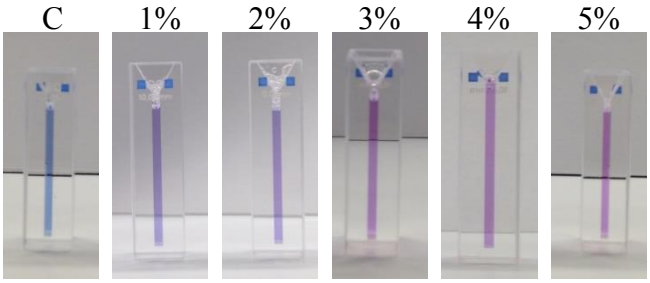

Figure 3.10: Representative OBM solutions for Day 7 of the alamarBlue® assay for control and 1-5% HA.

On Day 1 the normalized average absorbance was: control CaAlO: 1.00 ± 0.02, 1% HA: 1.00 ± 0.03, 2% HA: 1.06 ± 0.02, 3% HA: 1.12 ± 0.03, 4% HA: 1.24 ± 0.02, and 5% HA: 1.22 ± 0.03 (Figure 3.11). Based on the absorbance, the 4% and 5% HA composites exhibited a statistically greater amount of cell proliferation compared to all other samples, while the 2% and 3% HA were higher than 1% HA and control.

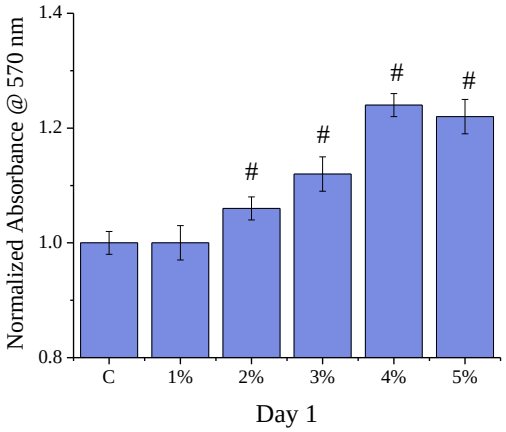

Figure 3.11: Day 1 normalized absorbance at 570 nm of control and 1-5% HA composites. # = statistically higher than control. Data represented as mean ± standard error, $p<0.05$.

All of the composites had significantly increased cell proliferation compared to control by Day 4, however the 5% HA supported the greatest amount of proliferation. The normalized average absorbance on Day 4 was: control CaAlO: 1.00 ± 0.01, 1% HA: 1.09

± 0.02, 2% HA: 1.12 ± 0.01, 3% HA: 1.12 ± 0.01, 4% HA: 1.14 ± 0.02, and 5% HA: 1.20 ± 0.03 (Figure 3.12).

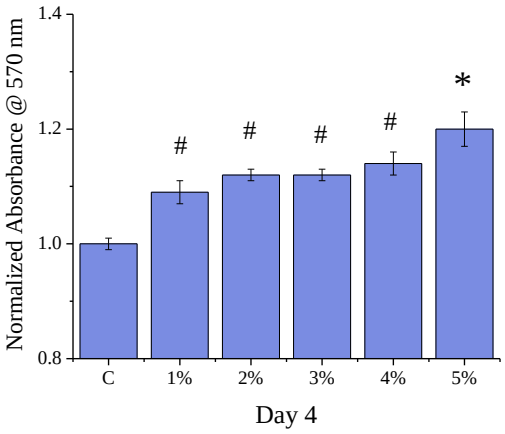

Figure 3.12: Day 4 normalized absorbance at 570 nm of control and 1-5% HA composites. # = statistically higher than control and * = statistically higher than control and all other composites. Data represented as mean ± standard error, $p<0.05$.

At Day 7 the normalized average absorbance was: control CaAlO: 1.00 ± 0.02, 1% HA: 1.22 ± 0.02, 2% HA: 1.23 ± 0.02, 3% HA: 1.34 ± 0.04, 4% HA: 1.41 ± 0.06 and 5% HA: 1.51 ± 0.03 (Figure 3.13). Similar to Day 4, all of the composites exhibited significantly greater cell proliferation than the control CaAlO. The cells on the 5% HA composite again supported the highest amount of proliferation.

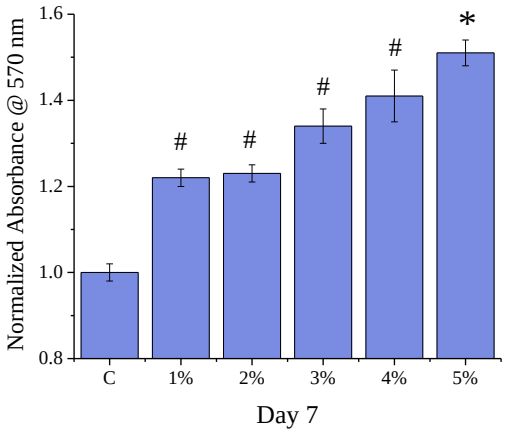

Figure 3.13: Day 7 normalized absorbance at 570 nm of control and 1-5% HA composites. # = statistically higher than control and * = statistically higher than control and all other composites. Data represented as mean ± standard error, $p<0.05$.

3.4 Discussion

The osteogenic HA phase was shown to be present at the composite surface without adversely affecting the mechanical integrity of the material. *In vitro* osteoblast tests examined if increasing the amount of HA at the interface played a significant role in bone cell performance when cultured on the composites. The composites were evaluated for their ability to increase osteoblast attachment and percent viability, and their ability to support increased cell proliferation. If the presence of the osteoinductive HA at the interface plays a significant role in the osteoblast response, the materials with increasing amounts of HA should result in the best composite material.

On the extended time points of the osteoblast assays (Days 4 and 7), the 5% HA composites had the greatest number of attached live cells and supported the greatest amount of cell proliferation, compared to control CaAlO and the 1-4% HA composites. Whereas the percent viability of attached cells was increased on all composites over control CaAlO. The greatest increase in cell attachment and proliferation on the 5% HA is the result of the exposure of the cells to the osteoconductive and osteoinductive HA at the tissue-material interface. This result is in agreement with the work of Pino-Minguez and coworkers, where they demonstrated the maximum amount of osteoblast growth, proliferation and differentiation at higher percentage composites of PMMA and HA.[25] In their work, they observed the maximum cellular response between 15% and 20% HA, and found that at greater than 20% HA the PMMA:HA composites lost their mechanical integrity.[25]

Based on the physical and biological evaluation of the 1-5% HA composites, the 5% HA composite is the most applicable for a cancellous bone scaffold material. The 5% HA had an elastic modulus and modulus of rupture similar to non-load bearing cancellous

bone and consistently resulted in increased osteoblast attachment, viability and proliferation on all days examined. This composite was the only one to enhance cellular response on each day examined. These results are in agreement with previous work in the literature that has demonstrated that composite materials containing HA increase bone regeneration more than the non-HA containing materials.[23-25] Further, this CaAlO:HA composite material is mechanically stronger than HA alone and is easier to synthesize.

More importantly, in the past increased *in vitro* osteoblast performance and *in vivo* bone regeneration using CaAlO based materials required interfacial modification with biomolecules.[6,23,28,33] Various organic molecules, cell adhesion peptides and osteogenic proteins have been immobilized to the CaAlO in order to increase bone cell response.[6,23,28,33] A result of the necessity to chemically modify the material is multiple synthetic reaction steps. These synthetic steps may introduce harmful chemicals to the materials, result in the deactivation of the linked biomolecule or require two separate reaction systems to simultaneously immobilize multiple functionalities on the material.[6,23,28,33] In using this materials-based approach, where composites that contain HA at the interface, bone cells are able to perform significantly better than control samples and interfacial modification of the material is not required.[25]

3.5 Conclusions

In vitro osteoblast attachment, percent viability and proliferation were all successfully enhanced on the RT formed 1-5% HA composites. Through the incorporation of osteogenic HA into the composite, and the HA phase presence at the material interface (confirmed using SEM-EDS) all of the indicators of cellular response were improved

compared to 100% CaAlO at the extended time points, Days 4 and 7. Further, the 5% HA composite was the only material that resulted in increased cell attachment, percent viability and proliferation at the short time point, Day 1. Not only was the 5% HA the only material to mechanically match the elastic modulus and modulus of rupture of non-load bearing cancellous bone, but it was also the only material that significantly increased osteoblast attachment, percent viability and proliferation on all days examined. Based on these results the 5% HA is the appropriate CaAlO:HA composite to use when increased cellular response is desired on mechanically relevant materials.

3.6 References

1. Adamczyk, Z.; Barbasz, J.; Cieśla, M. Mechanisms of fibrinogen adsorption at solid substrates. *Langmuir* **2011**, *27*, 6868-6878.

2. Fuss, C.; Palmaz, J. C.; Sprague, E. A. Fibrinogen: Structure, function, and surface interactions. *J. Vasc. Interv. Radiol.* **2001**, *12*, 677-682.

3. Ratner, B.; Hoffman, A.; Schoen, F.; Lemons, J. *Biomaterials Science: An Introduction to Materials in Medicine*, 3rd ed; Elsevier: London, 2004.

4. Siegismund, D.; Keller, T. F.; Jandt, K. D.; Rettenmayr, M. Fibrinogen adsorption on biomaterials–A numerical study. *Macromol. Biosci.* **2010**, *10*, 1216-1223.

5. Hersel, U.; Dahmen, C.; Kessler, H. RGD modified polymers: Biomaterials for stimulated cell adhesion and beyond. *Biomaterials* **2003**, *24*, 4385-4415.

6. Palchesko, R. N.; Romeo, J. D.; McGowan, K. A.; Gawalt, E. S. Increased osteoblast adhesion on physically optimized KRSR modified calcium aluminate. *J. Biomed. Mater. Res., Part A* **2012**, *100*, 1229-1238.

7. Sun, S.; Yu, W.; Zhang, Y.; Zhang, F. Increased preosteoblast adhesion and osteogenic gene expression on TiO_2 nanotubes modified with KRSR. *J. Mater. Sci. Mater. Med.* **2013**, *24*, 1079-1091.

8. Mann, B. K.; West, J. L. Cell adhesion peptides alter smooth muscle cell adhesion, proliferation, migration, and matrix protein synthesis on modified surfaces and in polymer scaffolds. *J. Biomed. Mater. Res.* **2002**, *60*, 86-93.

9. Xiao, S. J.; Textor, M.; Spencer, N. D.; Sigrist, H. Covalent attachment of cell-adhesive,(Arg-Gly-Asp)-containing peptides to titanium surfaces. *Langmuir* **1998**, *14*, 5507-5516.

10. Maddikeri, R.; Tosatti, S.; Schuler, M.; Chessari, S.; Textor, M.; Richards, R.; Harris, L. Reduced medical infection related bacterial strains adhesion on bioactive RGD modified titanium surfaces: A first step toward cell selective surfaces. *J. Biomed. Mater. Res., Part A* **2008**, *84*, 425-435.

11. Sawyer, A.; Hennessy, K.; Bellis, S. Regulation of mesenchymal stem cell attachment and spreading on hydroxyapatite by RGD peptides and adsorbed serum proteins. *Biomaterials* **2005**, *26*, 1467-1475.

12. Sawyer, A. A.; Hennessy, K. M.; Bellis, S. L. The effect of adsorbed serum proteins, RGD and proteoglycan-binding peptides on the adhesion of mesenchymal stem cells to hydroxyapatite. *Biomaterials* **2007**, *28*, 383-392.

13. Salinas, C. N.; Anseth, K. S. The influence of the RGD peptide motif and its contextual presentation in PEG gels on human mesenchymal stem cell viability. *J. Tissue Eng. Regener. Med.* **2008**, *2*, 296-304.

14. Shu, X. Z.; Ghosh, K.; Liu, Y.; Palumbo, F. S.; Luo, Y.; Clark, R. A.; Prestwich, G. D. Attachment and spreading of fibroblasts on an RGD peptide–modified injectable hyaluronan hydrogel. *J. Biomed. Mater. Res., Part A* **2004**, *68*, 365-375.

15. Lai, Y.; Xie, C.; Zhang, Z.; Lu, W.; Ding, J. Design and synthesis of a potent peptide containing both specific and non-specific cell-adhesion motifs. *Biomaterials* **2010**, *31*, 4809-4817.

16. Lee, M. H.; Brass, D. A.; Morris, R.; Composto, R. J.; Ducheyne, P. The effect of non-specific interactions on cellular adhesion using model surfaces. *Biomaterials* **2005**, *26*, 1721-1730.

17. Mrksich, M. A surface chemistry approach to studying cell adhesion. *Chem. Soc. Rev.* **2000**, *29*, 267-273.

18. Woo, K. M.; Seo, J.; Zhang, R.; Ma, P. X. Suppression of apoptosis by enhanced protein adsorption on polymer/hydroxyapatite composite scaffolds. *Biomaterials* **2007**, *28*, 2622-2630.

19. Dee, K. C.; Andersen, T. T.; Bizios, R. Design and function of novel osteoblast-adhesive peptides for chemical modification of biomaterials. *J. Biomed. Mater. Res.* **1998**, *40*, 371-377.

20. Balasundaram, G.; Webster, T. J. Increased osteoblast adhesion on nanograined Ti modified with KRSR. *J. Biomed. Mater. Res., Part A* **2007**, *80*, 602-611.

21. Schuler, M.; Hamilton, D. W.; Kunzler, T. P.; Sprecher, C. M.; de Wild, M.; Brunette, D. M.; Textor, M.; Tosatti, S. G. Comparison of the response of cultured osteoblasts and osteoblasts outgrown from rat calvarial bone chips to nonfouling KRSR and FHRRIKA-peptide modified rough titanium surfaces. *J. Biomed. Mater. Res., Part B* **2009**, *91*, 517-527.

22. Nelson, M.; Balasundaram, G.; Webster, T. J. Increased osteoblast adhesion on nanoparticulate crystalline hydroxyapatite functionalized with KRSR. *Int.J. Nanomed.* **2006**, *1*, 339-349.

23. Miljkovic, N. D.; Cooper, G. M.; Hott, S. L.; DiSalle, B. F.; Gawalt, E. S.; Smith, D. M.; McGowan, K.; Marra, K. G. Calcium aluminate, RGD-modified calcium aluminate, and β-tricalcium phosphate implants in a calvarial defect. *J. Craniofac. Surg.* **2009**, *20*, 1538-1543.

24. Ball, M.; Downes, S.; Scotchford, C.; Antonov, E.; Bagratashvili, V.; Popov, V.; Lo, W. J.; Grant, D.; Howdle, S. Osteoblast growth on titanium foils coated with hydroxyapatite by pulsed laser ablation. *Biomaterials* **2001**, *22*, 337-347.

25. Pino-Mínguez, J.; Jorge-Mora, A.; Couceiro-Otero, R.; García-Santiago, C. Study of the viability and adhesion of osteoblast cells to bone cements mixed with hydroxyapatite at different concentrations to use in vertebral augmentation techniques. *Rev. Esp. Cir. Ortop. Traumatol.* **2015**, *59*, 122-128.

26. Mujeeb, A.; Miller, A. F.; Saiani, A.; Gough, J. E. Self-assembled octapeptide scaffolds for in vitro chondrocyte culture. *Acta Biomater.* **2013**, *9*, 4609-4617.

27. Chen, S.; Mantei, N.; Dong, L.; Schachner, M. Prevention of neuronal cell death by neural adhesion molecules L1 and CHL1. *J. Neurobiol.* **1999**, *38*, 428-439.

28. Palchesko, R. N.; Buckholtz, G. A.; Romeo, J. D.; Gawalt, E. S. Co-immobilization of active antibiotics and cell adhesion peptides on calcium based biomaterials. *Mater. Sci. Eng., C* **2014**, *40*, 398-406.

29. Shor, L.; Güçeri, S.; Wen, X.; Gandhi, M.; Sun, W. Fabrication of three-dimensional polycaprolactone/hydroxyapatite tissue scaffolds and osteoblast-scaffold interactions in vitro. *Biomaterials* **2007**, *28*, 5291-5297.

30. San Thian, E.; Huang, J.; Best, S. M.; Barber, Z. H.; Brooks, R. A.; Rushton, N.; Bonfield, W. The response of osteoblasts to nanocrystalline silicon-substituted hydroxyapatite thin films. *Biomaterials* **2006**, *27*, 2692-2698.

31. Nakayama, G. R.; Caton, M. C.; Nova, M. P.; Parandoosh, Z. Assessment of the alamarBlue assay for cellular growth and viability in vitro. *J. Immunol. Methods* **1997**, *204*, 205-208.

32. Voytik-Harbin, S. L.; Brightman, A. O.; Waisner, B.; Lamar, C. H.; Badylak, S. F. Application and evaluation of the alamarBlue assay for cell growth and survival of fibroblasts. *In Vitro Cell. Dev.-An.* **1998**, *34*, 239-246.

33. Clafshenkel, W. P.; Rutkowski, J. L.; Palchesko, R. N.; Romeo, J. D.; McGowan, K. A.; Gawalt, E. S.; Witt-Enderby, P. A. A novel calcium aluminate-melatonin scaffold enhances bone regeneration within a calvarial defect. *J. Pineal Res.* **2012**, *53*, 206-218.

Chapter 4: Creating a Multifunctional Composite Ceramic by Antimicrobial Peptide Immobilization to the 5% HA

4.1 Introduction

The formation of bacterial biofilms on the surfaces of medical implants is a serious clinical problem that may result in infection, implant failure, revision surgery and death.[1-7] Between 5-14% of initial orthopedic joint replacement surgeries result in implant failure.[8-10] Bacterial biofilms are chronic infections that occur on implant surfaces and are one of the most serious causes of implant failure.[11-13] Infection typically occurs at the time of surgery, where bacteria on the skin can enter the wound and colonize the implant surface.[3,12-17] Therefore, limiting bacterial attachment to the implant is important in limiting implant failure.

Upon attachment the planktonic bacteria undergo a phenotype change into sessile organisms which produce a protective polysaccharide matrix and have a reduced need for nutrients.[14,16,18] The extracellular matrix protects the bacteria from their surrounding environment, including any antibiotics that may be employed for treatment.[19-21] Further, the matrix-enclosed bacteria can spread to other regions of the body, through shedding of biofilm clusters or the release of planktonic cells, making it difficult to determine the infection location and can lead to severe infections and even death (Figure 4.1).[2,10,13,14,17,22] Conventional treatments are frequently insufficient because they require high doses of antibiotics and contribute to antibiotic resistance in the biofilm.[5,23-26] Frequently the only way to treat a biofilm infection is to remove the implant and install a new one, however this does not eliminate the risk of re-infection of the new material.[12,13,15,17,27]

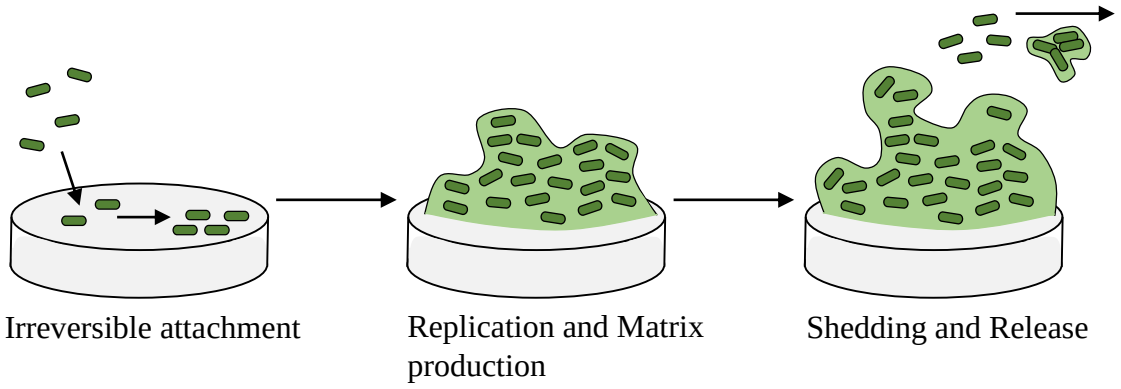

Figure 4.1: Steps in biofilm formation on the implant surface include irreversible bacterial attachment of planktonic bacteria, bacterial replication and polysaccharide matrix production and shedding of biofilm clusters and release of planktonic cells.

Since the bacteria within the biofilm are sessile and tend to not grow and divide, current research aims to prevent biofilm formation by limiting the initial bacterial attachment.[28-30] Some approaches include the use of physical adsorption of antibiotics into the biomaterials, that way when placed into the physiological environment, the antibiotics leach from the material and treat the bacteria that are in the biomaterials vicinity.[31-33] In using this approach, groups have seen that the majority of the antibiotics tend to release from the material very rapidly and do not remain localized to surgical site.[34,35] In other studies, antibiotics have been covalently immobilized to the materials in an attempt to keep the treatment localized to the surgical site.[36,37] Many studies have shown that this approach keeps the antibiotic localized to the material and that the antibiotics maintain some form of activity against bacterial challenge.[36,37] However, other work has shown that the immobilization of antimicrobials reduces their effectiveness against bacteria.[38] Also, reaction schemes must be developed that use functional groups within the antibiotic that are not part of the mechanism of action, and because the antibiotics have specific modes of action, the orientation of the immobilized molecules must be considered.[39,40]

As an approach to limit the risk of development of antibiotic resistant bacterial strains, antimicrobial peptides (AMP) are being investigated.[41-43] AMPs are short peptides that are part of the innate immune response to pathogens.[44] Many AMPs have broad spectrum efficacy against both gram positive and gram negative bacteria.[44,45] Most importantly AMPs have low minimum inhibitory concentrations and a fast-acting mechanism.[44] AMPs form membrane pores that compromise cell viability, this is important in biofilm applications because the AMP mechanism of action does not rely on bacteria growth and division like it does in many common antibiotics (Figure 4.2).[44,46-48]

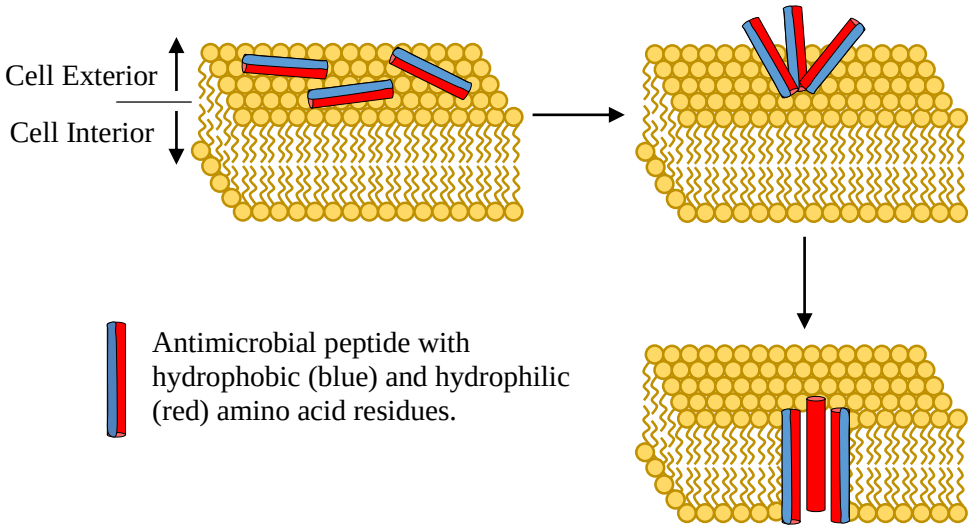

Figure 4.2: A proposed mechanism of AMP action is membrane pore formation where hydrophobic amino acids allow for intercalation of the peptide into the phospholipid membrane of bacteria, and hydrophilic amino acids form the interior of the pore.

Inverso-CysHHC10 is a synthetic AMP (H-CKRWWKWIRW-NH_2, all D-amino acids, Scheme 4.1) shown to be highly effective against common biofilm forming bacteria either when in solution or when covalently incorporated into a flexible polyethylene glycol hydrogel.[49,50] HHC10 has an LC99.9 (lethal concentration to 99.9% of inocula) of 8 μM against the common biofilm forming bacteria, *S. aureus*, *S. epidermidis* and *E. coli*.[49,50]

HHC10 is also proteolytically stable because it is composed of the nonproteinogenic D-amino acids. It has been shown that greater than 90% of HHC10 remains intact after soaking in pooled human serum for 25 hours.[49] The HHC10 was also shown to be non-cytotoxic to sheep erythrocytes, as only 1% of the initially seeded cells did not survive after incubation with HHC10.[49] Lastly, HHC10 has been amended to include the cysteine residue at the N-terminus of the peptide. Cleophas et al demonstrated that the addition of this cysteine residue does not affect the activity of the AMP in solution, and the cysteine residue facilitates the ease of immobilization of HHC10 to materials.[50]

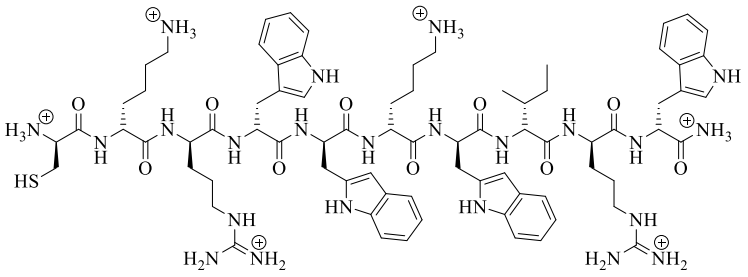

Scheme 4.1: Inverso-CysHHC10 containing the hydrophobic tryptophan and isoleucine amino acids and hydrophilic arginine and lysine amino acids. The sacrificial cysteine is appended to the N-terminus.

The goal in this work was to covalently attach HHC10 to the mechanically optimized and biologically preferred 5% HA composite to add antimicrobial properties to the synthetic graft material. Each of the two steps in the attachment were verified using DRIFT and the activity of the linked HHC10 against *E. coli* was evaluated using the NPN uptake assay and a bacterial turbidity test. Lastly, in an ideal multifunctional system the function of one modification should not affect the function of another. Therefore osteoblast performance on the HHC10 modified 5% HA discs was also re-examined.

4.2 Materials and Methods

4.2.1 Materials

Calcium aluminum oxide (CaAlO) was supplied by CAberTech, Inc. (Monessen, PA). Calcium phosphate tribasic and 2-hydroxy-4'-(2-hydroxyethoxy)-2-methylpropiophenone (Irgacure 2959, 98%) were purchased from Sigma-Aldrich. Phosphoric acid (Certified ACS), tetrahydrofuran (THF, Optima, 99.9%) and 4-(2-hydroxyethyl)-piperazine ethanesulfonic acid (HEPES, 99%) were obtained from Thermo Fisher Scientific. The THF was distilled over sodium and benzophenone prior to use. 16-heptadecenoic acid (16-ene, 97%) was purchased from Apollo Scientific and N,N-dimethylformamide (DMF, 99.8%) from Acros Organics. The antimicrobial peptide, Inverso-CysHHC10, (HHC10, >90.0%, H-CKRWWKWIRW-NH_2) was obtained from GenScript USA, Inc. as a lyophilized powder and reconstituted in doubly distilled water (ddH_2O). N-phenylnaphthylamine (NPN, 98%) was purchased from Ultra Scientific and Luria Bertani medium (LB media) was from MP Biomedicals. The LB media capsules were dissolved in 50 mL of ddH_2O and autoclaved before use. *Escherichia coli* (ATCC® 25922) was obtained from ATCC. Normal human osteoblasts, osteoblast subculturing reagents (HEPES buffered saline, Trypsin/EDTA, Trypsin neutralizing solution) and osteoblast basal medium (OBM) were purchased from LONZA (Walkersville, MD). The Live/Dead® Viability/Cytotoxicity Assay Kit and alamarBlue® reagent were purchased from Life Technologies. All materials and chemicals were used as received unless otherwise noted.

4.2.2 Casting Composite 5% HA

Calcium aluminum oxide:hydroxyapatite (HA) composite discs (5% HA only) were cast using the same method previously described in Chapter 2 and 3. First the three different aggregate sizes of CaAlO (-30+60, -60 and -200) were dry mixed in a 1:1:2 ratio. Upon thorough mixing, ground $Ca_3(PO_4)_2$ was added to the mixed CaAlO powder at a mass appropriate for the final composition to be 5% HA. The powders were thoroughly dry mixed together and hydrated with 0.3 mL of ddH_2O per gram CaAlO and 1.1 mL H_3PO_4 per gram $Ca_3(PO_4)_2$ in the composite. The paste thickened for 10 minutes, then was poured into the 6x2 mm cylindrical molds. The paste set for four hours, then was rehydrated using H_3PO_4 and allowed to set overnight. Composites were hydrated again the next day with H_3PO_4 and permitted to set overnight. The following day composites were removed from the mold and rehydrated in H_3PO_4 for 24 hours. The 5% HA discs were sterilized before cellular and bacterial studies by autoclaving at 121°C and 18 psi of steam for 60 minutes with fast exhaust.

4.2.3 Covalent Antimicrobial Peptide Immobilization

The antimicrobial peptide Inverso-CysHHC10 was attached to the 5% HA surface using a two-step solution deposition method. First, warm (60°C) 5% HA discs were immersed in a 1 mM 16-heptadecenoic acid (16-ene) solution (dry THF) for one hour at room temperature. Excess solvent was removed by placing the discs on a 0.1 torr vacuum line for 24 hours. The 16-ene modified discs were then placed into a solution of 1 mg/mL HHC10 and 0.5 mg/mL Irgacure 2959 in 10:1 ddH_2O:DMF.[51] The HHC10 solution

containing the 16-ene modified discs was then reacted under 365 nm UV light for 3 hours with N_2 purge. Again, excess solvent was removed on a 0.1 torr vacuum line for 24 hours (Scheme 4.2). Both 16-ene and HHC10 modified 5% HA discs were rinsed in solvent prior to analysis. Discs were sterilized by autoclaving at 121°C and 18 psi of steam for 60 minutes with fast exhaust prior to cellular and bacterial assays.

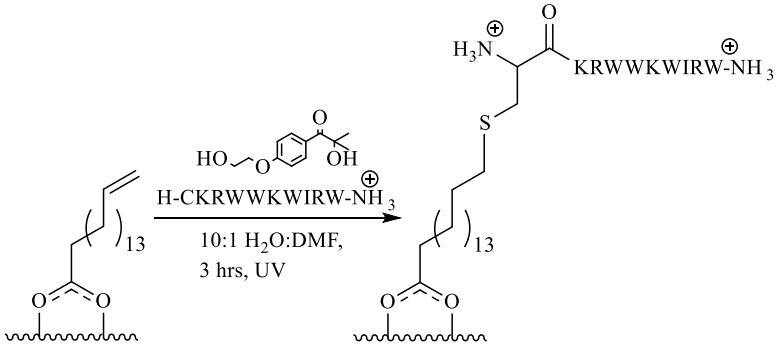

Scheme 4.2: Reaction sequence utilized for the covalent immobilization of HHC10 to composite 5% HA. First the material is modified with 16-heptadecenoic acid, then an alkene-thiol click reaction is used to link HHC10 at the interface.

4.2.4 Diffuse Reflectance Infrared Fourier Transform Spectroscopy

A Thermo Nicolet Nexus 470 FT-IR spectrophotometer equipped with a diffuse reflectance attachment was used to obtain spectra of the modified composites following each step of HHC10 immobilization. Each step of the covalent modification served as the background spectra for the subsequent step in the sequence. Spectra were collected for 1024 spectral scans (4000-400 cm^{-1}) with a resolution of 4 cm^{-1}.

4.2.5 Quantification of Antimicrobial Peptide Immobilization on 5% HA

Using a Horiba Scientific Fluoromax-4 Spectrofluorometer, the amount of HHC10 immobilized to the 5% HA was measured. Quantification using fluorimetry was possible because HHC10 contains four tryptophan residues, with the fluorescent indole side chain, and an excitation wavelength of 285 nm.[52,53] A five point calibration curve with stock concentrations of 0.025, 0.050, 0.075, 0.100 and 0.200 mg of HHC10 per mL of 10:1 ddH_2O:DMF was prepared (n=5 per concentration). The stock solutions were prepared using the same reaction conditions that were used to immobilize HHC10 to the 5% HA, described in Section 4.2.3. Fluorescence emission spectra were collected from 250-450 nm with the maximum emission used for quantification observed at 342 nm. Ten HHC10 modified 5% HA discs were prepared using a 1 mg/mL HHC10 solution with 0.5 mg/mL Irgacure 2959 in 10:1 ddH_2O:DMF and 16-heptadecenoic acid modified 5% HA discs (prepared as described in Section 4.2.3). After the immobilization reaction was complete, the 5% HA discs were removed from the solution and the solution fluorescence was collected. The concentration of HHC10 remaining in the solution was quantified using the calibration curve. The resulting average change in concentration from before HHC10 immobilization to after was correlated to how much HHC10 had been immobilized to the 5% HA discs (n=10).

4.2.6 Quantification of Antimicrobial Peptide Released from Modified 5% HA

To quantify the amount of HHC10 that remained immobilized to the 5% HA discs, direct infusion mass spectrometry was used. Six HHC10 modified 5% HA discs were soaked in 2 mL of ddH_2O for 1, 3.5 and 24 hours. At each time point the discs were removed from the water and moved into a fresh 2 mL of ddH_2O. The ddH_2O from each time point was filtered using a 0.2 μm syringe filter and 0.1% formic acid (total volume) was added to assist in the HHC10 ionization process. A five point calibration curve based on the instrument signal at $[HHC10+3H]^{3+}$ was prepared with concentrations of $9.0x10^{-9}$, $5.0x10^{-8}$, $1.5x10^{-7}$, $3.0x10^{-7}$ and $5.0x10^{-7}$ M, all with 0.1% formic acid (n=5 per concentration). The six samples at each time point were then analyzed with an Agilent Technologies 6530 Accurate-Mass Quadrupole-Time of Flight Liquid Chromatography/Mass Spectrometry (Q-TOF MS) with High Performance Liquid Chromatography-Chip Cube Mass Spectrometry Interface using an FIA-Chip (II). Samples were analyzed in positive ionization mode using the following instrument settings: Gas temperature=325°C, Drying gas=4.0 L/min, Capillary voltage=1900 V, Fragmentor voltage=175 V, Skimmer voltage=65 V and Octapole1 voltage=750 V. Sample and stock solutions were subtracted from a ddH_2O and 0.1% formic acid background and the concentration of HHC10 in solution was quantified using the calibration curve (n=6). Based on the volume of the samples, the mass of HHC10 in solution was determined and the percent of HHC10 remaining linked after soaking was calculated based on the amount immobilized determined in Section 4.2.5.

4.2.7 *Escherichia coli* Culture

Escherichia coli (*E. coli*) purchased for American Type Culture Collection (ATCC® 25922) were thawed from a -80°C freezer and placed into a T-25 cm^2 cell culture flask. One full inoculation loop of *E. coli* was added to 15 mL of the prepared LB media and placed onto the shaker incubator. Flasks of *E. coli* were left in the shaker incubator long enough to grow to an optical density at 600 nm ($OD_{600\ nm}$) of 0.5 for the N-phenylnaphthylamine uptake assay and 0.1 for the bacterial turbidity test.

4.2.8 *Escherichia coli* NPN Uptake Factor on Modified 5% HA

A fluorescence assay based on the uptake of a nonpolar probe, N-phenylnaphthylamine (NPN), was used to monitor the changes in permeability of the membrane of *E. coli* when mixed with HHC10 modified 5% HA discs.[54,55] If the bacteria membrane is compromised, NPN enters the phospholipid environment and increased fluorescence can be observed (Figure 4.3).

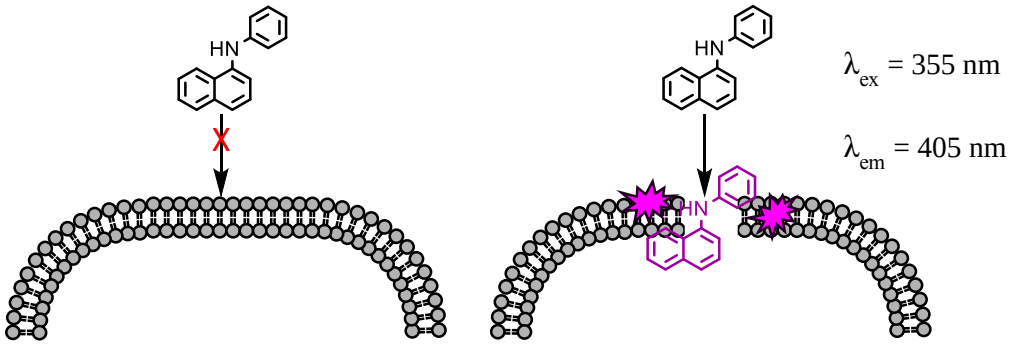

Figure 4.3: NPN uptake assay for determination of *E. coli* membrane permeability. If the HHC10 effectively lyses the membrane the NPN can enter the hydrophobic environment and increased fluorescence of NPN can be observed. If the membrane remains intact the NPN cannot enter and fluorescence is not observed.

A planktonic *E. coli* culture was grown to an initial optical density at 600 nm ($OD_{600\ nm}$) of 0.5 in Luria-Bertani media (LB media). The cells were centrifuged for 10 minutes at 1000 g, then resuspended in one-half of their initial volume of 5 mM HEPES at pH 7.2. A 5 mM NPN solution, in acetone, was prepared, and diluted to 40 μM with HEPES immediately before use.

For a standard fluorescence measurement using the PerkinElmer VICTOR^3 Multilabel Plate Reader, the microtitre plate wells (ten/sample) were supplemented with 200 μL total of HEPES, *E. coli*, NPN and 5% HA discs, dependent on the sample. Wells that contained *E. coli* and NPN always had 100 μL and 50 μL respectively, with HEPES accounting for the remaining volume. Sample wells were (i) HEPES + unmodified 5% HA disc; (ii) HEPES + NPN + unmodified 5% HA disc; (iii) HEPES + *E. coli* + unmodified 5% HA disc; (iv) HEPES + *E. coli* + NPN + unmodified 5% HA disc; (v) HEPES + *E. coli* + HHC10 modified 5% HA disc; (vi) HEPES + *E. coli* + NPN + HHC10 modified 5% HA disc. The *E. coli* solution was always added last, immediately preceding fluorescent measurement, and the values were collected within three minutes of *E. coli* addition. The NPN uptake factors were then calculated as a ratio of background-corrected (subtracted by the value in the absence of NPN) fluorescence values of the *E. coli* suspension and of the HEPES buffer.[54,55] The NPN uptake factor of the treated *E. coli* was normalized to the NPN uptake factor of untreated *E. coli* (n=1000).

4.2.9 *Escherichia coli* Bacterial Turbidity Tests with Modified 5% HA

An analysis based on bacterial optical density was used to monitor the effect of immobilized HHC10 on the growth of the gram-negative *E. coli* (Figure 4.4).[36,56] A planktonic culture of *E. coli* was diluted to an initial $OD_{600\ nm}$ of 0.1 in LB media. Two milliliters of the planktonic *E. coli* solution were placed into 15 mL centrifuge tubes. There were four tubes of each sample: (i) *E. coli* + unmodified 5% HA disc and (ii) *E. coli* + HHC10 modified 5% HA disc. After preparing the samples, the centrifuge tubes were placed in a shaker incubator at 37°C for 2.5 hours. After the incubation period, the $OD_{600\ nm}$ of each sample was recorded using an Agilent Technologies Cary 100 UV-VIS spectrometer. Three replicates of each sample were collected and the average $OD_{600\ nm}$ of HHC10 modified 5% HA (ii) treated *E. coli* was normalized to the untreated *E. coli* (i).

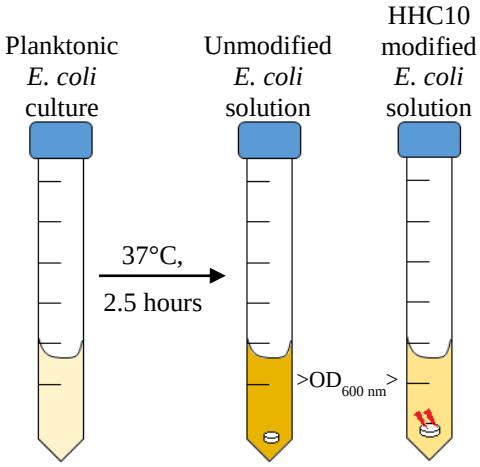

Figure 4.4: Bacterial turbidity test for the evaluation of *E. coli* growth in culture. If HHC10 reduces bacterial growth, the concentration of *E. coli* in solution will be smaller and the $OD_{600\ nm}$ will be lower than untreated bacteria.

4.2.10 Inverso-CysHHC10 Antimicrobial Activity in Solution and on Modified 5% HA

Using the NPN uptake factor and bacterial turbidity tests previously described in Section 4.2.8 and 4.2.9, the efficacy of the immobilized HHC10 against *E. coli* was compared to the free, in solution HHC10 to determine the concentration dosage that the linked AMP was equally as effective as.

In the NPN assay eight samples were prepared and treated using the same approach.[54,55] The first six samples were the same as those in Section 4.2.8 and now included (vii) HEPES + *E. coli* + 10 μM HHC10 solution (50 μL) + unmodified disc and (viii) *E. coli* + 10 μM HHC10 solution (50 μL) + NPN + unmodified 5% HA. The NPN uptake factors were calculated using the same method and the treated *E. coli* (both 10 μM solution and linked to 5% HA) were normalized to the untreated *E. coli*.

In the bacterial turbidity test, the bacteria was prepared using the same method and the two samples in Section 4.2.9 were the same and one additional sample was added (iii) *E. coli* + 10 μM HHC10 + unmodified 5% HA disc.[36,56] The average $OD_{600\,nm}$ of the treated *E. coli* (both solution and linked) was normalized to the untreated *E. coli*.

4.2.11 Osteoblast Cell Culture

NHOsts isolated from a 2 year old male were thawed from a -200°C liquid N_2 dewar and plated into T-25 cm^2 tissue culture flasks with at least 125,000 cells per flask in 5 mL of OBM. Tissue culture flasks were placed into an incubator at 37°C and 5% CO_2 for 24 hours so live osteoblasts could adhere to the interior. In the flasks, NHOst attachment and

division was monitored daily until approximately 80% confluence. OBM was changed daily after initial seeding during the days leading up to 80% confluence in the flask.

Once cells reached 80% confluence they were subcultured out of the flasks and a cell trial was begun. NHOsts were subcultured according to the protocol provided by LONZA and counted using the hemocytometer with Trypan Blue. Nine autoclaved HHC10 modified 5% HA discs per time point were placed into individual wells of 48 well plates labeled as Days 1, 4 and 7. NHOsts were then diluted to 10,000 cells per mL in OBM, and 1 mL of this NHOst solution was added to each well containing a disc. OBM was changed daily in the individual wells leading up to each time point.

4.2.12 Osteoblast Attachment to Modified 5% HA

NHOsts isolated from a 2 year old male were purchased from LONZA, cultured until 80% confluent and diluted to a concentration of 10,000 cells per mL of OBM. Three sample sets of three discs per time point (Days 1, 4 and 7, nine total discs) were autoclaved and seeded with 10,000 NHOsts. After 1, 4 and 7 days the number of attached live and dead cells was determined using the Live/Dead® Viability/Cytotoxicity assay kit from Life Technologies.[56-59] The number of live cells was counted on all 45 images for control unmodified 5% HA and HHC10 modified 5% HA. The amount of attached lived cells on HHC10 modified 5% HA was normalized to the control unmodified 5% HA.

4.2.13 Osteoblast Viability on Modified 5% HA

NHOsts isolated from a 2 year old male were cultured and treated the same as described in Section 4.2.11. Cells were again assayed using the Live/Dead®

Viability/Cytotoxicity assay kit and both the living (green) and dead (red) cells were counted on the 45 images collected for control and HHC10 modified 5% HA, obtaining a total number of cells. The number of live cells was divided by the number of total cells to determine percent viability.

4.2.14 Osteoblast Proliferation on Modified 5% HA

NHOsts isolated from a 2 year old male were cultured to 80% confluence and diluted to 10,000 cell per mL of OBM. Then 1 mL of the NHOst solution was added to nine wells containing autoclaved 5% HA discs. NHOst proliferation was evaluated using the alamarBlue® assay from Life Technologies.[14,60-63] The absorbance of the alamarBlue reagent in the OBM was collected for all nine samples at each time point. The absorbance of the OBM from the HHC10 modified 5% HA was normalized to the control unmodified 5% HA.

4.2.15 Statistics

A one-way analysis of variance (ANOVA) with a Bonferroni post-hoc test was used to determine the averages and statistical differences between the HHC10 immobilization and amount released, the *E. coli* NPN uptake factor and $OD_{600\ nm}$ for linked and free HHC10, and the NHOst attachment, viability and proliferation all at the $p<0.05$ level of significance and all data is reported as mean ± standard error.

4.3 Results

4.3.1 Covalent Antimicrobial Peptide Immobilization

To add antimicrobial activity to the 5% HA composite HHC10 was covalently immobilized to the surface. The covalent linkage of HHC10 to the 5% HA controls the location of the antimicrobial, resulting in a localized treatment aimed at preventing bacterial colonization and possible biofilm formation. The 5% HA composite was the only composite evaluated due to its mechanical similarity to non-loading bearing bone (Chapter 2) and the consistent, increased osteoblast attachment and proliferation on all days examined (Chapter 3).

To immobilize HHC10 to the surface of the 5% HA discs, warm (60°C) samples were immersed in a 1 mM solution of 16-ene (THF) for 1 hour at room temperature. Samples were removed from solution and placed onto a 0.1 torr vacuum line for 24 hours. The modified samples were analyzed using diffuse reflectance infrared Fourier transform (DRIFT) spectroscopy. The peaks corresponding to the asymmetric and symmetric methylene stretches, at 2921 and 2852 cm^{-1}, confirm the presence of the 16-ene on the surface (Figure 4.5).[36,56,59] The peak positions are indicative of an organic acid film that contains *gauche* and *trans* interactions. The presence of both types of interactions is a result of the surface topography of the 5% HA material, observed using SEM.

The acid head group binding mode and tail group functionality was determined by looking at the carboxylic acid region of the DRIFT spectrum (Figure 4.5). The solid 16-ene spectrum contains peaks at 1709, 1434 and 1295 cm^{-1} corresponding to the $\nu_{C=O}$, ν_{C-O} and ν_{C-O-H} of the free carboxylic acid and the peak attributed to the $\nu_{C=C}$ at 1642 cm^{-1}. The spectrum of the modified substrate contains a broad peak centered at 1540 cm^{-1} that is the

result of the carboxylate stretch, which indicates a bidentate organic acid binding mode. Most importantly, the immobilized acid spectrum also contains a peak at 1651 cm^{-1} which is attributed to the alkene ($\nu_{C=C}$), free at the film interface that may be used for subsequent organic reactions.

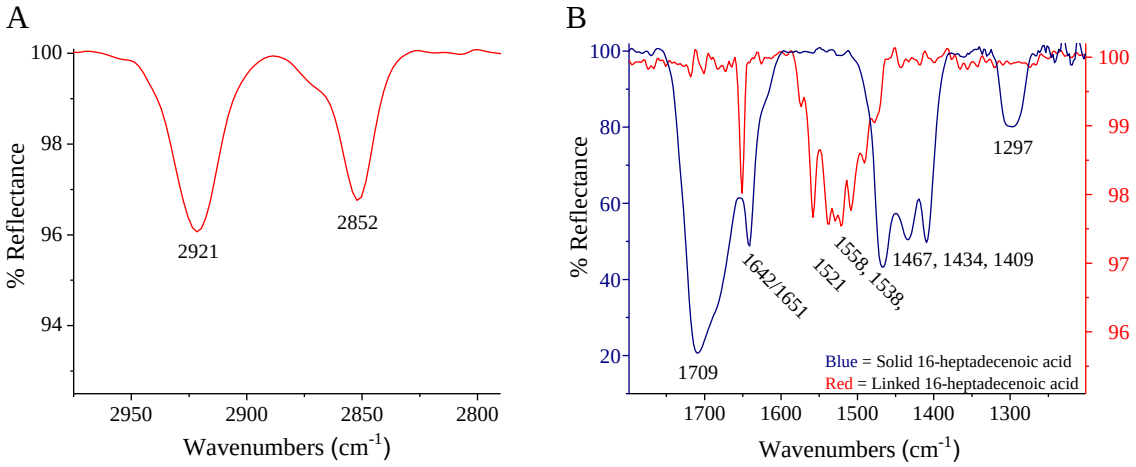

Figure 4.5: DRIFT spectra indicating successful surface modification of 5% HA with 16-heptadecenoic acid. A) Methylene stretching region, $\nu_{CH2\ asymm}$= 2921 cm^{-1} and $\nu_{CH2\ symm}$= 2852 cm^{-1} indicating the presence of the acid film after solvent rinse. B) Acid head group binding region with peaks indicative of a bidentate binding mode for the attached acid (red spectra) at 1558, 1538 and 1521 cm^{-1} and the free interfacial $\nu_{C=C}$ at 1651 cm^{-1}.

The immobilization of HHC10 was achieved using a one-step alkene-thiol click reaction, where a sacrificial cysteine residue (thiol side chain) appended to the AMP reacts with the terminal alkene of the formed film. 16-ene modified 5% HA discs were placed in a 1 mg/mL HHC10 solution containing 0.5 mg/mL Irgacure 2959 in 10:1 ddH_2O:DMF.[51] The HHC10 solution, containing the 16-ene modified 5% HA discs, was reacted under 365 nm UV light for 3 hours with N_2 purge. The successful linkage of HHC10 to the 16-ene films was confirmed using DRIFT spectroscopy, by comparing lyophilized HHC10 solid powder to HHC10 that had been linked to 5% HA discs (Figure 4.6).

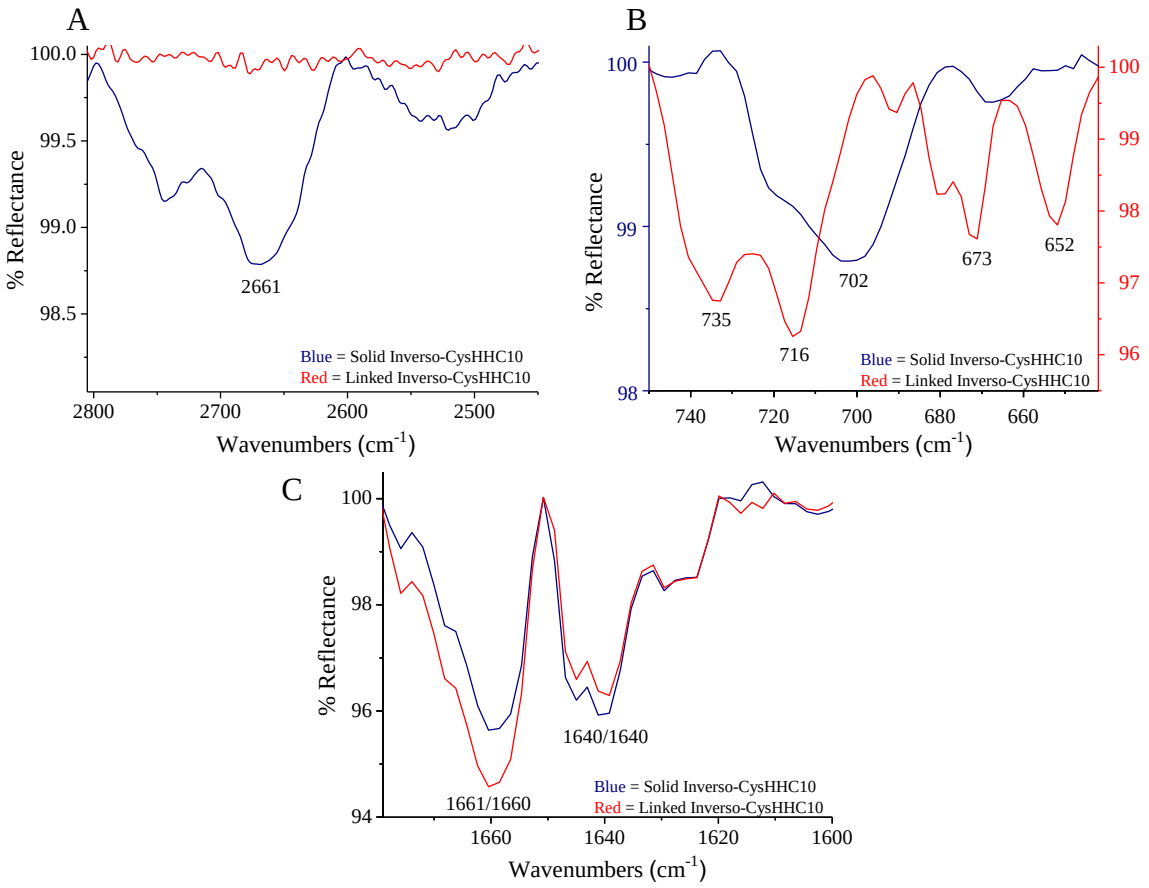

Figure 4.6: DRIFT spectra indicating successful immobilization of HHC10. A) Thiol stretching before (blue) and after (red) peptide linking, showing the loss of the S-H stretch. B) Sulfide bond stretches before (blue) and after (red) peptide immobilization corresponding to $\nu_{C\text{-}S\ cysteine,\ solid}$ at 702 cm^{-1} and $\nu_{C\text{-}S\ cysteine}$ and $\nu_{C\text{-}S\ acid\ to\ peptide}$ at 735, 716, 673 and 652 cm^{-1}. C) Amide I ($\nu_{C=O}$) and amide II ($\nu_{N\text{-}H}$) bands for solid (blue) and linked peptide (red) indicating the presence on the peptide on the 5% HA composite.

The solid HHC10 contained peaks corresponding to the $\nu_{S\text{-}H}$ at 2661 cm^{-1}, $\nu_{C\text{-}S}$ at 702 cm^{-1} and $\nu_{amide\ I}$ and $\nu_{amide\ II}$ at 1661 and 1640 cm^{-1}. In the linked HHC10 spectra, the $\nu_{S\text{-}H}$ peak is no longer present and the single $\nu_{C\text{-}S}$ stretch has split into two sets of peaks that are shifted to 735, 716, 673 and 652 cm^{-1}. These changes are indicative of successful immobilization of HHC10 because the click reaction takes place between the cysteine's side chain thiol and forms a new sulfide bond. The amide I and II region of the DRIFT spectrum was also examined. In the linked HHC10 the $\nu_{amide\ I}$ was observed at 1660 cm^{-1}

and the $\nu_{amide\ II}$ at 1640 cm^{-1}, matching those observed in the solid HHC10. The changes observed in the thiol and sulfide regions, coupled with the persistence of the amide I and II, confirm the successful immobilization of HHC10 to the 5% HA composite.

4.3.2 Quantification of Antimicrobial Peptide Immobilization on 5% HA

The amount of HHC10 that was covalently linked to the 5% HA composites was determined using fluorescence. HHC10 modified 5% HA discs were prepared using the alkene-thiol linker system described in Section 4.2.3. Ten discs were covalently modified and the fluorescence of the reaction solution at 342 nm, due to the four tryptophan residues within HHC10, was correlated to the amount of HHC10 that had been linked.

By monitoring the fluorescence emission and using the calibration curve (Figure 4.7), the average amount of AMP immobilized using this alkene-thiol linker system was found to be 470 ± 20 μg HHC10 per 5% HA disc. The 5% HA discs used here weigh on average 0.053 grams, which translates to an antimicrobial loading of 8850 ± 90 μg HHC10 per gram of modified 5% HA composite.

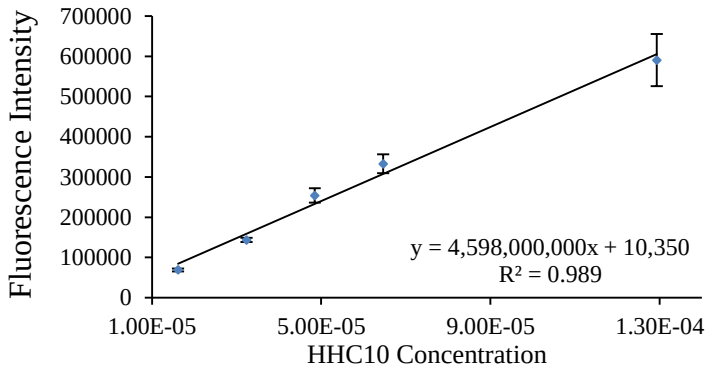

Figure 4.7: Calibration curve used for the quantification of the amount of immobilized HHC10 on the 5% HA composites.

4.3.3 Quantification of Antimicrobial Peptide Released from HHC10 Modified 5% HA

The quantity remaining and stability of immobilized HHC10 over time in aqueous solution was evaluated using Direct Infusion Q-TOF MS. HHC10 modified 5% HA discs were soaked in ddH_2O for 1, 3.5 and 24 hours. At each time point the discs were removed and the ddH_2O was analyzed. The limit of detection of HHC10 in ddH_2O using this method was found to be $9.9x10^{-9}$ M and the limit of quantification was $3.0x10^{-8}$ M (Figure 4.8).

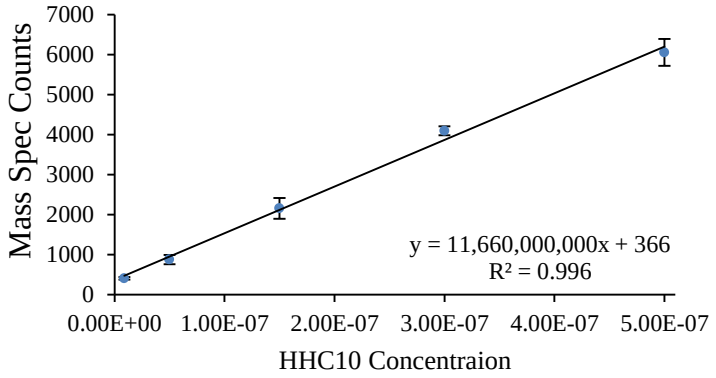

Figure 4.8: Calibration curve used to quantify the amount of HHC10 released into solution.

After 1 hour the concentration of HHC10 in the ddH_2O was $3.71x10^{-7} \pm 0.73x10^{-7}$ M, after 3.5 hours the total concentration of HHC10 in solution was $5.01x10^{-7} \pm 0.50x10^{-7}$ M and following 24 hours of soaking the total concentration of HHC10 in solution was $5.67x10^{-7} \pm 0.20x10^{-7}$ M. Using the determined concentrations and the sample volume, the corresponding mass of HHC10 in solution was determined. After 1 hour the average mass of HHC10 released from the modified 5% HA discs was 1.15 ± 0.23 μg, then after 3.5 hours the total amount of HHC10 released was 1.55 ± 0.15 μg and after soaking for 24 hours the total mass of HHC10 released from the composite and into the ddH_2O was 1.75 ± 0.06 μg. The amount of HHC10 liberated from the modified 5% HA significantly

increased between 1 and 3.5 hours, but the increase was not significant between 3.5 and 24 hours. The average percentage of HHC10 that remained linked to the 5% HA was quantified using the average loading determined in Section 4.3.2. After 24 hours of soaking the modified 5% HA discs, the average amount of HHC10 that remained immobilized using the developed alkene-thiol linker system was 99.63 ± 0.01% (Figure 4.9).

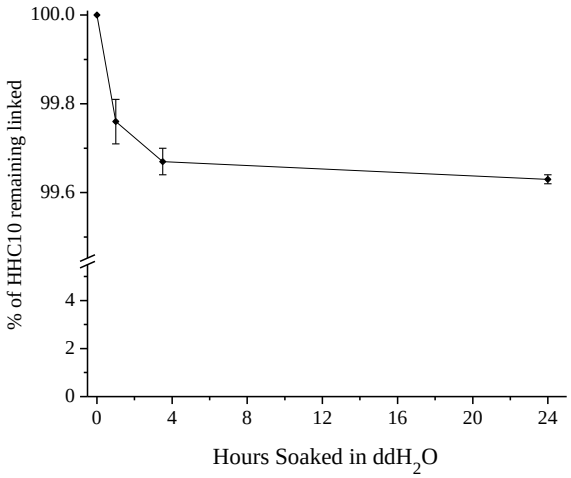

Figure 4.9: The percentage of Inverso-CysHHC10 that remains linked to 5% HA using the alkene-thiol linker system through a 24 hour soak in ddH_2O, shown as mean ± standard error, $p<0.05$.

4.3.4 *Escherichia coli* NPN Uptake Factor on Modified 5% HA

A proposed mechanism of AMP action is through cell membrane disruption, where the AMPs form trans-membrane pores that result in the collapse of the cell membrane and leads to cell death.[43,44,47] Changes in *E. coli* membrane permeability were evaluated using the NPN uptake assay. *E. coli* cultures were grown to 0.5 $OD_{600\,nm}$ and treated with HHC10 modified 5% HA discs. The fluorescence intensity of the samples was collected and the NPN uptake factors were determined and normalized to untreated *E. coli*. The normalized NPN uptake factors were: control untreated *E. coli*: 1.00 ± 0.01 and HHC10 modified 5% HA treated *E. coli*: 1.35 ± 0.02 (Figure 4.10). The normalized NPN uptake factor of the

treated *E. coli* was statistically higher than the NPN uptake factor of untreated *E. coli*, indicative of increased membrane permeability. Which clearly demonstrates that the HHC10 retains its activity against *E. coli* when it is covalently immobilized to a 5% HA composite using the developed alkene-thiol linker system.

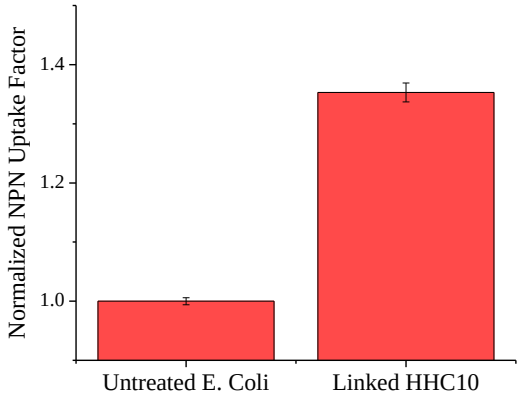

Figure 4.10: Normalized NPN uptake factor for untreated *E. coli* and *E. coli* treated with HHC10 modified 5% HA discs. Data shown as mean ± standard error, $p<0.05$. *E. coli* treated with modified discs exhibit increased membrane permeability.

4.3.5 *Escherichia coli* Bacterial Turbidity Tests with Modified 5% HA

The activity of linked HHC10 was further evaluated by monitoring the growth of *E. coli* in planktonic culture when incubated with HHC10 modified 5% HA. After incubating a 0.1 $OD_{600\ nm}$ *E. coli* solution for 2.5 hours with modified 5% HA, the $OD_{600\ nm}$ was measured for all samples and normalized to untreated *E. coli*. The normalized average $OD_{600\ nm}$ for *E. coli* solutions were: control untreated *E. coli*: 1.00 ± 0.02 and HHC10 modified 5% HA treated *E. coli*: 0.24 ± 0.01 (Figure 4.11). Based on the decreased $OD_{600\ nm}$, the growth of *E. coli* incubated with HHC10 modified 5% HA discs was

effectively inhibited. Further demonstrating the immobilized HHC10 retains its activity against the *E. coli*.

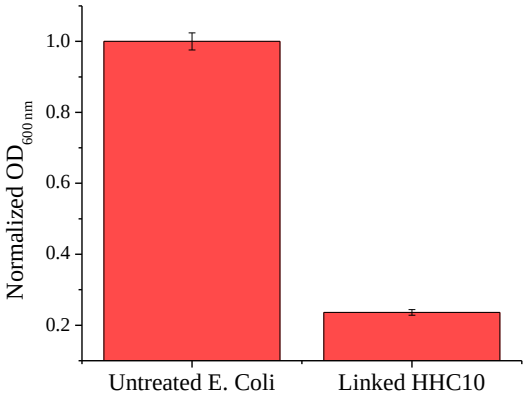

Figure 4.11: Normalized $OD_{600\ nm}$ for untreated *E. coli* and *E. coli* treated with HHC10 modified 5% HA discs. Data shown as mean ± standard error, $p<0.05$. *E. coli* treated with modified discs exhibit decreased $OD_{600\ nm}$ and decreased bacterial growth in culture.

4.3.6 Inverso-CysHHC10 Antimicrobial Activity in Solution and Linked to Modified 5% HA

Based on the NPN uptake assay and bacterial turbidity test, it was clearly shown that the immobilized HHC10 retains its antimicrobial activity against *E. coli*. The efficacy of the linked AMP was further compared to the free, in solution HHC10 to determine the concentration dosage that the linked AMP was equally as effective as.

E. coli was cultured and treated as described in Section 4.2.8. Using the NPN uptake assay, the fluorescence intensity of the samples was collected and the NPN uptake factors were determined and normalized to the untreated *E. coli*. The NPN uptake factors were: control untreated *E. coli*: 1.00 ± 0.01; 10 μM HHC10 treated *E. coli*: 1.36 ± 0.01 and HHC10 modified 5% HA treated *E. coli*: 1.35 ± 0.02. (Figure 4.12). The NPN uptake factors of the treated *E. coli*, both 10 μM HHC10 and HHC10 modified 5% HA discs, were statistically higher than that of untreated *E. coli*. Further, the NPN uptake factor of linked

and 10 μM HHC10 were statistically equivalent, demonstrating that immobilized HHC10 is as effective as a 10 μM AMP solution.

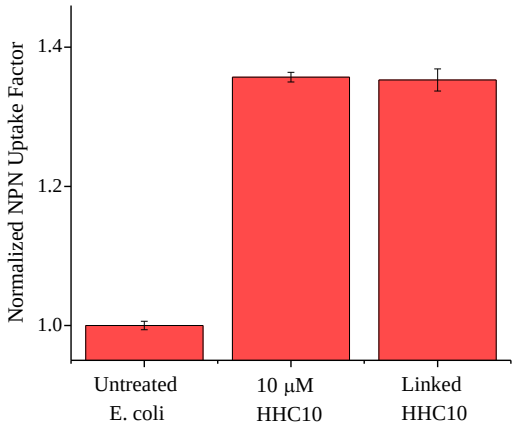

Figure 4.12: NPN uptake assay for *E.* coli treated with 10 μM and linked HHC10, shown as mean ± standard error, $p<0.05$. Both treated *E. coli* solutions have a statistically higher NPN uptake factor than untreated *E. coli* and are statistically equivalent.

E. coli was cultured and treated as described in Section 4.2.9. Using the bacterial turbidity test, the $OD_{600\ nm}$ of *E. coli* solutions were collected and normalized to the untreated bacteria solutions. The normalized $OD_{600\ nm}$ for the *E. coli* solutions were: control untreated *E. coli*: 1.00 ± 0.02; 10 μM HHC10 treated *E. coli*: 0.25 ± 0.02 and HHC10 modified 5% HA treated *E. coli*: 0.24 ± 0.01 (Figure 4.13). The $OD_{600\ nm}$ of the *E. coli* incubated with both the 10 μM HHC10 and HHC10 modified 5% HA discs were statistically lower than the untreated *E. coli*. Additionally, the $OD_{600\ nm}$ of *E. coli* treated with 10 μM HHC10 and linked HHC10 were statistically equal, confirming the linked HHC10 prevents *E. coli* growth as effectively as a 10 μM HHC10 solution.

Based on both the NPN uptake assay and *E. coli* bacterial turbidity test, the linked HHC10 is equally effective against *E. coli* as a 10 μM HHC10 solution.

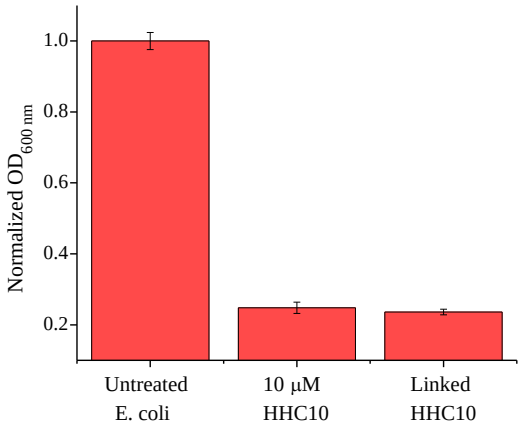

Figure 4.13: Bacterial turbidity tests for *E. coli* treated with 10 μM and linked HHC10, shown as mean ± standard error, $p<0.05$. Both treated *E. coli* solutions have a statistically lower $OD_{600\ nm}$ than untreated *E. coli* and are statistically equivalent.

4.3.7 Osteoblast Attachment to Modified 5% HA

To evaluate if the immobilization of HHC10 affected the increased osteoblast attachment observed on the unmodified 5% HA, NHOsts were cultured and seeded onto sterilized, HHC10 modified 5% HA discs. Nine discs were placed into a 48 well plate per time point and loaded with 10,000 NHOsts. After 1, 4 and 7 days the cells were imaged using the Live/Dead® Viability/Cytotoxicity assay kit. Five images per disc were collected (Figure 4.14) and the number of live cells was counted and normalized to the control.

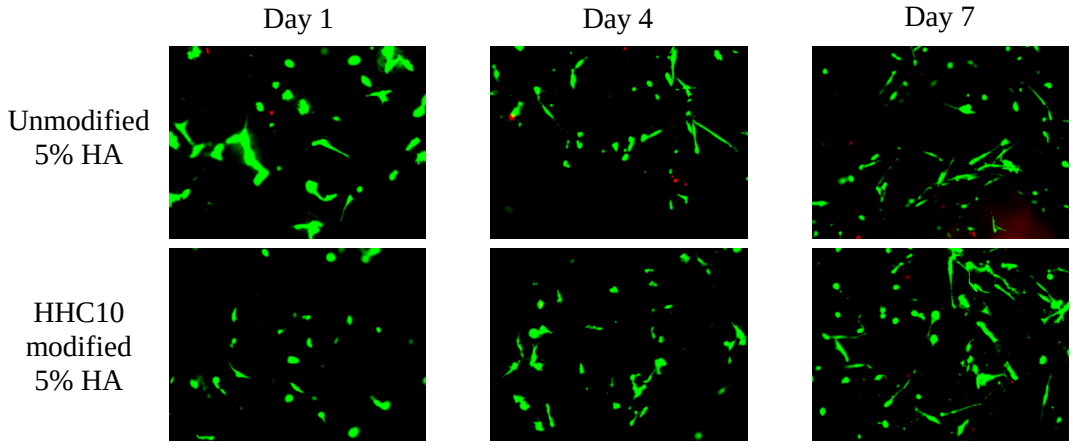

Figure 4.14: Representative Live/Dead® fluorescent images of osteoblasts attached to control unmodified and HHC10 modified 5%HA composites on Days 1, 4 and 7.

On Day 1 the normalized average number of live osteoblasts per view was: control unmodified 5% HA: 100.0 ± 7.7 and HHC10 modified 5% HA: 105.5 ± 8.7 (Figure 4.15). The HHC10 modified 5% HA composites had statistically the same number of attached live cells as unmodified 5% HA on Day 1.

On Day 4 the normalized average number of live osteoblast cells per view was: control unmodified 5% HA: 100.0 ± 9.4 and HHC10 modified 5% HA: 101.1 ± 9.2 (Figure 4.15). Again, the HHC10 modified 5% HA discs had the statistically same number of cells per view as unmodified 5% HA.

The normalized average number of live osteoblast cells per view on Day 7 was: control unmodified 5% HA: 100.0 ± 6.1 and HHC10 modified 5% HA: 103.9 ± 4.8 (Figure 4.15). The amount of attached live cells was once again statistically the same for HHC10 modified and unmodified 5% HA.

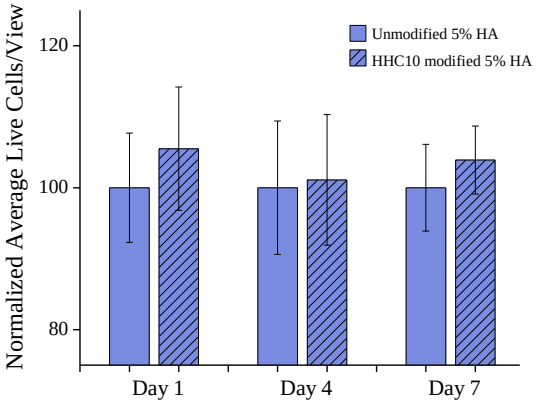

Figure 4.15: Days 1, 4 and 7 normalized average number of live osteoblasts attached to control unmodified and HHC10 modified 5% HA composites. Data represented as mean ± standard error, $p<0.05$. The average number of attached live cells is statistically equal on all days examined.

The number of live osteoblasts attached the HHC10 modified 5% HA was statistically equal to the number attached to unmodified 5% HA on all days examined.

These results prove that the covalent immobilization of the AMP does not have a negative effect on the osteoblasts cultured on the composites.

4.3.8 Osteoblast Viability on Modified 5% HA

To examine the effect of immobilizing HHC10 on osteoblast viability, NHOsts were cultured and seeded onto sterilized, HHC10 modified 5% HA discs. Nine sterilized discs per time point were placed into a 48 well plate and loaded with 10,000 NHOsts. After 1, 4 and 7 days the cells were imaged using the Live/Dead® Viability/Cytotoxicity assay kit. Five images per disc were collected. The number of live cells was divided by the total number of cells to determine the percent viability of the NHOsts.

On Day 1 the percent cell viability was: control unmodified 5% HA: 84.4 ± 1.8 and HHC10 modified 5% HA: 85.6 ± 1.7 (Figure 4.16). The HHC10 modified and unmodified 5% HA had same percentage of attached viable cells.

The percent cell viability on Day 4 was: control unmodified 5% HA: 74.4 ± 2.5 and HHC10 modified 5% HA: 78.6 ± 3.0 (Figure 4.16). Again both modified and unmodified 5% HA had statistically the same percent cell viability.

On Day 7 the percent cell viability was: control unmodified 5% HA: 81.6 ± 1.2 and HHC10 modified 5% HA: 87.1 ± 1.3 (Figure 4.16). The percentage of viable cells on the HHC10 modified 5% HA was statistically higher than that of cells on unmodified 5% HA.

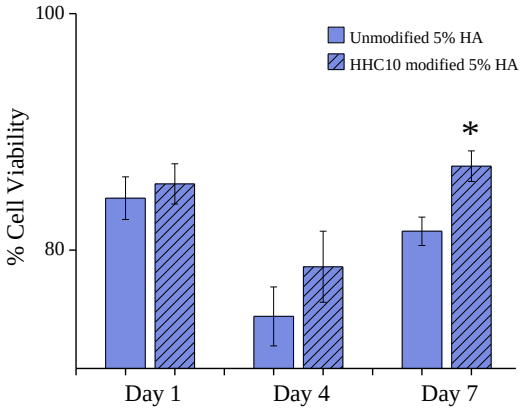

Figure 4.16: Days 1, 4 and 7 percent viability of attached cells on control unmodified and HHC10 modified 5% HA composites. * = statistically higher than control for that day. Data represented as mean ± standard error, $p<0.05$. The percent viability is equal on Day 1 and 4 and statistically higher on Day 7.

The immobilization of HHC10 also does not adversely affect the percent viability of the attached osteoblasts. At the longest time point the percent viability was greater on the HHC10 modified 5% HA.

4.3.9 Osteoblast Proliferation on Modified 5% HA

To determine if the presence of HHC10 had an effect on osteoblast proliferation, NHOsts were cultured and seeded onto sterilized, HHC10 modified 5% HA discs. Nine discs at each time point were placed into 48 well plates and loaded with 10,000 cells. Before evaluating proliferation, the alamarBlue® reagent was diluted into the OBM. After 1, 4 and 7 days the OBM was examined using UV-VIS spectroscopy. The absorbance of the OBM from each well was collected and normalized to control unmodified 5% HA.

On Day 1 the normalized average absorbance was: control unmodified 5% HA: 100.0 ± 2.5 and HHC10 modified 5% HA: 103.2 ± 4.2 (Figure 4.17). The amount of cell proliferation supported was statistically equal between modified and unmodified 5% HA.

The normalized average absorbance on Day 4 was: control unmodified 5% HA: 100.0 ± 1.8 and HHC10 modified 5% HA: 98.1 ± 2.8 (Figure 4.17). Again, cell proliferation was equally supported on both the control and HHC10 modified 5% HA discs.

By Day 7 the normalized average absorbance was: control unmodified 5% HA: 100.0 ± 4.6 and HHC10 modified 5% HA: 101.2 ± 4.3 (Figure 4.17). Similar to the previous days, the absorbance was statistically equal between control and modified samples.

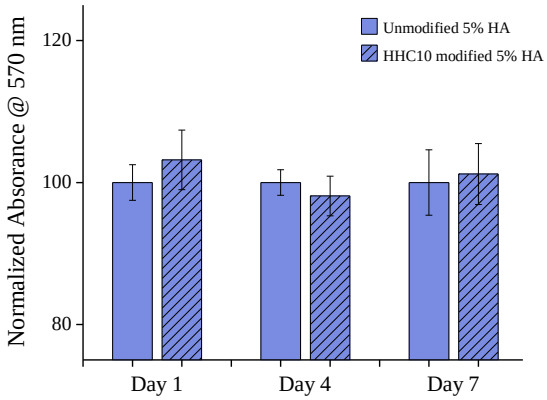

Figure 4.17: Days 1, 4 and 7 normalized absorbance of OBM for control unmodified and HHC10 modified 5% HA composites. Data represented as mean ± standard error, $p<0.05$. The amount of cell proliferation is statistically equal on all days examined.

The HHC10 modified 5% HA discs supported cell proliferation equally as well as the unmodified 5% HA on all days examined. Again, these results demonstrate that the immobilization of HHC10 does not affect the increased cell proliferation observed on the 5% HA composite.

4.4 Discussion

Implant associated infections are difficult to eliminate because of their antibiotic resistant characteristics.[15,19-21] Frequently, by the time the infection is discovered it is in an advanced stage, when the removal of the implant is the best approach for treatment.[2,13-

[15,17,27] To avoid this colonization, an antimicrobial molecule that is localized to the graft and is present upon implantation is desirable.[31-33,36,37] To also avoid the growing concern over antibiotic resistance, an immobilized antimicrobial peptide was investigated.[41-44] The AMP was covalently attached to the composite 5% HA materials through a two-step alkene-thiol click reaction. DRIFT spectroscopy confirmed both of the steps of the modification proceeded successfully and Q-TOF MS confirmed the quantity and stability of the attached HHC10. HHC10 modified 5% HA discs were then sterilized by autoclaving and evaluated biologically.

Antibacterial efficacy, of both the linked and in solution HHC10, was evaluated through the NPN uptake assay and bacterial turbidity tests.[36,54-56] A proposed mechanism of AMP action is through cell membrane disruption, where the AMPs form trans-membrane pores that results in the collapse of the cell membrane and cell death.[41,44] Changes in membrane permeability for *E. coli* treated with HHC10 modified 5% HA and 10 μM HHC10 were evaluated using the NPN uptake assay. NPN uptake was increased by 40% for the *E. coli* treated using both types of HHC10. Further, the uptake was statistically equal for both the linked HHC10 and the 10 μM HHC10 ($p<0.05$), demonstrating that the linked AMP permeabilizes the *E. coli* membrane as well as a 10 μM solution. The LC99.9 of "free" HHC10 is 8 μM and the effective dosage of the linked HHC10 is 10 μM, showing that the linked HHC10 retains its activity against *E. coli* through linkage.[49]

The prevention of bacterial growth in culture was monitored using the bacterial turbidity test.[36,56] As bacteria are grown in culture, they create a turbid solution, where the greater the concentration of bacteria, the greater the turbidity of that solution. Through this assay a similar HHC10 effectiveness was observed to seen in the NPN uptake assay. Both

the HHC10 modified 5% HA discs and with 10 μM HHC10 resulted in a 75% decrease in *E. coli* solution turbidity. This decrease was equal for both HHC10 treated *E. coli* samples. This assay confirmed that the linked AMP is equally as effective at preventing the growth of *E. coli* in culture as the 10 μM HHC10 solution. The bacterial turbidity test coupled with the NPN uptake assay verified that the covalent immobilization of HHC10 does not render the AMP inactive, but rather the activity is only slightly diminished.

Since the goal was to develop a material that increased osteoblast performance and simultaneously decreased bacterial attachment, once the HHC10 had been immobilized to the 5% HA the material and evaluated for its antibacterial properties, osteoblast performance on the HHC10 modified 5% HA materials was re-examined. The presence of HA at the composite interface was shown to increase osteoblast response on unmodified 5% HA discs. When the osteoblast attachment, viability and proliferation were examined on HHC10 modified 5% HA, it was shown that the immobilization of HHC10 does not affect the bone cell performance. On Day 1 and Day 4, the number of attached cells, percent cell viability and cell proliferation were all comparable on HHC10 modified and unmodified 5% HA. On Day 7 the number of attached cells and cell proliferation were statistically the same and the percent cell viability was increased on HHC10 modified 5% HA over control.

These osteoblast performance assays consistently demonstrated that the HHC10 modification did not impede with the osteoblast response. This indicates that despite the immobilization of HHC10 onto the 5% HA composites, there is still sufficient surface contact area available for cells to interact. If the HHC10 formed a complete layer on the CaAlO:HA surface the cells would not be able to interact with the composite and the

cellular response would decrease. Previous work had demonstrated that "free" HHC10 induced hemolysis in only 1% of erythrocytes.[49] Although the work here did not explicitly quantify the amount of cell death, it was clearly shown that HHC10 immobilization did not decrease the number of attached live cells or the percent viability of those cells.

Based on the biological evaluation of the HHC10 modified 5% HA composite, the multifunctional material had been developed. The 5% HA had an elastic modulus and modulus of rupture that was similar to non-load bearing cancellous bone and consistently resulted in increased osteoblast attachment, viability and proliferation. Chemical functionalization with an antimicrobial peptide added antibacterial properties to the material and did not sacrifice the bone cell performance. Based on the mechanical and biological evaluation performed on the HHC10 modified 5% HA it was determined that this composite is suitable for a synthetic bone graft and has the ability to address multiple physiological stresses that would be placed on it.

4.5 Conclusions

DRIFT analysis confirmed the RT-formed 5% HA composite was successfully functionalized with the potent antimicrobial peptide Inverso-CysHHC10. Immobilization was achieved using the highly efficient alkene-thiol click reaction and the HHC10 remained localized on the 5% HA disc for at least 24 hours. Through covalent immobilization the HHC10 retained its bactericidal activity and functioned with the potency of a 10 μM HHC10 solution, based on the increased *E. coli* membrane permeability and the reduced growth of *E. coli* in culture. Most importantly, the linked HHC10 did not adversely affect the increased osteoblast response observed on the unmodified 5% HA

composites. Cell attachment and proliferation on HHC10 modified and unmodified 5% HA was statistically equivalent on all the days examined and percent cell viability was increased on the longest time point. These results clearly demonstrate that the increased osteoblast response is not affected by the attachment of the antimicrobially active HHC10. Further the alkene-thiol linker system utilized here can be extended to other system where the material contains reactive surface hydroxyl groups and the antimicrobial molecule contains or can be amended to include a sacrificial thiol functionality.

4.6 References

1. Arciola, C. R.; Campoccia, D.; Speziale, P.; Montanaro, L.; Costerton, J. W. Biofilm formation in Staphylococcus implant infections. A review of molecular mechanisms and implications for biofilm-resistant materials. *Biomaterials* **2012**, *33*, 5967-5982.

2. Costerton, J.; Stewart, P. S.; Greenberg, E. Bacterial biofilms: A common cause of persistent infections. *Science* **1999**, *284*, 1318-1322.

3. Donlan, R. M. Biofilms and device-associated infections. *Emerging Infect. Dis.* **2001**, *7*, 277-281.

4. Fitzpatrick, F.; Humphreys, H.; O'Gara, J. The genetics of staphylococcal biofilm formation—Will a greater understanding of pathogenesis lead to better management of device-related infection?. *Clin. Microbiol. Infect.* **2005**, *11*, 967-973.

5. Hall-Stoodley, L.; Costerton, J. W.; Stoodley, P. Bacterial biofilms: From the natural environment to infectious diseases. *Nat. Rev. Microbiol.* **2004**, *2*, 95-108.

6. Mack, D.; Rohde, H.; Harris, L.; Davies, A.; Horstkotte, M. A.; Knobloch, J. Biofilm formation in medical device-related infection. *Int. J. Artif. Organs* **2006**, *29*, 343-359.

7. Pavithra, D.; Doble, M. Biofilm formation, bacterial adhesion and host response on polymeric implants—Issues and prevention. *Biomed. Mater.* **2008**, *3*, 034003.

8. Campoccia, D.; Montanaro, L.; Moriarty, T. F.; Richards, R.; Ravaioli, S.; Arciola, C. R. The selection of appropriate bacterial strains in preclinical evaluation of infection-resistant biomaterials. *Int. J. Artif. Organs* **2008**, *31*, 841-847.

9. Martinez, L.; Bryan, R.; Apostolidis, C.; Morgenstern, A.; Casadevall, A.; Dadachova, E. Antibody-guided alpha radiation effectively damages fungal biofilms. *Antimicrob. Agents Chemother.* **2006**, *50*, 2132-2136.

10. Moriarty, T. F.; Schlegel, U.; Perren, S.; Richards, R. G. Infection in fracture fixation: Can we influence infection rates through implant design?. *J. Mater. Sci. Mater. Med.* **2010**, *21*, 1031-1035.

11. Del Pozo, J. L.; Patel, R. Infection associated with prosthetic joints. *N. Eng. J. Med.* **2009**, *361*, 787-794.

12. Katsikogianni, M.; Missirlis, Y. Concise review of mechanisms of bacterial adhesion to biomaterials and of techniques used in estimating bacteria-material interactions. *Eur. Cell. Mater.* **2004**, *8*, 37-57.

13. Subbiahdoss, G.; Pidhatika, B.; Coullerez, G.; Charnley, M.; Kuijer, R.; van der Mei, H. C.; Textor, M.; Busscher, H. J. Bacterial biofilm formation versus mammalian cell growth on titanium-based mono-and bi-functional coating. *Eur. Cell. Mater.* **2010**, *19*, 205-213.

14. Childs, S. G. Biofilm: The pathogenesis of slime glycocalyx. *Orthop. Nurs.* **2008**, *27*, 361-369.

15. Sampedro, M. F.; Patel, R. Infections associated with long-term prosthetic devices. *Infect. Dis. Clin. N. Am.* **2007**, *21*, 785-819.

16. Sauer, K. The genomics and proteomics of biofilm formation. *Genome Biol.* **2003**, *4*, 219.

17. Tunney, M.; Dunne, N.; Einarsson, G.; McDowell, A.; Kerr, A.; Patrick, S. Biofilm formation by bacteria isolated from retrieved failed prosthetic hip implants in an in vitro model of hip arthroplasty antibiotic prophylaxis. *J. Orthop. Res.* **2007**, *25*, 2-10.

18. Stoodley, P.; Sauer, K.; Davies, D.; Costerton, J. W. Biofilms as complex differentiated communities. *Annu. Rev. Microbiol.* **2002**, *56*, 187-209.

19. Davies, D. Understanding biofilm resistance to antibacterial agents. *Nat. Rev. Drug Discovery* **2003**, *2*, 114-122.

20. Høiby, N.; Bjarnsholt, T.; Givskov, M.; Molin, S.; Ciofu, O. Antibiotic resistance of bacterial biofilms. *Int. J. Antimicrob. Agents* **2010**, *35*, 322-332.

21. Stewart, P. S.; Costerton, J. W. Antibiotic resistance of bacteria in biofilms. *Lancet* **2001**, *358*, 135-138.

22. Stoodley, P.; Hall-Stoodley, L.; Lappin-Scott, H. M. Detachment, surface migration, and other dynamic behavior in bacterial biofilms revealed by digital time-lapse imaging. *Methods Enzymol.* **2001**, *337*, 306-319.

23. Jose, B.; Antoci, V.; Zeiger, A. R.; Wickstrom, E.; Hickok, N. J. Vancomycin covalently bonded to titanium beads kills Staphylococcus aureus. *Chem Biol* **2005**, *12*, 1041-1048.

24. Olson, M. E.; Ceri, H.; Morck, D. W.; Buret, A. G.; Read, R. R. Biofilm bacteria: Formation and comparative susceptibility to antibiotics. *Can. J. Vet. Res.* **2002**, *66*, 86.

25. Walsh, C. Molecular mechanisms that confer antibacterial drug resistance. *Nature* **2000**, *406*, 775-781.

26. Zimmerli, W.; Trampuz, A.; Ochsner, P. E. Prosthetic-joint infections. *N. Eng. J. Med.* **2004**, *351*, 1645-1654.

27. Campoccia, D.; Montanaro, L.; Arciola, C. R. The significance of infection related to orthopedic devices and issues of antibiotic resistance. *Biomaterials* **2006**, *27*, 2331-2339.

28. Bridgett, M.; Davies, M.; Denyer, S. Control of staphylococcal adhesion to polystyrene surfaces by polymer surface modification with surfactants. *Biomaterials* **1992**, *13*, 411-416.

29. Bazaka, K.; Jacob, M. V.; Crawford, R. J.; Ivanova, E. P. Plasma-assisted surface modification of organic biopolymers to prevent bacterial attachment. *Acta Biomater.* **2011**, *7*, 2015-2028.

30. Chapman, R. G.; Ostuni, E.; Liang, M. N.; Meluleni, G.; Kim, E.; Yan, L.; Pier, G.; Warren, H. S.; Whitesides, G. M. Polymeric thin films that resist the adsorption of proteins and the adhesion of bacteria. *Langmuir* **2001**, *17*, 1225-1233.

31. Gautier, H.; Merle, C.; Auget, J.; Daculsi, G. Isostatic compression, a new process for incorporating vancomycin into biphasic calcium phosphate: Comparison with a classical method. *Biomaterials* **2000**, *21*, 243-249.

32. Radin, S.; Ducheyne, P. Controlled release of vancomycin from thin sol–gel films on titanium alloy fracture plate material. *Biomaterials* **2007**, *28*, 1721-1729.

33. Obadia, L.; Amador, G.; Daculsi, G.; Bouler, J. M. Calcium-deficient apatite: Influence of granule size and consolidation mode on release and in vitro activity of vancomycin. *Biomaterials* **2003**, *24*, 1265-1270.

34. Stigter, M.; De Groot, K.; Layrolle, P. Incorporation of tobramycin into biomimetic hydroxyapatite coating on titanium. *Biomaterials* **2002**, *23*, 4143-4153.

35. Cauda, V.; Onida, B.; Platschek, B.; Mühlstein, L.; Bein, T. Large antibiotic molecule diffusion in confined mesoporous silica with controlled morphology. *J. Mater. Chem.* **2008**, *18*, 5888-5899.

36. Palchesko, R. N.; McGowan, K. A.; Gawalt, E. S. Surface immobilization of active vancomycin on calcium aluminum oxide. *Mater. Sci. Eng., C* **2011**, *31*, 637-642.

37. Murugan, R.; Ramakrishna, S. Coupling of therapeutic molecules onto surface modified coralline hydroxyapatite. *Biomaterials* **2004**, *25*, 3073-3080.

38. Bagheri, M.; Beyermann, M.; Dathe, M. Immobilization reduces the activity of surface-bound cationic antimicrobial peptides with no influence upon the activity spectrum. *Antimicrob. Agents Chemother.* **2009**, *53*, 1132-1141.

39. Bechinger, B. The structure, dynamics and orientation of antimicrobial peptides in membranes by multidimensional solid-state NMR spectroscopy. *Biochim. Biophys. Acta* **1999**, *1462*, 157-183.

40. Kruszewski, K. M.; Nistico, L.; Longwell, M. J.; Hynes, M. J.; Maurer, J. A.; Hall-Stoodley, L.; Gawalt, E. S. Reducing Staphylococcus aureus biofilm formation on stainless steel 316L using functionalized self-assembled monolayers. *Mater. Sci. Eng., C* **2013**, *33*, 2059-2069.

41. Gordon, Y. J.; Romanowski, E. G.; McDermott, A. M. A review of antimicrobial peptides and their therapeutic potential as anti-infective drugs. *Curr. Eye Res.* **2005**, *30*, 505-515.

42. Costa, F.; Carvalho, I. F.; Montelaro, R. C.; Gomes, P.; Martins, M. C. L. Covalent immobilization of antimicrobial peptides (AMPs) onto biomaterial surfaces. *Acta Biomater.* **2011**, *7*, 1431-1440.

43. Onaizi, S. A.; Leong, S. S. Tethering antimicrobial peptides: Current status and potential challenges. *Biotechnol. Adv.* **2011**, *29*, 67-74.

44. Jenssen, H.; Hamill, P.; Hancock, R. E. Peptide antimicrobial agents. *Clin. Microbiol. Rev.* **2006**, *19*, 491-511.

45. Howden, B. P.; Davies, J. K.; Johnson, P. D.; Stinear, T. P.; Grayson, M. L. Reduced vancomycin susceptibility in Staphylococcus aureus, including vancomycin-intermediate and heterogeneous vancomycin-intermediate strains: Resistance mechanisms, laboratory detection, and clinical implications. *Clin. Microbiol. Rev.* **2010**, *23*, 99-139.

46. Friedrich, C. L.; Moyles, D.; Beveridge, T. J.; Hancock, R. E. Antibacterial action of structurally diverse cationic peptides on gram-positive bacteria. *Antimicrob. Agents Chemother.* **2000**, *44*, 2086-2092.

47. Fulmer, P. A.; Lundin, J. G.; Wynne, J. H. Development of antimicrobial peptides (AMPs) for use in self-decontaminating coatings. *ACS Appl. Mater. Interfaces* **2010**, *2*, 1266-1270.

48. Powers, J. P. S.; Hancock, R. E. The relationship between peptide structure and antibacterial activity. *Peptides* **2003**, *24*, 1681-1691.

49. Cleophas, R. T.; Riool, M.; Quarles van Ufford, H. C.; Zaat, S. A.; Kruijtzer, J. A.; Liskamp, R. M. Convenient preparation of bactericidal hydrogels by covalent attachment of stabilized antimicrobial peptides using thiol–ene click chemistry. *ACS Macro Lett.* **2014**, *3*, 477-480.

50. Cleophas, R. T.; Sjollema, J.; Busscher, H. J.; Kruijtzer, J. A.; Liskamp, R. M. Characterization and activity of an immobilized antimicrobial peptide containing bactericidal PEG-hydrogel. *Biomacromolecules* **2014**, *15*, 3390-3395.

51. Ma, Y.; Zheng, J.; Amond, E. F.; Stafford, C. M.; Becker, M. L. Facile fabrication of "dual click" one-and two-dimensional orthogonal peptide concentration gradients. *Biomacromolecules* **2013**, *14*, 665-671.

52. Lee, F. S.; Auld, D. S.; Vallee, B. L. Tryptophan fluorescence as a probe of placental ribonuclease inhibitor binding to angiogenin. *Biochemistry* **1989**, *28*, 219-224.

53. Hott, J.; Borkman, R. F. The non-fluorescence of 4-fluorotryptophan. *Biochem. J.* **1989**, *264*, 297-299.

54. Helander, I.; Mattila-Sandholm, T. Fluorometric assessment of gram-negative bacterial permeabilization. *J. Appl. Microbiol.* **2000**, *88*, 213-219.

55. Helander, I. M.; Mattila-Sandholm, T. Permeability barrier of the gram-negative bacterial outer membrane with special reference to nisin. *Int. J. Food Microbiol.* **2000**, *60*, 153-161.

56. Palchesko, R. N.; Buckholtz, G. A.; Romeo, J. D.; Gawalt, E. S. Co-immobilization of active antibiotics and cell adhesion peptides on calcium based biomaterials. *Mater. Sci. Eng., C* **2014**, *40*, 398-406.

57. Chen, S.; Mantei, N.; Dong, L.; Schachner, M. Prevention of neuronal cell death by neural adhesion molecules L1 and CHL1. *J. Neurobiol.* **1999**, *38*, 428-439.

58. Mujeeb, A.; Miller, A. F.; Saiani, A.; Gough, J. E. Self-assembled octapeptide scaffolds for in vitro chondrocyte culture. *Acta Biomater.* **2013**, *9*, 4609-4617.

59. Palchesko, R. N.; Romeo, J. D.; McGowan, K. A.; Gawalt, E. S. Increased osteoblast adhesion on physically optimized KRSR modified calcium aluminate. *J. Biomed. Mater. Res., Part A* **2012**, *100*, 1229-1238.

60. Gloeckner, H.; Jonuleit, T.; Lemke, H. D. Monitoring of cell viability and cell growth in a hollow-fiber bioreactor by use of the dye Alamar Blue™. *J. Immunol. Methods* **2001**, *252*, 131-138.

61. San Thian, E.; Huang, J.; Best, S. M.; Barber, Z. H.; Brooks, R. A.; Rushton, N.; Bonfield, W. The response of osteoblasts to nanocrystalline silicon-substituted hydroxyapatite thin films. *Biomaterials* **2006**, *27*, 2692-2698.

62. Shor, L.; Güçeri, S.; Wen, X.; Gandhi, M.; Sun, W. Fabrication of three-dimensional polycaprolactone/hydroxyapatite tissue scaffolds and osteoblast-scaffold interactions in vitro. *Biomaterials* **2007**, *28*, 5291-5297.

63. Voytik-Harbin, S. L.; Brightman, A. O.; Waisner, B.; Lamar, C. H.; Badylak, S. F. Application and evaluation of the alamarBlue assay for cell growth and survival of fibroblasts. *In Vitro Cell. Dev.-An.* **1998**, *34*, 239-246.

Chapter 5: Conclusions

5.1 Effect of Hydroxyapatite Incorporation into Calcium Aluminum Oxide

To improve the biocompatibility and osteogenic ability of the CaAlO material, it was cast as part of a composite with the osteoinductive and osteoconductive calcium phosphate material, HA.[1-3] HA was utilized due to its chemical similarity to the mineral component of natural bone and its previously demonstrated ability to increase *in vivo* bone regeneration.[2,4-6] By pairing small amounts of the osteogenic HA with the mechanically strong CaAlO, a new potential bone scaffold material was developed and evaluated.

5.1.1 Phase Composition of Cast Composites

The composites were formed using a room temperature cast where three different aggregate sizes of CaAlO were mixed with ground $Ca_3(PO_4)_2$ and hydrated using a dilute H_3PO_4 solution. Composites containing 1-5, 10, 15, 20 and 25% HA were successfully formed and evaluated for their phase composition. When CaAlO was exclusively cast, three different calcium aluminum phases were found using PXRD, $CaAl_4O_7$, $CaAl_2O_4$ and $Ca_3Al_2(OH)_{12}$, and when $Ca_3(PO_4)_2$ was cast two difference phases were detected $Ca_5(PO_4)_3OH$ (HA) and $CaHPO_4 \cdot 2H_2O$. When CaAlO and $Ca_3(PO_4)_2$ were cast together the same five phases were observed, indicating that there are no cross reactions taking place and there is no mixing of the two primary materials (CaAlO and $Ca_3(PO_4)_2$). SEM-EDS further confirmed the presence, abundance and distribution of the cast HA at the composite interface where *in vitro* cellular interactions can occur.

5.1.2 Mechanical Properties of Cast Composites

Two different post hydration processes were examined to determine the effect on the mechanical properties of the cast composites. The post hydration methods tested were 1) drying at room temperature and 2) sintering at 1000°C for 4 hours. These methods were evaluated because CaAlO derives its strength from hydration with water at room temperature, whereas HA derives its strength from sintering. The materials were evaluated for both the effect of increasing amount of HA in the composite and the effect of post hydration processing. The addition of HA to the composite was shown to significantly decrease the mechanical strength with larger amounts of HA (>10%), to the point where these composites were not similar in strength to natural non-load bearing cancellous bone. Post hydration processing also played a significant role in composite strength. All sintered composites had statistically lower elastic moduli and >10% HA composites had lower moduli of rupture. Ultimately the low percentage HA composites were the closest match to structural cancellous bone and were evaluated for ability to increase osteoblast response.

Table 5.1: Mechanical properties of natural bone and the 5% HA developed in this work.

	Elastic Modulus (GPa)	Modulus of Rupture (MPa)
Load Bearing Cortical Bone	15-22	60-75
Non-Load Bearing Cancellous Bone	3-11	4-9
RT-formed 5% HA Composite	8.8-11	5.7-7.1

5.1.3 Osteoblast Response on 1-5% HA

The low percentage of HA composites that were mechanically similar to non-load bearing cancellous bone were examined for increased osteoblast response. Osteoblast cells were cultured and seeded onto sterilized 1-5% HA discs and evaluated for cellular attachment, percent viability and proliferation on Days 1, 4 and 7 after seeding. Significantly increased osteoblast attachment was observed on all 1-5% HA composites on Days 4 and 7. However, on Day 1 only the 5% HA had significantly increased osteoblast attachment. Cell viability was significantly increased on all composites on Days 4 and 7, and on 1%, 4% and 5% HA on Day 1. Cell proliferation was increased on Days 4 and 7 for all composites and on 4% and 5% HA on Day 1. The 5% HA had osteoblast attachment and proliferation that was significantly higher than all other composites on the days examined. Therefore the 5% HA is the composite that is mechanically the most similar to non-load bearing cancellous bone and also increases osteoblast response the most over all other composites.

5.2 Inverso-CysHHC10 Antimicrobial Activity: Surface Immobilized vs. in Solution

After determining that the 5% HA composite was the most suitable material mechanically and for increased osteoblast response, the composite was functionalized to prevent *E. coli* growth.[7-9] The broad spectrum antimicrobial peptide HHC10 was covalently linked to the 5% HA in a two-step alkene-thiol click reaction, where the material serves as the delivery vehicle for the antimicrobial, and the 16-ene film serves as the organic spacer

group giving the AMP steric freedom at the interface.[10,11] Mass spectral analysis revealed the stability of the newly formed sulfide bond that kept greater than 99.6% of the HHC10 localized to the material through 24 hours soaking in water. The activity of the linked HHC10 was determined through the NPN uptake factor and bacterial turbidity test. Increased bacteria cell membrane permeability was evaluated using the NPN uptake assay.[12,13] Results indicated increased NPN uptake for *E. coli* treated with HHC10 modified 5% HA versus unmodified 5% HA, as a result of AMP activity and membrane pore formation. The growth of *E. coli* in planktonic culture was also significantly reduced as indicated by the $OD_{600\,nm}$ in the bacterial turbidity test.[14,15] The amount of AMP covalently linked to the 5% HA composite was as effective against *E. coli* as a 10 μM HHC10 solution, which is slightly greater than the 8 μM LC99.9 of free Inverso-CysHHC10.[10,11] Both of these assays confirm that HHC10 retains its antimicrobial activity through the alkene-thiol immobilization, resulting in the antimicrobially active 5% HA interface.

5.3 Osteoblast Response on Inverso-CysHHC10 Modified 5% HA

In an ideal multifunctional system, the function of one modification should not be affected by the other. Therefore, once the covalent attachment and antimicrobial evaluation of HHC10 was completed, the increased osteoblast response observed on unmodified 5% HA was re-examined. Osteoblasts were cultured and seeded onto sterilized HHC10 modified 5% HA and examined for their attachment, viability and proliferation on Days 1, 4 and 7. Statistically equivalent cellular attachment was observed on HHC10 modified and unmodified 5% HA on all days examined. The extent of osteoblast proliferation on the

HHC10 modified 5% HA was again statistically equal to the unmodified 5% HA on Days 1, 4 and 7. Finally percent cell viability was the same on HHC10 modified and unmodified 5% HA on Days 1 and 4, and was statistically higher on modified 5% HA on Day 7. These outcomes demonstrate that the independent functions of the 5% HA composite are not compromised when the AMP is immobilized to the material surface.

5.4 Impact and Future Work

Through the execution of this project, the CaAlO material was physically and chemically improved for applicability as a bone scaffold material. The incorporation of the osteogenic HA into the material resulted in increased osteoblast response without the implementation of chemical modification. The use of an alkene-thiol click reaction to link an antimicrobial peptide to the composite also demonstrates an improved method for the addition of antibacterial activity to these bone scaffold materials.[11,16]

Literature has shown that through the chemical immobilization of cell adhesion peptides and osteoinductive proteins osteoblast performance can be significantly increased on a variety of materials.[14,17-20] However, the enhanced osteoblast response observed on the unmodified CaAlO based composites that remain mechanically similar to non-load bearing bone is the first result of this nature. By increasing bone cell response through this materials-based approach the extent of functionalization and introduction of chemicals to the materials has been significantly reduced.

The covalent immobilization of Inverso-CysHHC10 to the 5% HA composite that remains active through sterilization is a significant contribution towards the limitation of implant associated infections. The significance of the antimicrobial peptide being localized

to the material is that it allows for effective broad spectrum antimicrobial activity that is persistent at the location of implantation. Most importantly, by using an AMP instead of an antibiotic, this modification approach plays a critical role in limiting the development of antibacterial resistance among strains of bacteria *in vitro* and *in* vivo.[21-24]

The design of a multifunctional composite material that actively enhances osteoblast response and decreases bacterial growth is significant because it represents an advancement in the development of biomaterials that are able to address multiple physiological strains that may be placed on the material in an *in vivo* setting. Further, in an ideal multifunctional material one function would not be effected by the other, and the system developed here demonstrates that these biological functions work in synergy on the material. The modified composites designed here cooperatively address the problems associated with mechanical and biological bone graft failure.

The reaction sequence used to modify the 5% HA interface is further applicable to other relevant biomaterial surfaces. Any interface that contains the reactive surface hydroxyl and μ-oxo groups can be functionalized with using this alkene-thiol approach. Many current metal oxides used in total joint replacements and arterial and venous stents contain these groups and their functionality could be improved through antimicrobial modification using an alkene-thiol click linker system.

In the future, methods to create macroporosity in the materials without compromising mechanical strength would be desirable. A potential approach is to integrate the fibrous protein collagen into the material, as natural bone is approximately 60% hydroxyapatite and 40% collagen by dry mass. Also, composites that are between 5-10% HA may be examined mechanically and biologically because the trend observed in this

work is that as the HA percentage increases the osteoblast response increases, but the mechanical strength decreases. The alkene-thiol linker system could be utilized to link a natural AMP. The HHC10 used here is effective *in vitro*, however it is a synthetic AMP. The human immune system is composed of a large variety of natural AMP's including defensins, cathelicidins and histatins that may be more attractive options in human biomaterial applications.[25-28]

Ultimately, *in vivo* studies using a critical sized bone defect are necessary to evaluate the ability of the unmodified and HHC10 modified 5% HA to increase new bone formation in a physiological setting.[6] Further *in vitro* bacterial testing with additional biofilm forming bacteria including *S. aureus* and *S. epidermidis* would be beneficial to demonstrate that the linked AMP retains its broad spectrum antibacterial activity.[21,29-31] Upon completing these additional *in vitro* studies, an *in vivo* implant associated infection model would be necessary to fully evaluate the material for its applicability as a synthetic bone scaffold.

5.5 References

1. Clafshenkel, W. P.; Rutkowski, J. L.; Palchesko, R. N.; Romeo, J. D.; McGowan, K. A.; Gawalt, E. S.; Witt-Enderby, P. A. A novel calcium aluminate-melatonin scaffold enhances bone regeneration within a calvarial defect. *J. Pineal Res.* **2012**, *53*, 206-218.

2. LeGeros, R. Z. Properties of osteoconductive biomaterials: Calcium phosphates. *Clinical orthopaedics and related research* **2002**, *395*, 81-98.

3. Pino-Mínguez, J.; Jorge-Mora, A.; Couceiro-Otero, R.; García-Santiago, C. Study of the viability and adhesion of osteoblast cells to bone cements mixed with hydroxyapatite at different concentrations to use in vertebral augmentation techniques. *Rev. Esp. Cir. Ortop. Traumatol.* **2015**, *59*, 122-128.

4. Charalambous, C. P. In *Classic Papers in Orthopaedics*; Banaszkiewicz, P.A., Kader, D. F., Eds.; Springer: London, 2014; Part VIII , pp. 419-421.

5. Jarcho, M. Calcium phosphate ceramics as hard tissue prosthetics. *Clin. Orthop. Relat. Res.* **1981**, *157*, 259-278.

6. Miljkovic, N. D.; Cooper, G. M.; Hott, S. L.; DiSalle, B. F.; Gawalt, E. S.; Smith, D. M.; McGowan, K.; Marra, K. G. Calcium aluminate, RGD-modified calcium aluminate, and β-tricalcium phosphate implants in a calvarial defect. *J. Craniofac. Surg.* **2009**, *20*, 1538-1543.

7. Boman, H. G.; Agerberth, B.; Boman, A. Mechanisms of action on Escherichia coli of cecropin P1 and PR-39, two antibacterial peptides from pig intestine. *Infect. Immun.* **1993**, *61*, 2978-2984.

8. Kim, H. K.; Chun, D. S.; Kim, J. S.; Yun, C. H.; Lee, J. H.; Hong, S. K.; Kang, D. K. Expression of the cationic antimicrobial peptide lactoferricin fused with the anionic peptide in Escherichia coli. *Appl. Microbiol. Biotechnol.* **2006**, *72*, 330-338.

9. Kovach, M. A.; Ballinger, M. N.; Newstead, M. W.; Zeng, X.; Bhan, U.; Yu, F. S.; Moore, B. B.; Gallo, R. L.; Standiford, T. J. Cathelicidin-related antimicrobial peptide is required for effective lung mucosal immunity in Gram-negative bacterial pneumonia. *J. Immunol.* **2012**, *189*, 304-311.

10. Cleophas, R. T.; Riool, M.; Quarles van Ufford, H. C.; Zaat, S. A.; Kruijtzer, J. A.; Liskamp, R. M. Convenient preparation of bactericidal hydrogels by covalent attachment of stabilized antimicrobial peptides using thiol–ene click chemistry. *ACS Macro Lett.* **2014**, *3*, 477-480.

11. Cleophas, R. T.; Sjollema, J.; Busscher, H. J.; Kruijtzer, J. A.; Liskamp, R. M. Characterization and activity of an immobilized antimicrobial peptide containing bactericidal PEG-hydrogel. *Biomacromolecules* **2014**, *15*, 3390-3395.

12. Helander, I.; Mattila-Sandholm, T. Fluorometric assessment of gram-negative bacterial permeabilization. *J. Appl. Microbiol.* **2000**, *88*, 213-219.

13. Helander, I. M.; Alakomi, H. L.; Latva-Kala, K.; Koski, P. Polyethyleneimine is an effective permeabilizer of gram-negative bacteria. *Microbiol.* **1997**, *143*, 3193-3199.

14. Palchesko, R. N.; Buckholtz, G. A.; Romeo, J. D.; Gawalt, E. S. Co-immobilization of active antibiotics and cell adhesion peptides on calcium based biomaterials. *Mater. Sci. Eng., C* **2014**, *40*, 398-406.

15. Palchesko, R. N.; McGowan, K. A.; Gawalt, E. S. Surface immobilization of active vancomycin on calcium aluminum oxide. *Mater. Sci. Eng., C* **2011**, *31*, 637-642.

16. Ma, Y.; Zheng, J.; Amond, E. F.; Stafford, C. M.; Becker, M. L. Facile fabrication of "dual click" one-and two-dimensional orthogonal peptide concentration gradients. *Biomacromolecules* **2013**, *14*, 665-671.

17. Hersel, U.; Dahmen, C.; Kessler, H. RGD modified polymers: Biomaterials for stimulated cell adhesion and beyond. *Biomaterials* **2003**, *24*, 4385-4415.

18. Palchesko, R. N.; Romeo, J. D.; McGowan, K. A.; Gawalt, E. S. Increased osteoblast adhesion on physically optimized KRSR modified calcium aluminate. *J. Biomed. Mater. Res., Part A* **2012**, *100*, 1229-1238.

19. Sun, S.; Yu, W.; Zhang, Y.; Zhang, F. Increased preosteoblast adhesion and osteogenic gene expression on TiO_2 nanotubes modified with KRSR. *J. Mater. Sci. Mater. Med.* **2013**, *24*, 1079-1091.

20. Xiao, S. J.; Textor, M.; Spencer, N. D.; Sigrist, H. Covalent attachment of cell-adhesive,(Arg-Gly-Asp)-containing peptides to titanium surfaces. *Langmuir* **1998**, *14*, 5507-5516.

21. Costa, F.; Carvalho, I. F.; Montelaro, R. C.; Gomes, P.; Martins, M. C. L. Covalent immobilization of antimicrobial peptides (AMPs) onto biomaterial surfaces. *Acta Biomater.* **2011**, *7*, 1431-1440.

22. Gordon, Y. J.; Romanowski, E. G.; McDermott, A. M. A review of antimicrobial peptides and their therapeutic potential as anti-infective drugs. *Curr. Eye Res.* **2005**, *30*, 505-515.

23. Jenssen, H.; Hamill, P.; Hancock, R. E. Peptide antimicrobial agents. *Clin. Microbiol. Rev.* **2006**, *19*, 491-511.

24. Onaizi, S. A.; Leong, S. S. Tethering antimicrobial peptides: Current status and potential challenges. *Biotechnol. Adv.* **2011**, *29*, 67-74.

25. De Smet, K.; Contreras, R. Human antimicrobial peptides: Defensins, cathelicidins and histatins. *Biotechnol. Lett.* **2005**, *27*, 1337-1347.

26. Ganz, T. Defensins: Antimicrobial peptides of innate immunity. *Nat. Rev. Immunol.* **2003**, *3*, 710-720.

27. Kavanagh, K.; Dowd, S. Histatins: Antimicrobial peptides with therapeutic potential. *J. Pharm. Pharmacol.* **2004**, *56*, 285-289.

28. Zanetti, M. Cathelicidins, multifunctional peptides of the innate immunity. *J. Leukocyte Biol.* **2004**, *75*, 39-48.

29. Alvarez-Bravo, J.; Kurata, S.; Natori, S. Novel synthetic antimicrobial peptides effective against methicillin-resistant Staphylococcus aureus. *Biochem. J.* **1994**, *302*, 535-538.

30. Midorikawa, K.; Ouhara, K.; Komatsuzawa, H.; Kawai, T.; Yamada, S.; Fujiwara, T.; Yamazaki, K.; Sayama, K.; Taubman, M. A.; Kurihara, H. Staphylococcus aureus susceptibility to innate antimicrobial peptides, β-defensins and CAP18, expressed by human keratinocytes. *Infect. Immun.* **2003**, *71*, 3730-3739.

31. Rieg, S.; Steffen, H.; Seeber, S.; Humeny, A.; Kalbacher, H.; Dietz, K.; Garbe, C.; Schittek, B. Deficiency of dermcidin-derived antimicrobial peptides in sweat of patients with atopic dermatitis correlates with an impaired innate defense of human skin in vivo. *J. Immunol.* **2005**, *174*, 8003-8010.